PERIODICAL

Volume 4, No. 2
New Series

March 1958

RECORDS
OF
OCEANOGRAPHIC WORKS
IN JAPAN

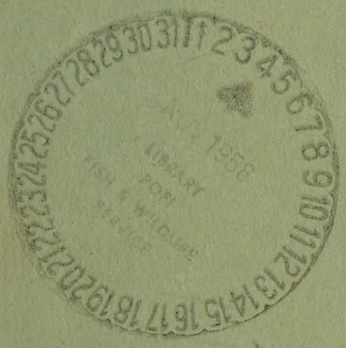

Published by

Science Council of Japan

BOARD OF EDITORS

Editor-in-Chief
Shinkishi HATAI

Editors
Yoshio HIYAMA — Kōji HIDAKA
Yasuo MIYAKE — Hiroshi NIINO

With the Co-operation of

Physical Oceanography
Kōji FUKUTOMI — Shōichirō HAYAMI
Mashito NAKANO — Tadayoshi SASAKI
Kanji SUDA — Ryūtarō TAKAHASHI
Michitaka UDA

Chemical Oceanography
Masayoshi ISHIBASHI — Yasuo MATSUDAIRA
Ken SUGAWARA

Geological Oceanography
Shōzaburō HANZAWA

Biological Oceanography
Denzaburò MIYADI — Yō K. OKADA
Isao TAKI — Yukio YAMADA

Fisheries
Hiroaki AIKAWA — Motosaku FUJINAGA
Takeo IMAI

Secretary
Buei ARAYA

SUGGESTION TO AUTHORS OF PAPERS FOR THE RECORDS OF OCEANOGRAPHIC WORKS IN JAPAN

An author wishing to contribute a paper to the RECORDS OF OCEANOGRAPHIC WORKS IN JAPAN should submit in compliance with the following suggestions:

1. Manuscripts will be accepted within the scope of
   Physical Oceanography — Geological Oceanography
   Chemical Oceanography — Biological Oceanography and
   Fisheries
2. An original and a copy of his manuscript should be type-written double-spaced in 21×29.5 cm paper, within 12 sheets, making 6 printed pages including plates and tables.
3. The manuscript should be addressed to the competent editor and mailed to the official in charge of the Science Council of Japan, Ueno Park, Tokyo, Japan.
4. The author is asked to follow this publication for forms of headings and references, etc.
5. The editors reserve the right to accept the manuscripts and to make minor editorial changes in them, so that all paper may conform to overall style of this publication.

CONTENTS

Computation of the Wind Stresses over the Oceans ..... Koji HIDAKA.. 77
On the Seasonal Variations of Surface Divergence of the Ocean Currents in Terms of Wind Stresses in the Oceans.. Koji HIDAKA and Kiheiji OGAWA.. 124
Depth Determination in Oceanographic Observations.... Toshihiko TERAMOTO.. 170
A Study on Upwelling ..... Kozo YOSHIDA.. 186
Productibility of Plankton-feeders in the Off-shore Area of Japan ..... Yoshio HIYAMA and Fujio YASUDA.. 193
Mophometric Comparison of the Albacore from the Northwest, the Equatorial and the Southwest Pacific.... Kenji KUROGANE and Yoshio HIYAMA.. 200

Digitized by the Internet Archive
in 2025

https://archive.org/details/records-of-oceanographic-works-in-japan-new-series_1958-03_4_2

Records of Oceanographic Works
in Japan Vol. 4, No. 2
March 1958

Computation of the Wind Stresses over the Oceans

By
Koji Hidaka
(Geophysical Institute, University of Tokyo)

Abstract

The field of wind stress over the North Pacific Ocean were computed by the Scripps Institution of Oceanography after Munk's formula. This is the result of an at tempt to extend this work to three big worlds oceans.

Mechanism at the air-sea boundary is still not clear, and there are much to be done for better understanding of processes going on at this interface. Several formulae for computing the wind stresses on the sea surface from the wind velocity data have been proposed. Walter H. Munk published in 1947 that there is a jump of wind streess at a critical wind velocity 6.6 m/sec or at the wind force 4 on the Beaufort scale. (Munk, 1947). A few years later Gerhard Neumann stated that there is no such a particular jump of wind stress at the wind speed which Munk mentioned (Neumann, 1951). This problem was afterwards examined by several authors, including William G. Van Dorn who made a series of experiments in an large artificial basin (Van Dorn, 1953).

Nevertheless, the problem of wind stresses still remains unsettled. Recent progress in the field of dynamical oceanography, however, urgently requires the information as to the field of wind stress over the oceans.

In 1948, the Scripps Institution of Oceanography, University of California, published a series of tables of the field of mean monthly wind stress over the North Pacific as down as the latitude 2.5°S. (SIO, 1948). The present paper involves tha result of an attempt to extend the computation of the wind stress fields to the South Pacific, Indian and Atlantic Oceans for four seasons and of their annual mean values.

To keep pace with Scripps computation the formula by Munk:

$$\tau = 0.008\rho W^2 \quad (W < 6.6 \text{ m/s})$$
$$= 0.026\rho W^2 \quad (W > 6.6 \text{ m/s})$$

was employed in this report, where W is the wind speed in cm/sec and ρ the density of the air. (Munk, 1947). The result is given in Tables I–XV.

The material was exclusively adopted from the Pilot Charts of wind roses for 5° squares of the U. S. Navy Hydrographic Office. For the practical computation, method of Robert O. Reid was also referred to (Reid, 1948),

For the data for the North Pacific down to 2.5°S the tables for the months of January, April, July and October are reproduced from the Scripps report. (SIO, 1948). For the South Pacific are tabulated the averages of the data for three months centering at January, April, July and October. For the Indian Ocean, the data for January, April, July and October are tabulated, while the Atlantic data consist of the averages of three months centering at January, April, July and October. In addition, the fields of annual mean wind stress were computed and are tabulated at the same time.

Dynamically speaking, there are many questions and difficulties in the exact computation of wind stresses over the sea surface. In this respect, it would be hard to say that these data present the field of wind stress over the oceans very accurately. The author will, however, be happy if this computation would, though approximately, give an idea of the wind stress distribution over the oceans, and help the research workers who are interested in dynamical oceanography in this direction.

This research has been partly financed by the funds of the Japanese National Commission for Unesco, to whom the author wishes to express his sincerest thanks. The author is also much idebted to Mr. K. OGAWA and Misses. T. OSADA and K. MARUYAMA for tedious computations.

References

MUNK, W. H. (1947): A critical wind speed for air-sea boundary processes. J. Mar. Res. **6**, 203–218.

NEUMANN, Gerhard (1951): Gibt es eine „Kritische Windgeschwindigkeit" für die Grenzfläche Wasser-Luft. Deutsche Hydrographische Zeitshrift **4**, 6–13.

REID, R. O. (1948): The equatorial currents of the eastern Pacific as maintained by the stress of the wind. J. Mar. Res. **7**, 74, 74–99.

Scripps Institution of Oceanography (1948): The field of mean wind stress over the North Pacific Ocean. Oceanographic Report No. 14, 1–12.

Van DORN, W. G. (1953): Wind stress on an artificial pond. J. Mar. Res. **12**, 249–276.

Table 1. Computed Wind Stresses over the Pacific Ocean—Dec., Jan. and Feb.

(τ_x and τ_y are given by the upper and lower figures, respectively, of each compartment, the unit being 10^{-2} dynes/cm^2).

	E 122.5°	127.5°	132.5°	137.5°	142.5°	147.5°	152.5°	157.5°	162.5°	167.5°	172.5°	177.5°	W 177.5°	172.5°	167.5°	162.5°
N 57.5°													+ 84	+ 25	+ 40	+ 49
52.5°													+ **66**	+ **23**	+ **11**	+ **26**
47.5°							+143	+178	+159	+154	+110	+ 52	+ 31	+ 27	+ 40	+ 55
							−**133**	−**118**	− **57**	− **31**	+ **23**	+ **47**	+ **31**	+ **27**	+ **37**	+ **15**
42.5°					+159	+141	+142	+156	+180	+163	+150	+ 95	+ 64	+ 76	+ 88	+ 84
					− **80**	−**108**	−**125**	− **78**	− **56**	− **22**	− **22**	− **3**	+ **53**	+ **8**	+ **49**	+ **56**
37.5°					+ 83	+129	+189	+199	+188	+152	+205	+145	+135	+127	+114	+104
					−**122**	−**126**	−**128**	−**121**	− **57**	− **20**	+ **1**	− **2**	+ **34**	+ **16**	+ **7**	+ **35**
32.5°	+ 22	+ 62	+39	+103	+132	+143	+147	+170	+187	+158	+143	+116	+ 64	+ 95	+ 80	+ 87
	− **84**	−**100**	−**81**	−**104**	− **55**	− **63**	− **44**	− **20**	− **10**	+ **28**	+ **27**	− **3**	+ **29**	+ **5**	+ **13**	+ **23**
27.5°	− 71	− 8	+32	+ 27	+ 25	+ 66	+ 91	+ 99	+ 74	+ 56	+ 23	+ 9	+ 23	+ 19	+ 3	− 47
	−**174**	−**167**	−**61**	− **41**	− **41**	− **42**	− **46**	− **13**	− **3**	− **22**	− **3**	− **21**	− **3**	− **14**	− **15**	− **5**
22.5°	− 45	− 64	−55	− 46	− 27	− 34	− 30	− 45	− 21	− 14	− 29	− 34	− 14	− 21	− 22	− 28
	−**177**	−**112**	−**58**	− **71**	− **39**	− **38**	− **34**	− **38**	− **24**	− **6**	− **14**	− **15**	− **13**	− **19**	− **15**	− **20**
17.5°	− 0	− 96	−90	− 76	− 57	− 67	− 40	− 26	− 61	− 40	− 62	− 48	− 46	− 57	− 59	− 73
	−**102**	− **83**	−**81**	− **63**	− **39**	− **48**	− **26**	− **11**	− **20**	− **18**	− **27**	− **11**	− **10**	− **14**	− **24**	− **30**
12.5°		− 62	−79	− 93	− 56	− 67	−117	−133	−168	− 60	− 96	− 57	−147	−129	− 75	− 96
		− **47**	−**52**	− **51**	− **35**	− **33**	− **55**	− **70**	− **90**	− **31**	− **44**	− **30**	− **70**	− **62**	− **42**	− **51**
7.5°		− 22	−45	− 39	− 89	− 80	− 95	− 89	−112	− 96	− 81	− 57	− 91	−108	−102	−116
		− **36**	−**40**	− **43**	− **32**	− **45**	− **40**	− **47**	− **78**	− **45**	− **48**	− **45**	− **68**	− **59**	− **57**	− **54**
2.5°		− 6	+ 2	+ 2	− 12	+ 5	− 25	− 46	− 28	− 32	− 32	−109	− 40	− 43	− 61	− 9
		− **17**	− **7**	− **8**	− **12**	+ **13**	− **10**	− **44**	− **23**	− **26**	− **26**	−**101**	− **15**	− **24**	− **15**	− **1**
S 2.5°					+ 30	+ 30	+ 25	+ 9	+ 2	+ 6	− 11	− 17	− 19	− 25	− 36	− 16
					− **0**	− **6**	− **4**	− **12**	− **14**	− **11**	− **46**	− 35	− **9**	− **21**	− **15**	− **5**

Table 1. (continued)

	157.5°	152.5°	147.5°	142.5°	137.5°	132.5°	127.5°	122.5°	117.5°	112.5°	107.5°	102.5°	97.5°	92.5°	87.5°	82.5°
N		− 6	− 35	− 65	− 30											
57.5°		− **2**	+ **43**	+ **17**	− **1**											
52.5°	+ 57	+ 90	+ 96	+105	+114	+ 64	+ 48									
	+ **36**	+ **38**	+ **50**	+ **68**	+ **71**	+ **52**	− **1**									
47.5°	+ 83	+ 83	+ 29	+ 86	+ 96	+ 32	+ 1									
	+ **43**	+ **23**	+ **33**	+ **52**	+ **66**	+ **50**	+**109**									
42.5°	+ 95	+ 89	+104	+ 62	+ 89	+ 75	+ 51									
	+ **38**	+ **14**	+ **71**	+ **41**	+ **29**	+ **13**	+ **64**									
37.5°	+ 75	+ 76	+ 59	+ 49	+ 52	+ 54	+ 38	+ 10								
	+ **85**	+ **91**	+ **59**	+ **52**	+ **12**	− **1**	− **28**	− **17**								
32.5°	+ 46	+ 44	+ 5	+ 14	+ 18	+ 19	+ 30	+ 45	+ 8							
	+ **12**	+ **61**	+ **23**	+ **37**	+ **13**	− **15**	− **41**	− **68**	− **9**							
27.5°	− 30	− 29	− 28	− 26	− 28	− 37	− 24	− 15	+ 15							
	− **3**	− **2**	+ **6**	+ **18**	− **10**	− **33**	− **38**	− **43**	− **21**							
22.5°	− 43	− 41	− 55	− 70	− 85	− 65	− 76	− 50	− 22	+ 4	+ 3					
	− **23**	− **14**	− **10**	− **14**	− **35**	− **41**	− **55**	− **46**	− **31**	−**12**	−**12**					
17.5°	− 62	− 95	− 77	−117	−133	− 84	− 86	−117	− 54	− 7	+ 4	+ 1				
	− **21**	− **41**	− **41**	− **60**	− **72**	− **49**	− **54**	− **58**	− **59**	−**15**	−**11**	− **3**				
12.5°	−169	−136	−113	−163	−150	− 91	−183	−166	−104	−59	−26	− 6	−32	− 5	−34	
	− **95**	− **69**	− **57**	− **94**	−**102**	− **72**	− **95**	− **76**	− **67**	−**45**	−**14**	− **6**	−**60**	−**10**	−**28**	
7.5°	−125	−108	− 85	−141	− 93	− 75	− 61	− 71	− 48	−28	−52	−51	−19	− 8	−16	0
	− **86**	− **59**	− **22**	− **40**	− **45**	− **17**	− **25**	+ **6**	− **7**	− **6**	−**24**	− **9**	− **6**	− **5**	−**22**	− **7**
2.5°	− 41	− 73	− 83	− 79	− 63	− 59	− 55	− 51	− 32	−22	−12	− 8	−22	0	− 3	− 0
	+ 8	+ **20**	+ **32**	+ **25**	+ **3**	+ **36**	+ **48**	+ **55**	+ **24**	+**16**	+ **9**	+**30**	+**40**	+ **9**	+ **7**	+ **7**
S	− 77	− 73	− 58	− 82	− 94	−114	− 92	− 77	− 63	−27	−16	−20	−34	− 5	− 4	+ 4
2.5°	+ **2**	+ **33**	+ **11**	− **9**	+ **10**	+ 42	+ **42**	+ 50	+ **22**	+**10**	+**10**	+**23**	+**45**	+ **9**	+ **8**	+**11**

Table 1. (continued)

		E 122.5°	127.5°	132.5°	137.5°	142.5°	147.5°	152.5°	157.5°	162.5°	167.5°	172.5	E 177.5°	W 177.5°	172.5°	167.5°	162.5°	157.5°
S	E.C.	+ 24	+ 9	+359	+151		+106	+ 67	+ 2	+ 13	+ 3	+ 13	+ 11	− 4	+ 10	− 13	− 17	− 12
7.5°	N.C.	+ 5	− 0	− 10	− 3		− 30	− 66	− 2	− 1	− 17	− 17	− 4	− 5	− 17	− 51	− 32	− 8
12.5°		− 69	+ 6	+ 14	+321	+ 57	− 2	− 66	+ 19	+ 16	− 2	− 2	− 5	− 6	− 6	− 6	+ 0	− 10
		+156	+ 3	− 69	− 43	−147	− 0	− 25	+ 36	− 14	− 11	− 1	− 7	− 1	− 2	− 16	− 3	− 4
17.5°		− 1	−780			− 51	−387	−413	−629	− 59	− 17	− 47	− 57	− 40	− 26	− 34	− 31	− 30
		+ 3	−107			− 1	+ 19	+ 83	+215	+ 6	− 6	+ 20	+ 15	+ 3	+ 17	− 10	+ 4	− 0
22.5°							− 5	− 92	−114	− 47	− 70	− 59	− 69	− 43	− 55	− 44	− 32	− 83
							− 0	+ 25	+ 19	− 22	+ 11	+ 21	+ 17	+ 16	+ 5	− 14	− 2	− 17
27.5°								− 64	− 44	− 58	− 88	− 56	− 50	− 61	− 57	− 42	− 52	− 24
								+ 50	+ 4	+ 10	+ 37	+ 17	+ 12	+ 7	+ 12	+ 5	+ 16	− 16
32.5°		+ 69	− 14	− 85	+ 7			−308	−319	− 28	− 31	− 31	− 37	− 27	− 10	− 6	− 15	+ 3
		+ 17	+ 7	−192	+ 39			−149	+148	− 12	− 17	+ 13	+ 8	− 10	+ 25	+ 16	+ 22	+ 7
37.5°		+ 76	+ 50	+ 24	+ 46	+322	+300	+ 21	− 44	− 3	− 3	+ 22	+ 16	+ 41	+ 9	+ 11	+ 38	− 19
		+ 49	+ 47	+ 12	− 68	+390	+374	+254	− 58	+ 12	+ 12	+ 20	− 2	− 15	− 12	− 11	− 41	− 10
42.5°		+146	+111	+119	+ 65	+524	+608	− 32	+410	+ 40	+ 27	+ 14	+ 9	+ 18	+ 24	+ 2	+ 7	+ 23
		− 38	− 24	+ 7	+ 35	−148	+450	+ 12	− 42	− 1	+ 48	+ 2	− 0	− 42	− 50	− 12	+ 12	+ 2
47.5°		+171	+147	+128	+138	+100	+145	+125	+ 63	+ 94	+101	+126	+ 83	+ 59	+174	+ 53	+105	+ 96
		+ 48	− 11	− 45	− 87	+ 16	− 22	− 55	+ 58	+ 33	− 34	+ 10	+ 92	+ 26	+ 23	− 5	+ 7	+ 58
52.5°										− 6	+ 80	+102	− 26	+169	+ 84	+181	+115	+194
										+108	−123	−110	−151	− 69	+ 86	+174	− 76	−100
S	E.C.																	
57.5°	N.C.																	

Table 1. (continued)

		152.5°	147.5°	142.5°	137.5°	W 132.5°	W 127.5°	122.5°	117.5°	112.5°	107.5°	102.5°	97.5°	92.5°	87.5°	82.5°	77.5°	W 72.5°
S	E.C.	− 30	− 48	− 4	− 74	−223	− 91	−122	− 76	− 89	− 85	− 75	− 69	+ 15	− 12	− 0	− 3	
7.5°	N.C.	− 8	− 17	− 4	− 3	+ 9	+ 21	+ 40	+ 9	+ 27	+ 28	+ 44	+ 69	+ 12	+ 11	+ 0	− 12	
12.5°		− 4	− 38	− 1	− 56	− 98	−218	− 83	−101	− 96	− 85	− 97	− 62	− 82	− 38	− 5	− 9	
		− 25	− 16	− 2	− 5	+ 14	− 2	+ 2	− 23	+ 10	− 9	+ 16	+ 5	+ 44	− 1	− 1	+ 9	
17.5°		− 8	− 11	− 1	− 69	− 78	− 82	− 63	− 60	− 33	− 78	−104	− 62	− 80	− 35	− 57	− 13	− 6
		− 7	− 3	+ 0	+ 3	− 1	+ 9	− 0	− 2	− 13	+ 7	− 34	− 4	+ 27	+ 23	+ 24	+ 8	+ 7
22.5°		− 62	− 42	− 4	− 69	− 79	− 54	− 53	− 12	− 34	− 8	− 63	− 57	− 70	− 43	− 56	− 10	− 4
		− 17	+ 9	− 1	+ 37	+ 5	− 2	− 3	− 5	− 20	− 6	− 3	− 2	+ 28	+ 5	+ 45	+ 12	+ 6
27.5°		− 25	− 48	− 0	− 48	− 65	− 50	− 56	− 5	− 78	− 11	− 50	− 43	− 30	− 40	− 55	− 41	− 2
		− 1	− 12	− 3	+ 14	− 2	+ 5	− 3	− 3	+ 2	+ 3	− 23	− 10	− 3	+ 36	+ 45	+ 42	+ 12
32.5°		− 39	+ 16	− 2	− 5	− 41	− 28	+ 1	+ 12	− 11	− 12	+ 12	− 4	+ 4	+ 7	− 4	− 12	+ 0
		− 10	− 20	+ 0	− 2	+ 19	− 1	− 13	− 15	+ 65	+ 10	− 27	+ 0	− 1	+ 12	+ 18	+ 61	+ 61
37.5°		− 31	+ 49	+ 3	+ 17	− 3	+ 7	+ 31	+ 35	+ 21	− 16	+ 45	+ 16	+ 32	+ 48	+ 38	+ 15	+ 0
		+ 6	+ 35	+ 1	− 2	− 24	− 9	+ 3	+ 13	− 3	− 34	− 2	− 4	+ 13	+ 7	+ 35	+ 59	+ 58
42.5°		+ 81	+ 57	+ 8	+ 21	+ 18	+ 17	+ 83	+114	+131	+102	+119	+103	+198	+128	+139	+ 97	+ 53
		+ 17	− 50	− 1	− 59	+ 17	− 15	− 11	+ 16	− 5	+ 55	+ 73	+ 78	+115	− 3	+ 47	+ 35	+ 35
47.5°		+127	+104	+ 17	+108	+ 78	+104	+138	+201	+257	+260	+279	+246	+148	+218	+215	+167	
		− 12	+ 2	− 5	− 70	− 44	+ 14	− 25	− 66	+ 7	+ 32	+ 43	+ 96	+ 75	+ 14	− 37	− 3	
52.5°		+ 82	+356	+201	+194	+ 24	+ 45	+151	+163	+203	+266	+281	+354	+294	+201	+222	+320	+137
		+ 41	− 22	+ 34	+ 32	− 51	+ 15	− 7	+ 18	+ 90	+ 71	+ 40	+ 96	+ 26	+ 51	− 9	− 7	+ 2
S	E.C.								+113	+113	+104	+114	+119	+203	+241	+142	+257	+255
52.5°	N.C.								− 18	− 18	+ 26	+ 17	+162	+ 38	+ 29	− 24	− 48	− 59

Table 2. Computed Wind Stresses over the Pacific Ocean—Mar., Apr. and May.

(τ_x and τ_y are given by the upper and lower figures, respectively, of each compartment, the unit being 10^{-2} dynes/cm^2).

	E 122.5°	127.5°	132.5°	137.5°	142.5°	147.5°	152.5	157.5°	162.5°	167.5°	172.5°	177.5°	W 177.5°	172.5°	167.5°	162.5°
N 57.5°																
													+120	+ 82	+ 86	+ 86
52.5°													+ 13	+ 41	+ 8	+ 23
							+58	+ 86	+ 82	+ 73	+80	+74	+ 94	+ 68	+ 83	+ 69
47.5°							− 2	− 24	0	+ 19	+23	+41	+ 6	+ 15	+ 38	+ 37
					+28	+30	+54	+ 72	+ 76	+ 75	+57	+89	+ 54	+ 82	+ 70	+106
42.5°					+ 2	−17	−26	− 29	− 19	− 25	− 4	+35	+ 2	+ 22	+ 31	+ 20
					+ 6	+ 26	+ 51	+ 54	+ 55	+ 43	+56	+74	+ 46	+ 41	+ 27	+ 35
37.5°					−26	+ 8	−10	− 23	− 14	− 2	+30	+26	+ 10	+ 36	+ 11	+ 6
	− 2	+ 8	0	+18	+17	+11	+ 33	+ 14	+ 33	+ 22	+16	+12	+ 12	− 2	− 3	+ 1
32.5°	−14	−47	−23	−37	− 5	+14	+24	+ 12	+ 33	+ 12	−12	− 8	− 7	− 9	− 11	− 6
	−27	− 1	− 7	− 9	− 1	−13	− 5	+ 6	+ 1	+ 3	−13	−20	− 31	− 23	− 23	− 41
27.5°	−48	−32	−11	+ 6	−11	−19	−24	− 0	− 10	− 7	−10	−12	− 23	− 20	− 25	− 24
	−43	−24	−20	−21	−25	−15	−45	− 24	− 28	− 29	−36	−36	− 39	− 43	− 38	− 46
22.5°	−51	−12	−15	− 7	−16	− 5	−23	− 11	− 20	− 19	−14	−24	− 14	− 28	− 29	− 34
	−20	−31	−36	−28	−35	−42	−44	− 49	− 31	− 41	−43	−68	−100	− 67	− 99	− 81
17.5°	− 9	−17	−20	−14	−16	−25	−10	− 14	− 12	− 14	−21	−21	− 31	− 31	− 38	− 34
		−19	−33	−28	−25	−54	−98	−122	−111	−113	−91	−91	−107	−127	−114	− 91
12.5°		−12	−20	−15	− 9	−23	−57	− 72	− 66	− 18	−43	−49	− 43	− 57	− 59	− 46
		−14	−30	−35	−33	−20	−51	− 61	− 88	− 75	−84	−85	− 70	− 96	− 71	− 77
7.5°		−11	−16	−22	−15	−10	−33	− 47	− 56	− 31	−45	−44	− 15	− 44	− 40	− 53
		+ 1	0	+ 2	− 7	−19	−27	− 21	− 25	− 18	−35	−41	− 21	− 27	− 31	− 23
2.5°		− 3	− 9	− 2	− 5	− 9	−25	− 18	− 20	− 11	− 6	−16	− 4	− 2	− 4	− 8
S 2.5°					+16	+12	+ 4	− 9	− 18	− 4	− 2	−29	− 24	− 13	− 17	− 29
					−20	+ 1	+ 3	+ 3	− 19	− 10	− 3	−11	− 10	− 4	− 5	− 11

Table 2. (continued)

	157.5°	152.5°	147.5°	142.5°	137.5°	132.5°	127.5°	122.5°	117.5°	112.5°	107.5°	102.5°	97.5°	92.5°	87.5°	82.5°
N	− 7	+ 28	− 28	− 83	− 22											
57.5°	**− 22**	**− 50**	**− 16**	**+ 19**	**+ 21**											
52.5°	+102	+ 93	+ 75	+ 64	+ 63	+ 41	− 19									
	+ 18	**+ 25**	**+ 25**	**+ 35**	**+ 47**	**+ 19**	**+ 32**									
47.5°	+108	+ 80	+ 81	+ 99	+101	+ 54	+ 27									
	− 8	**+ 3**	**+ 14**	**+ 25**	**+ 19**	**+ 19**	**+ 29**									
42.5°	+ 82	+ 96	+ 85	+ 81	+ 61	+ 62	+ 40									
	+ 56	**+ 26**	**+ 30**	**+ 12**	**+ 15**	**− 2**	**− 11**									
37.5°	+ 19	+ 46	+ 38	+ 42	+ 48	+ 47	+ 46	+ 63								
	− 11	**− 7**	+ 8	**− 2**	**− 11**	**− 30**	**− 64**	**− 73**								
32.5°	+ 16	+ 7	0	− 4	+ 6	+ 9	+ 36	+ 58	− 15							
	− 28	**− 35**	**− 12**	**− 23**	**− 7**	**− 38**	**− 73**	**− 36**	**− 10**							
27.5°	− 59	− 25	− 18	− 7	− 17	− 22	− 2	+ 2	+ 40							
	− 22	− 8	**− 12**	**− 7**	**− 14**	**− 32**	**− 27**	**− 56**	**− 50**							
22.5°	− 42	− 41	− 70	− 66	− 71	− 54	− 42	− 36	− 17	+ 9	+ 8					
	− 21	**− 20**	**− 26**	**− 28**	**− 35**	**− 47**	**− 42**	**− 43**	**− 61**	**−11**	− 8					
17.5°	− 74	− 96	−104	−118	−106	− 65	− 62	− 80	− 33	− 2	+ 6	+ 3				
	− 23	**− 56**	**− 46**	**− 66**	**− 74**	**− 51**	**− 53**	**− 62**	**− 42**	**−12**	**−10**	**− 1**				
12.5°	−165	−115	−115	−146	− 80	−122	−138	−113	−110	−49	− 7	− 1	− 6	− 2	−11	
	−104	**− 82**	**− 57**	**− 93**	**− 58**	**−100**	**−124**	**− 81**	**− 95**	**−41**	**− 9**	**− 4**	**−14**	**− 5**	**− 8**	
7.5°	− 82	−140	− 91	− 88	− 92	−128	− 94	− 64	− 47	−27	−21	−24	−18	− 4	− 3	− 1
	− 46	**−100**	**− 68**	**− 60**	**− 73**	**− 74**	**− 65**	**− 27**	**− 19**	**−12**	**− 6**	**− 8**	**− 6**	**− 3**	**− 9**	**− 3**
2.5°	− 28	− 41	− 29	− 24	− 16	− 59	− 12	− 14	− 12	−11	− 6	− 5	− 3	0	− 3	+ 2
	− 6	+ 8	**− 2**	**− 3**	**− 1**	**+ 28**	**+ 9**	**+ 14**	**+ 8**	**+12**	**+ 6**	**+ 1**	**+ 6**	**+ 6**	+ 8	**+ 6**
S	− 23	− 18	− 28	− 20	− 48	− 72	− 26	− 66	− 34	−26	−18	−10	− 8	− 6	− 6	+ 1
2.5°	**− 2**	**− 4**	**− 2**	**− 1**	+ 2	**+ 21**	**+ 13**	**+ 38**	**+ 27**	**+16**	**+12**	**+ 7**	**+ 9**	**+ 6**	**+ 6**	+ 8

Table 2. (continued)

		E											E	W				
		122.5°	127.5°	132.5°	137.5°	142.5°	147.5°	152.5°	157.5°	162°5°	167°5°	172.5°	177.5°	177.5°	172.5°	167°5°	162.5°	157.5°
S	E.C.	− 0	− 7	+ 0	− 10	+ 50	+ 29	− 5	− 9	− 16	− 2	+ 17	− 8	− 5	− 5	− 8	− 5	− 12
7.5°	N.C.	+ 1	− 5	− 0	− 0	− 12	+ 0	+ 3	+ 3	− 9	− 6	− 11	− 19	− 3	− 2	− 6	+ 2	+ 9
12.5°		+ 13	− 35	+ 47	− 18	− 36	− 74	− 7	− 4	− 31	− 25	+ 6	− 40	− 8	− 8	− 10	− 12	− 30
		+ 12	− 5	+ 3	− 3	+ 5	+ 39	+ 5	− 3	− 1	− 1	− 6	− 8	− 2	− 1	− 3	+ 0	+ 3
17.5°		− 3					− 70	− 72	− 13	− 63	− 8	− 70	− 57	− 60	−54	− 48	− 59	− 12
		− 3					+ 39	− 30	+ 3	+ 39	+ 22	+ 22	+ 23	+ 19	+20	+ 24	+ 20	+ 14
22.5°							− 55	− 72	− 67	− 7	− 69	− 58	− 53	− 76	−60	− 54	− 49	− 33
							+ 5	+ 12	+ 36	+ 25	+ 20	+ 23	+ 30	− 3	+13	+ 15	+ 11	− 15
27.5°								− 70	− 78	− 76	−107	− 49	− 43	− 73	−51	− 82	− 65	+ 18
								+ 43	+ 50	+ 21	+ 17	+ 21	+ 17	− 9	+14	+ 6	+ 25	+ 22
32.5°								+ 11	− 7	− 43	− 37	− 12	− 39	− 14	− 6	− 20	+ 35	+ 3
								+ 27	+ 40	+ 13	+ 19	+ 5	+ 26	+ 15	+12	+ 53	+ 66	+ 13
37.5°		+ 35	+ 64	+ 18	+ 69	+ 66	+ 61	+ 31	+ 16	+ 9	+ 30	+ 6	+ 18	+ 5	−25	− 31	+ 81	+ 91
		+ 15	+ 22	+ 12	+ 38	+ 32	+ 30	+ 23	+ 46	− 41	+ 16	+ 10	+ 17	+ 9	− 2	+ 38	+ 58	+ 46
42.5°		+137	+250	+159	+ 66	+ 98	+109	+ 93	+ 9	+ 48	+ 16	+ 5	+ 29	+138	+41	− 48	+ 18	+102
		− 12	− 20	− 31	− 10	+ 12	+ 25	+ 29	− 11	− 20	+ 10	+ 12	+ 47	− 25	+38	+ 54	− 78	+ 7
47.5°		+189	+236	+197	+163	+145	+102	+132	+177	+152	+122	+140	+122	+ 59	+52	+112	+192	+158
		− 68	−182	− 30	− 53	− 46	+ 2	+ 48	+ 14	+ 69	− 2	+119	+ 39	+ 15	+81	+ 41	+ 5	+ 62
52.5°																+184	+163	+112
																− 27	+ 2	+ 6
57.5°																		

Table 2. (continued)

		W														
		152.5°	147.5°	142.5°	137.5°	132.5°	127.5°	122.5°	117.5°	112.5°	107.5°	102.5°	97.5°	92.5°	87.5°	82.5°	77.5°	72.5°
S	E.C.	− 11	− 14	− 2	− 42	− 75	− 87	− 83	− 53	− 86	− 49	− 84	− 78	− 49	− 33	− 10	− 17	
7.5°	N.C.	− 5	− 4	− 0	− 24	+ 28	+ 28	+ 41	− 11	+ 29	+ 6	− 40	+ 49	+ 43	+ 9	+ 10	+ 3	
12.5°		− 50	− 14	− 6	− 46	− 76	− 84	− 87	− 84	− 84	− 69	− 88	− 86	− 79	− 37	− 12	− 10	
		− 6	− 2	+ 0	− 6	+ 9	+ 14	− 15	+ 8	+ 25	+ 4	+ 30	+ 33	+ 39	+ 9	+ 10	+ 9	
17.5°		− 32	− 12	− 1	− 69	− 54	− 57	− 52	− 59	− 53	− 64	− 67	− 79	− 82	− 81	− 49	− 13	− 3
		− 3	− 2	− 0	+ 11	+ 1	+ 1	− 4	− 16	+ 15	+ 13	+ 0	+ 23	+ 18	+ 34	+ 43	+ 9	+ 3
22.5°		+ 2	− 35	− 2	− 24	− 54	− 56	− 33	− 33	− 87	− 30	− 7	− 61	− 53	− 31	− 64	− 50	− 3
		− 5	− 16	+ 1	− 0	+ 19	+ 7	− 18	+ 4	+ 24	− 13	− 15	− 3	+ 16	+ 29	+ 44	+ 41	+ 7
27.5°		− 29	− 25	− 7	− 22	− 75	− 25	− 15	+ 4	+ 9	+ 5	− 36	− 8	− 4	− 35	− 38	− 27	− 1
		+ 41	− 17	+ 1	+ 18	+ 43	+ 11	+ 11	− 8	− 16	− 84	− 13	− 4	+ 0	+ 10	+ 25	+ 29	+ 11
32.5°		− 80	− 28	− 6	+ 5	− 39	− 23	+ 15	+ 18	+ 25	+ 24	+ 24	− 2	+ 26	+ 6	+ 34	− 15	+ 1
		+ 14	+ 59	+ 9	− 37	+ 12	− 0	− 3	+ 34	− 41	+ 35	+ 61	+ 24	+ 4	+ 1	+ 59	+ 39	+ 50
37.5°		− 56	− 66	+ 3	+ 35	− 68	+ 9	+ 41	+125	+ 74	+ 82	+ 56	+ 72	+ 38	+ 39	+ 42	+ 7	+ 13
		+ 25	+ 28	+ 6	+ 13	+ 5	− 42	− 0	+102	+ 51	+ 46	− 16	+ 28	− 13	+ 21	+ 14	+ 34	+ 28
42.5°		− 70	− 15	− 9	+155	− 35	+ 17	+ 8	+123	+ 94	+121	+111	+ 53	+ 84	+ 61	+110	+ 85	+ 26
		+ 52	+ 52	+ 8	−118	− 39	− 8	+ 38	+ 52	+ 42	+ 91	+ 93	+ 29	− 1	+ 30	+ 19	− 5	− 60
47.5°		+ 89	+148	+ 13	+186	+ 34	+115	+ 33	+156	+136	+170	+178	+131	+ 76	+186	+216	+173	
		+ 78	− 67	− 7	− 75	− 50	+ 13	+ 46	− 16	+ 10	+ 72	+ 87	+155	+124	+ 14	+ 38	− 78	
52.5°		+243	+165	+362	+295	+151	+151	+153	+128	+110	+152	+109	+243	+239	+202	+225	+321	+156
		+151	+ 18	+167	+ 78	− 22	+124	+ 40	+ 27	+ 19	+ 32	− 47	− 4	− 7	+ 39	+ 33	− 41	+ 9
57.5°											+110	+133	+113	+171	+191	+227	+226	+224
											− 40	− 69	− 34	−192	− 84	− 53	− 1	+ 16

Table 3. Computed Wind Stresses over the Pacific Ocean—Jun. Jul. and Aug.

(τ_x and τ_y are given by the upper and lower figures, respectively, of each compartment, the unit being 10^{-2} dynes/cm^2).

	E 122.5°	127.5°	132.5°	137.5°	142.5°	147.5°	152.5°	157.5°	162.5°	167.5°	172.5°	177.5°	W 177.5°	172.5°	167.5°	162.5°
N 57.5°															+ 5	+25
52.5°													+46 +38	+51 +35	+45 +38	+42 +34
47.5°							+ 7 − 2	+ 7 + 6	0 +11	+ 1 +26	+ 2 +15	+17 +18	+20 +30	+31 +36	+37 +27	+36 +31
42.5°					− 7 + 5	− 5 + 4	− 3 + 7	− 6 + 3	− 6 +11	+15 + 9	+ 1 +24	+13 +31	+ 6 +20	+15 +13	+17 + 8	+12 +15
37.5°					−10 + 7	−16 + 3	− 4 + 6	− 1 +13	+ 4 +18	− 3 +10	0 +14	− 1 +28	+ 2 +17	+ 6 +18	+ 1 +11	+ 5 + 8
32.5°	−12 +13	− 5 + 5	−10 + 4	−12 − 2	+16 +22	+ 3 +22	− 9 +21	+ 8 +23	− 1 +18	− 5 +13	0 + 5	−15 +14	−11 + 2	−11 − 4	−27 − 5	−11 − 4
27.5°	+ 5 +21	−18 + 8	− 5 +18	− 4 + 3	− 5 +12	−24 +11	− 5 + 8	−13 +10	− 8 + 8	−15 − 7	−13 − 1	−33 − 2	−12 + 1	−18 −15	−51 −19	−41 −18
22.5°	+ 9 +11	− 4 +30	−15 +18	− 6 +18	−16 +10	−19 + 6	−20 + 8	−15 +11	−28 + 2	−21 + 7	−20 + 1	−42 −19	−28 −12	−30 −10	−46 −20	−67 −27
17.5°	+13 +14	+ 5 +14	− 1 +28	− 4 +17	−10 + 9	−13 + 4	−16 + 6	−28 + 3	−17 0	−50 − 8	−31 − 8	−58 − 5	−43 − 4	−57 −14	−47 −23	−73 −30
12.5°		+20 +11	+12 +20	+ 4 + 9	− 3 + 7	− 4 + 8	−21 − 5	−27 − 8	−33 −11			−75 −30	−75 −17	−79 −15	−68 −36	−79 −29
7.5°		+ 8 +15	+22 +15	+18 +15	+13 + 9	− 4 + 2	+ 2 + 5	−16 + 4	−15 − 4	−23 + 5	−18 − 3		−35 −18	−38 − 6	−35 −15	−48 −23
2.5°		+ 2 +22	+10 +13	+ 2 + 4	+ 4 +10	−13 +10	−20 +14	− 4 + 5	−23 + 7	−30 + 2	−15 + 2	−25 + 1	−34 + 5	−15 + 1	−40 + 6	−46 +11
S 2.5°					− 5 + 3	− 9 + 6	−51 +17	−13 +29	−15 + 7	−19 + 2	−45 − 4	−32 − 7	−37 + 6	−28 − 2	−29 − 2	−41 +13

Table 3. (continued)

	157.5°	152.5°	147.5°	142.5°	137.5°	132.5°	127.5°	122.5°	117.5°	112.5°	107.5°	102.5°	97.5°	92.5°	87.5°	82.5°
57.5°	−20 **+11**	−19 **+ 2**	+ 2 **+ 1**	**+ 4**	**+ 3**											
52.5°	+48 **+42**	+41 **+27**	+46 **+38**	+39 **+30**	+48 **+16**	+33 **− 7**	0 **− 1**									
47.5°	+29 **+36**	+48 **+28**	+41 **+36**	+28 **+16**	+29 **+ 7**	+35 **−19**	+ 33 **− 31**									
42.5°	+12 **+13**	+ 6 **+ 9**	+30 **+15**	+ 6 **− 1**	+14 **− 9**	+15 **−44**	+ 35 **− 88**									
37.5°	+ 7 **+ 8**	− 1 **+13**	+ 9 **− 8**	+ 1 **− 9**	− 1 **−17**	+ 1 **−74**	+ 50 **−116**	+64 **− 2**								
32.5°	−29 **−11**	−24 **− 9**	−12 **− 4**	−11 **− 8**	− 8 **−13**	− 8 **−31**	+ 20 **−103**	+56 **+32**	+10 **− 9**							
27.5°	−76 **−28**	−38 **−19**	−25 **− 9**	−21 **−10**	−43 **−42**	−39 **−55**	− 15 **− 36**	− 4 **−24**	+11 **−15**							
22.5°	−82 **−28**	−74 **−25**	−72 **−33**	−77 **−42**	−55 **−47**	−56 **−59**	− 32 **− 45**	−11 **−20**	+ 1 **−18**	+ 8 **− 8**	+ 6 **− 3**					
17.5°	−78 **−30**	−80 **−37**	−79 **−48**	−75 **−45**	−70 **−50**	−54 **−56**	− 44 **− 45**	−34 **−32**	−10 **−12**	0 **− 4**	0 **− 2**	+ 2 **− 2**				
12.5°	−80 **−33**	−69 **−41**	−61 **−37**	−70 **−46**	−48 **−43**	−42 **−36**	− 22 **− 21**	−10 **− 8**	+ 5 **+ 3**	+ 7 **+ 4**	0 **+ 2**	− 1 **+ 3**	− 6 **− 8**	− 6 **− 2**	− 9 **− 5**	
7.5°	−39 **−12**	−33 **− 5**	−25 **+ 4**	−23 **− 3**	−17 **+14**	−17 **+23**	− 5 **+ 19**	+ 1 **+35**	− 4 **+56**	+14 **+69**	+ 9 **+40**	+18 **+46**	+10 **+22**	+19 **+23**	+ 2 **− 1**	+ 4 **+ 2**
2.5°	−30 **+15**	−63 **+17**	−60 **+37**	−49 **+23**	−36 **+21**	−52 **+38**	− 52 **+ 57**	−53 **+70**	−59 **+75**	−45 **+70**	−22 **+39**	−20 **+48**	− 3 **+26**	+14 **+34**	+13 **+65**	+16 **+21**
S 2.5°	−61 **+ 7**	−67 **+17**	−74 **+ 4**	− 5 **+ 8**	−64 **+32**	−85 **+39**	− 86 **+ 40**	−74 **+42**	−68 **+36**	−61 **+38**	−33 **+29**	−43 **+32**	−23 **+24**	− 8 **+12**	− 3 **+17**	+ 3 **+17**

Table 3. (continued)

	E 122.5°	127.5°	132.5°	137.5°	142.5°	147.5°	152.5°	157.5°	162.5°	167.5°	172.5°	E 177.5°	W 177.5°	172.5°	167.5°	162.5°	157.5°
S 7.5°	− 32 + **27**	− 96 + **54**	− 71 + **50**	− 77 + **48**			− 43 + **51**	− 28 + **5**	−116 + **35**	− 66 + **39**	− 64 + **41**	− 25 + **24**	− 53 + **34**	− 67 + **25**	− 30 + **19**	− 77 − **5**	− 76 − **7**
12.5°	− 83 + **76**	− 31 + **22**	− 38 + **29**	− 43 + **43**	− 22 + **21**	− 56 + **53**	− 42 + **30**	−120 +**126**	−120 +**161**	− 62 + **37**	− 68 + **40**	− 65 + **35**	−120 + **99**	− 68 + **31**	−114 + **88**	− 42 + **5**	−126 + **11**
17.5°						− 20 + **8**	−142 + **14**	−118 +**115**	− 38 + **40**	− 57 + **52**	−113 +**137**	− 60 + **33**	− 56 + **44**	− 66 + **35**	− 61 + **33**	−143 + **58**	−113 + **45**
22.5°							− 27 + **32**	+ 11 + **69**	− 10 + **15**	− 36 + **14**	− 30 + **36**	− 12 + **31**	− 39 + **23**	− 42 + **36**	− 33 + **26**	− 65 + **16**	+ 6 − **27**
27.5°							+ 2 + **55**	+ 9 + **26**	+ 5 + **30**	+ 0 + **4**	− 24 + **11**	+ 19 + **34**	+ 57 + **3**	+ 12 + **22**	+ 58 + **62**	+ 26 + **23**	+ 11 − **2**
32.5°							+ 53 +**111**	+ 1 +**102**	+ 21 + **35**	+ 9 + **20**	+ 45 + **24**	+ 11 + **1**	+ 94 − **11**	+ 33 − **35**	+ 60 + **14**	+ 83 + **2**	+115 + **11**
37.5°	+111 − **95**	+ 18 − **46**	+ 43 − **1**	+ 37 + **27**	+ 20 + **18**	+ 83 + **43**	+ 91 + **63**	+ 16 − **4**	+ 63 + **31**	− 27 − **47**	− 6 − **14**	− 17 + **4**	+ 39 + **24**	− 12 + **17**	+ 59 + **26**	+141 − **23**	+ 73 + **46**
42.5°	+ 91 − **4**	+ 97 −**173**	+ 87 −**105**	+ 94 −**143**	− 20 − **81**	+120 − **51**	+ 58 + **43**	+ 73 + **47**	+ 64 + **55**	+ 62 + **83**	+ 67 + **80**	+ 28 + **65**	+ 50 +**158**	+ 6 +**132**	− 0 + **27**	+ 2 − **41**	+ 24 − **1**
47.5°	+126 − **98**	+116 −**121**	+ 9 − **0**	+ 59 − **32**	+103 − **65**	+195 − **81**	+ 62 − **81**	+ 16 + **33**	+ 36 +**108**	+111 + **71**	+128 + **5**	+132 + **88**	+ 33 + **93**	+163 + **12**	+ 7 − **61**	+ 74 + **19**	+ 25 − **0**
52.5°																	
S 57.5°																	

Table 3. (continued)

	152.5°	147.5°	142.5°	137.5°	132.5°	127.5°	122.5°	117.5°	112.5°	107.5°	102.5°	97.5°	92.5°	87.5°	82.5°	77.5°	72.5°
S 7.5°	−131 − **16**	− 79 − **20**	− 3 + **1**	− 85 + **25**	− 85 + **38**	−141 + **92**	−145 +**103**	−136 − **33**	−147 +**107**	−148 +**115**	− 76 + **46**	−154 +**122**	−55 +**52**	−57 +**57**	− 42 + **43**		
12.5°	− 69 + **14**	− 79 + **2**	− 9 + **3**	− 75 + **27**	− 71 + **27**	− 82 + **28**	−122 + **71**	− 66 + **41**	−152 + **34**	−193 + **74**	−151 + **27**	− 51 + **45**	−77 +**43**	−52 +**48**	− 57 + **58**	− 42 + **45**	
17.5°	− 89 + **18**	− 78 + **19**	− 7 − **1**	− 68 + **11**	− 61 − **0**	− 59 + **13**	− 68 + **2**	− 80 + **11**	− 78 + **9**	− 67 + **20**	−129 + **19**	− 88 + **59**	−52 +**20**	−56 +**31**	−134 +**118**	− 73 + **61**	− 23 + **52**
22.5°	− 56 + **18**	− 22 − **35**	− 3 + **2**	− 35 + **2**	− 33 + **10**	− 31 + **41**	− 75 + **24**	− 39 + **18**	− 50 + **2**	− 53 − **20**	− 51 + **23**	− 60 + **39**	−38 +**16**	− 5 − **1**	− 16 + **23**	− 13 + **62**	− 1 + **8**
27.5°	+ 26 + **5**	+ 27 + **17**	− 3 + **3**	− 70 + **12**	− 25 + **4**	+ 26 + **6**	− 24 + **41**	+ 11 − **10**	− 9 − **1**	+ 22 − **30**	+ 17 + **46**	+ 42 − **5**	+ 6 − **9**	− 2 +**11**	+ 4 + **17**	+ 25 + **34**	+ 2 + **40**
32.5°	+144 − **1**	+107 + **6**	+ 1 + **2**	− 28 − **37**	+ 37 − **63**	+ 68 + **20**	+ 53 − **10**	+ 53 − **32**	+ 18 − **7**	+ 32 + **6**	+ 24 − **7**	+ 37 − **30**	+42 −**35**	+12 −**10**	+ 65 + **44**	+ 29 + **0**	+ 1 − **15**
37.5°	+ 77 + **70**	+134 + **64**	+13 + **6**	+113 + **42**	+ 53 − **43**	− 4 − **78**	+ 58 + **12**	+111 + **25**	+ 74 + **11**	+ 17 − **14**	+ 75 − **2**	+ 45 − **25**	+74 +**59**	+54 −**22**	+ 82 − **3**	+ 62 + **21**	+ 23 − **5**
42.5°	− 51 + **9**	+103 + **52**	+22 +**13**	+ 96 +**100**	− 6 − **42**	− 11 + **0**	− 65 − **40**	+ 56 − **33**	+148 + **33**	+ 63 + **22**	− 16 + **11**	+ 8 + **26**	+64 +**19**	+12 +**24**	+130 + **75**	+135 + **21**	
47.5°	− 77 + **20**	+ 63 − 8	+18 + **3**	− 99 − **36**	− 35 + **37**	− 63 − **57**	− 26 + **52**	+ 40 + **10**	+ 46 + **24**	+ 72 + **40**	+ 58 + 66	− 11 − **21**	− 2 +**66**	+21 +**38**	+164 + **32**	+107 − **5**	
52.5°				−133 + **13**	−143 − **43**	+ 3 + **48**	− 22 − **12**	− 27 − **94**	+ 74 − **65**	− 2 + **3**	− 64 + **40**	− 7 + **49**	+20 +**35**	+23 +**37**	+ 45 + **2**	+139 − **20**	+ 88 − **7**
S 57.5°											− 29 − **34**	− 38 + **52**	+52 −**20**	+11 + **9**	+ 98 − **32**	+ 70 + **20**	+142 − **65**

Table 4. Computed Wind Stresses over the Pacific Ocean—Sep., Oct. and Nov.

(τ_x and τ_y are given by the upper and lower figures, respectively, of each compartment, the unit being 10^{-2} dynes/cm^2).

	E 122.5°	127.5°	132.5°	137.5°	142.5°	147.5°	152.5°	157.5°	162.5°	167.5°	172.5°	177.5°	W 177.5°	172.5°	167.5°	162.5°
57.5°																
52.5°													+119 − 35	+112 + 5	+144 − 17	+108 − 19
47.5°							+58 −68	+111 − 49	+110 − 39	+109 − 5	+142 − 5	+111 − 43	+ 91 − 43	+125 − 17	+116 + 2	+138 + 20
42.5°					+43 −11	+16 −12	+28 −14	+ 50 + 2	+ 52 − 13	+ 49 − 17	+ 52 − 22	+ 81 − 6	+100 − 23	+ 79 − 22	+ 93 + 1	+ 72 + 23
37.5°					−17 −32	0 −28	+ 9 −27	+ 17 − 16	+ 43 + 16	+ 45 + 4	+ 32 + 4	+ 65 − 45	+ 75 − 31	+ 82 − 8	+ 65 − 31	+ 66 + 1
32.5°	− 14 − 69	−11 −79	−29 −41	−28 −51	−11 −21	−12 − 8	+17 + 9	+ 1 + 7	− 11 + 19	− 5 − 4	− 20 − 22	− 7 − 32	+ 10 − 8	+ 46 − 20	+ 32 − 8	+ 26 − 2
27.5°	− 59 −107	−33 −78	−21 −40	−22 −37	−15 −15	−33 − 9	−26 − 4	− 13 − 2	− 27 − 9	− 26 − 5	− 18 − 9	− 24 − 18	− 9 − 14	− 21 − 18	− 20 − 15	− 28 − 26
22.5°	− 95 − 30	−41 −32	−44 −18	−31 −11	−23 + 7	−40 +10	−45 − 5	− 43 − 12	− 30 − 12	− 45 − 10	− 60 − 30	− 44 − 21	− 32 − 15	− 27 − 17	− 36 − 19	− 36 − 17
17.5°	− 65 − 61	−38 −23	−48 −11	−33 + 5	−44 + 5	−42 − 7	−32 − 3	− 51 − 10	− 52 − 13	− 40 − 16	− 42 − 4	− 44 − 21	− 68 − 27	− 54 − 16	− 58 − 32	− 70 − 21
12.5°		− 6 − 5	− 9 + 2	0 +12	−21 0	−29 − 9	−29 − 5	− 31 − 19	− 23 − 9	− 43 − 20	− 49 − 1	− 64 − 3	− 59 − 17	− 23 − 3	− 44 − 28	− 74 − 30
7.5°		+11 +10	+22 + 3	+22 + 5	− 5 +17	− 9 + 8	−13 − 5	− 19 − 15	− 10 + 5	− 11 + 7	− 30 0	− 5 − 2	− 28 − 7	− 22 − 2	− 31 + 2	− 41 0
2.5°		+14 +11	+19 + 9	+29 + 3	+ 4 0	−10 − 3	+ 1 + 3	− 8 + 2	− 15 + 2	− 16 + 8	− 13 + 8	− 15 − 4	− 17 0	− 22 + 12	− 24 + 9	− 19 + 12
S 2.5°					− 2 − 3	+12 − 4	− 2 + 5	− 4 + 6	− 11 − 10	− 12 0	− 24 − 3	− 13 + 1	− 24 − 2	− 21 − 12	− 18 − 4	− 47 − 9

Table 4. (continued)

	157.5°	152.5°	147.5°	142.5°	137.5°	132.5°	127.5°	122.5°	117.5°	112.5°	107.5°	102.5°	97.5°	92.5°	87.5°	82.5°
57.5°	+ 66 − **34**	+ 21 − **26**	+ 24 + **38**	− 45 + **49**	− 32 + **38**											
52.5°	+117 + **27**	+142 + **64**	+117 + **84**	+107 + **86**	+108 + **74**	+ 64 + **79**	−19 +**24**									
47.5°	+ 99 + **30**	+119 + **46**	+ 91 + **73**	+125 + **68**	+ 69 + **59**	+ 45 + **48**	+24 +**35**									
42.5°	+105 + **30**	+ 70 + **32**	+ 82 + **47**	+ 61 + **43**	+ 53 + **41**	+ 41 − **7**	+29 + **6**									
37.5°	+ 61 + **28**	+ 47 + **24**	+ 39 + **28**	+ 41 + **24**	+ 24 + **4**	+ 25 − **33**	+29 −**65**	+40 −**50**								
32.5°	+ 2 − **7**	+ 3 − **5**	+ 17 + **17**	+ 5 + **15**	+ 1 − **2**	− 4 − **15**	+20 −**81**	+49 −**77**	+ 9 −**10**							
27.5°	− 28 − **27**	− 22 − **7**	− 21 − **5**	− 10 − **1**	− 16 − **8**	− 28 − **31**	−10 −**22**	−11 −**37**	+10 −**12**							
22.5°	− 53 − **26**	− 37 − **9**	− 62 − **22**	− 76 − **29**	− 65 − **44**	− 60 − **48**	−44 −**51**	−39 −**42**	−21 −**26**	+ 6 −**10**	+ 3 − **4**					
17.5°	− 84 − **31**	− 93 − **41**	− 99 − **65**	−100 − **50**	− 83 − **56**	− 65 − **47**	−55 −**53**	−52 −**40**	−32 −**34**	− 3 − **1**	+ 1 − **1**	0 − **1**	 − **1**			
12.5°	− 71 − **26**	− 71 − **38**	− 56 − **35**	− 64 − **36**	− 55 − **28**	− 43 − **25**	−37 −**25**	−19 −**10**	− 9 **0**	− 5 + **2**	+21 +**11**	+ 9 + **8**	−12 −**34**	+ 2 − **3**	0 − **2**	
7.5°	− 34 + **6**	− 25 + **6**	− 24 + **11**	− 36 + **21**	− 32 + **19**	− 30 + **35**	−22 +**36**	+ 3 +**31**	+16 +**46**	+11 +**63**	+12 +**52**	− 5 +**37**	+28 +**24**	+30 +**42**	+ 7 **0**	+11 + **4**
2.5°	− 36 + **19**	− 45 + **16**	− 55 + **37**	− 41 + **29**	− 57 + **43**	− 77 + 64	−69 +**86**	−55 +**71**	−44 +**77**	−17 +**55**	− 9 +**53**	−10 +**47**	− 1 +**44**	+15 +**58**	+30 +**65**	+18 +**34**
S 2.5°	− 53 − **1**	− 59 − **5**	− 85 + **2**	− 66 + **9**	− 71 + **25**	−109 + **20**	−88 +**37**	−80 +**41**	−53 +**31**	−52 +**27**	−48 +**29**	−16 +**14**	−11 + **9**	− 7 + **9**	−12 +**28**	+ 5 +**17**

Table 4. (continued)

	E 122.5°	127.5°	132.5°	137.5°	142.5°	147.5°	152.5°	157.5°	162.5°	167.5°	172.5°	E 177.5°	W 177.5°	172.5°	167.5°	162.5°	157.5°
S	− 2	− 5	− 6	− 30	− 18	− 45	− 33	− 5	− 34	− 7	− 8	+ 8	− 11	− 19	− 12	− 17	− 18
7.5°	+ 1	+ 7	+ 5	− 11	+ 7	+ 21	+ 34	+ 6	+ 0	+ 9	− 2	+ 3	+ 1	+ 5	− 4	+ 1	+ 2
12.5°	− 19	+ 18	−120	− 34	− 76	− 45	− 79	− 53	− 72	− 9	−60	− 43	− 71	− 13	− 40	− 55	− 36
	+ 6	+ 5	− 5	− 16	+ 21	− 1	+ 29	+ 28	+ 87	− 17	+26	+ 1	+ 25	+ 1	− 1	+ 18	+ 4
17.5°	+ 8				− 76	− 61	− 77	− 50	−138	−100	−74	− 62	− 75	− 68	− 63	− 43	− 44
	+ 6				+ 29	+ 19	+ 36	+ 57	+ 18	+ 51	+28	+ 24	+ 32	+ 28	+ 30	− 7	+ 16
22.5°						− 5	− 50	− 45	− 61	− 63	−52	− 57	− 52	− 60	− 57	− 40	− 98
						− 2	+ 16	+ 8	+ 18	+ 22	+21	+ 27	+ 40	+ 17	+ 19	+ 14	+ 17
27.5°							− 21	− 18	− 36	− 32	− 4	− 24	− 18	− 16	− 23	+ 6	+ 3
							+ 20	+ 22	+ 8	+ 8	+ 2	+ 22	+ 22	+ 19	+ 14	− 1	+ 0
32.5°		+ 83	− 79	− 43			+ 13	− 5	+ 6	+ 15	+ 7	+ 77	+ 29	+ 15	+ 10	+ 68	+ 16
		− 5	+ 39	+ 16			+ 10	− 3	+ 49	+ 0	+31	− 1	− 1	− 30	+ 9	+ 62	+ 19
37.5°	+ 40	+ 85	+ 50	+ 77	+ 87	+144	+ 61	+ 65	+ 40	+ 27	+41	+ 17	+ 55	+ 58	+ 23	+ 95	+ 43
	− 4	+ 33	+ 32	+ 57	− 51	+ 59	+ 76	+ 7	− 5	− 67	−11	− 10	− 12	+ 31	+ 27	+ 3	− 5
42.5°	+162	+133	+197	+148	+116	+241	+113	+ 21	+ 21	+109	+28	+ 27	+ 6	+106	+158	+ 5	+ 83
	− 3	− 55	− 48	+ 10	+ 64	+ 61	− 13	+ 80	− 79	− 23	− 6	+ 36	+ 17	+ 96	+128	+ 38	+ 32
47.5°	+296	+130	+283	+174	+ 60	+208	+110	+155	+155	+193	+73	+ 69	+105	+162	+ 71	+ 91	+135
	−138	− 34	+ 18	− 53	− 63	− 57	+ 35	+ 17	− 38	− 5	+65	+ 27	− 30	+ 4	+ 28	+115	+ 84
52.5°										+ 45	+72	+164	+197	+163	+100	+104	+157
										− 34	−84	−235	−195	−126	+ 20	− 8	+ 49
57.5°																	

Table 4. (continued)

	152.5°	147.5°	142.5°	137.5°	132.5°	W 127.5°	122.5°	117.5°	112.5°	107.5°	102.5°	97.5	92.5°	87.5°	82.5°	77.5°	72.5°
S	− 71	− 78	− 2	− 90	− 89	−116	− 95	− 94	− 91	− 85	− 87	− 67	− 12	− 18	− 9	+ 1	
7.5°	− 21	− 29	− 0	− 5	− 2	+ 22	+ 23	+ 18	+ 18	+ 31	+ 38	+ 57	+ 16	+ 23	+ 13	+ 8	
12.5°	− 52	− 55	− 3	−109	− 75	− 81	− 96	− 86	− 94	− 96	− 85	− 95	− 86	− 69	− 58	− 10	
	÷ 65	− 4	+ 3	+ 41	+ 3	+ 7	+ 3	+ 10	+ 7	+ 7	+ 5	+ 33	+ 36	+ 44	+ 58	+ 10	
17.5°	− 43	− 50	− 7	− 76	− 67	− 57	− 77	− 66	− 63	−106	− 77	− 71	− 89	− 83	−124	− 12	− 7
	+ 3	− 1	− 0	− 4	− 13	− 2	− 10	+ 17	+ 11	+ 5	+ 16	− 5	+ 33	+ 36	+120	+ 11	+ 5
22.5°	− 46	− 37	− 13	− 68	− 71	− 53	−106	− 17	− 48	− 46	− 75	− 61	− 57	− 84	− 45	− 54	− 3
	+ 1	− 4	+ 8	+ 11	+ 9	+ 10	+ 0	− 6	+ 2	+ 7	− 5	− 5	+ 37	+ 14	+ 43	+ 50	+ 12
27.5°	+ 28	− 35	− 3	− 27	− 96	− 40	− 2	− 21	− 51	− 25	− 37	− 7	− 28	− 52	− 45	− 27	− 1
	− 15	+ 6	− 1	+ 2	+ 12	− 7	+ 25	+ 42	+ 2	− 29	− 1	− 5	+ 11	+ 32	+ 41	+ 69	+ 12
32.5°	+ 9	+ 13	+ 5	− 68	− 76	− 18	+ 10	− 15	+ 8	− 1	+ 4	+ 17	+ 13	− 3	− 4	− 9	− 4
	+ 23	+ 13	+ 3	+ 32	+ 9	− 18	+ 4	+ 1	− 14	− 2	+ 18	− 15	− 3	+ 31	+ 28	+ 33	+ 62
37.5°	+ 8	+ 83	+ 2	+ 1	− 11	− 47	+ 40	+ 99	+ 77	+ 8	+ 72	+ 35	+ 40	+ 33	+ 20	+ 24	+ 14
	+ 5	+ 10	− 1	+ 28	− 14	− 31	+ 13	+ 49	+ 8	− 35	+ 12	− 37	− 21	+ 2	+ 28	+ 35	+ 52
42.5°	+ 45	+100	+ 17	+ 85	+164	+ 27	+ 70	+ 87	+157	+ 88	+ 99	+ 64	+ 77	+139	+ 87	+ 68	+ 56
	+ 18	−103	− 2	+ 56	+ 29	+ 28	+ 8	+ 40	+ 22	+ 25	+ 12	− 24	− 9	− 26	+ 42	+ 44	+ 7
47.5°	+190	+194	+ 25	+171	+121	+ 62	+120	+188	+265	+154	+199	+143	+ 88	+136	+153	+145	
	+ 21	− 5	− 10	− 59	+ 46	+ 17	− 49	− 20	+ 2	+ 32	+ 76	+ 33	+ 28	+ 2	− 12	− 14	
52.5°	+ 98	+170	+131	+128	+150	+202	+268	+168	+211	+123	+120	+196	+170	+168	+262	+255	+194
	+ 53	+230	− 17	− 58	− 27	+ 11	− 57	− 11	− 25	+ 20	+ 25	− 7	+ 44	+ 73	− 14	− 50	+ 2
57.5°												+162	+122	+208	+244	+270	+362
												− 82	− 52	−116	− 17	− 17	+ 11

Table 5. Computed Wind Stresses over the Pacific Ocean—Annual Mean.

(τ_x and τ_y are given by the upper and lower figures, respectively, of each compartment, the unit being 10^{-2} dynes/cm^2).

	E 122.5°	127.5°	132.5°	137.5°	142.5°	147.5°	152.5°	157.5°	162.5°	167.5°	172.5°	E 177.5°	W 177.5°	172.5°	167.5°	162.5°
N 57.5°																
52.5°													+81 +21	+62 +16	+77 + 5	+64 +17
47.5°							+68 −49	+98 −47	+89 −23	+83 − 1	+81 +12	+60 +15	+56 + 9	+59 +20	+68 +27	+75 +28
42.5°					+54 −20	+49 −36	+58 −40	+73 −27	+75 −24	+76 −16	+67 + 1	+72 +11	+61 +15	+62 + 6	+67 +21	+69 +26
37.5°					+16 −46	+38 −35	+61 −39	+67 −35	+77 −10	+75 + 1	+81 +11	+77 + 3	+66 + 9	+66 +14	+55 0	+53 +11
32.5°	− 3 −39	+15 −55	0 −35	+23 −50	+39 −14	+35 −10	+42 + 3	+50 + 6	+55 +18	+43 +14	+40 + 1	+28 − 5	+19 + 5	+32 − 3	+21 − 1	+23 + 1
27.5°	−37 −77	−14 −67	− 2 −24	− 4 −16	+ 3 −11	+ 1 −14	+15 −15	+20 − 1	+10 − 4	+ 4 −11	− 6 − 5	−14 −11	− 6 − 9	− 9 −14	−19 −16	−13 −17
22.5°	−62 −84	−34 −33	−32 −18	−28 −18	−23 − 9	−29 − 8	−32 −12	−29 −10	−27 −14	−27 − 8	−35 −12	−38 −18	−30 −13	−31 −18	−33 −19	−42 −23
17.5°	−45 −44	−43 −30	−43 −23	−35 −15	−35 −12	−38 −18	−32 − 7	−37 − 7	−40 −11	−47 −14	−43 −16	−55 −16	−65 −18	−58 −20	−61 −30	−77 −28
12.5°		−14 −13	−26 −12	−28 −11	−26 − 9	−44 −13	−63 −28	−78 −43	−84 −41	−62 −18	−76 −27	−79 −32	−96 −36	−95 −40	−83 −40	−86 −40
7.5°		− 5 − 6	−10 − 8	− 7 −10	−27 − 6	−28 − 9	−38 −18	−43 −26	−55 −30	−51 −17	−55 −24	−44 −27	−59 −29	−61 −24	−63 −30	−73 −35
N 2.5°		+ 4 + 5	+ 9 + 2	+ 8 − 1	− 4 − 2	−11 + 1	−16 − 4	−19 −13	−21 − 9	−24 − 7	−28 − 5	−45 −25	−28 − 2	−28 − 4	−41 − 3	−37 + 4
S 2.5°					+ 9 −12	+14 − 6	+ 1 + 8	− 8 + 5	− 9 − 8	− 8 − 5	−19 −13	−21 −12	−27 − 4	−22 − 9	−26 − 7	−34 − 5

Table 5. (continued)

	157.5°	152.5°	147.5°	142.5°	137.5°	132.5°	127.5°	122.5°	117.5°	112.5°	107.5°	102.5°	97.5°	92.5°	87.5°	W 82.5°
N		+17	−17	− 48	−16											
57.5°		−11	+ 8	+ 25	+14											
52.5°	+ 76	+87	+85	+ 77	+83	+50										
	+ 33	+42	+51	+ 56	+52	+35	+15									
47.5°	+ 73	+80	+78	+ 80	+71	+45	+21									
	+ 23	+24	+40	+ 40	+40	+24	+35									
42.5°	+ 76	+65	+74	+ 53	+56	+46	+39									
	+ 31	+23	+40	+ 25	+18	− 9	− 4									
37.5°	+ 39	+38	+34	+ 34	+30	+32	+40	+48								
	+ 27	+33	+28	+ 20	− 4	−32	−67	−40								
32.5°	+ 8	+ 7	+ 2	0	+ 5	+ 5	+26	+51	+10							
	− 7	+19	+ 5	+ 8	− 3	−22	−73	−38	− 9							
27.5°	− 44	−28	−22	− 15	−26	−30	−13	− 7	+19							
	− 21	− 7	− 5	+ 1	−18	−38	−31	−42	−25							
22.5°	− 56	−48	−67	− 72	−67	−58	−47	−34	−14	+ 6	+ 5					
	− 25	−17	−22	− 29	−39	−48	−48	−40	−36	−10	− 6					
17.5°	− 74	−88	−89	−100	−98	−69	−60	−69	−32	− 3	+ 3	+ 2				
	− 27	−40	−49	− 58	−59	−52	−51	−43	−36	− 9	− 6	− 2				
12.5°	−121	−97	−95	−107	−81	−82	−91	−71	−52	−28	− 2	0	−14	− 2	−13	
	− 62	−55	−47	− 63	−54	−59	−64	−40	−36	−20	− 2	0	−27	− 5	−10	
7.5°	− 71	−84	−53	− 69	−56	−59	−42	−31	−19	− 9	−13	−13	0	+ 8	− 2	+ 4
	− 34	−38	−17	− 18	−18	− 6	− 4	+14	+19	+27	+16	+17	+ 9	+13	− 7	− 1
N	− 36	−59	−56	− 46	−41	−67	−47	−43	−37	−23	−12	−11	+ 2	+ 6	+ 9	+ 9
2.5°	+ 9	+18	+27	+ 16	+19	+43	+45	+52	+48	+38	+27	+31	+28	+27	+35	+14
S	− 55	−55	−58	− 56	−64	−90	−72	−74	−52	−41	−29	−21	−19	− 6	− 6	+ 3
2.5°	+ 1	− 2	− 4	+ 1	+18	+30	+33	+43	+28	+22	+11	+18	+21	+10	+15	+13

Table 5. (continued)

	E 122.5°	127.5°	132.5°	137.5°	142.5°	147.5°	152.5°	157.5°	162.5°	167.5°	172.5°	E 177.5°	W 177.5°	172.5°	167.5°	162.5°	157.5°
S	− 3	− 25	− 70	+ 9			− 4	− 10	− 38	− 18	− 11	− 4	−18	− 20	−16	− 29	− 29
7.5°	+ 8	+ 14	+ 11	+ 8			+ 6	+ 3	+ 6	+ 6	+ 3	+ 0	+ 7	+ 3	−11	− 8	− 1
12.5°	− 39	− 11	− 24	+ 56	− 19	− 44	− 48	− 40	− 52	− 25	− 31	− 38	−51	− 24	−42	− 27	− 51
	+ 63	+ 6	− 11	+ 5	− 25	+ 23	+ 10	+ 47	+ 58	+ 2	+ 15	+ 5	+30	+ 7	+17	+ 5	+ 3
17.5°						−134	−176	−203	− 74	− 46	− 76	− 69	−58	− 54	−52	− 69	− 50
						+ 22	+ 26	+ 98	+ 26	+ 29	+ 52	+ 24	+25	+ 25	+19	+ 19	+ 19
22.5°							− 60	− 54	− 31	− 59	− 50	− 48	−52	− 54	−47	− 47	− 52
							+ 21	+ 33	+ 9	+ 17	+ 25	+ 26	+19	+ 18	+18	+ 10	− 10
27.5°							− 38	− 33	− 41	− 57	− 33	− 25	−24	− 28	−22	− 21	+ 2
							+ 42	+ 25	+ 17	+ 17	+ 13	+ 21	+ 6	+ 17	+22	+ 16	+ 1
32.5°							− 58	− 82	− 11	− 11	+ 2	+ 3	+20	+ 8	+11	+ 43	+ 56
							− 0	+ 72	+ 21	+ 5	+ 18	+ 8	− 2	− 7	+23	+ 38	+ 13
37.5°	+ 66	+ 54	+ 34	+ 57	+124	+147	+ 51	+ 13	+ 27	+ 7	+ 16	+ 8	+35	+ 7	+16	+ 89	+ 47
	− 9	+ 14	+ 14	+ 13	+ 97	+127	+104	− 2	− 1	− 21	+ 1	+ 2	+ 1	+ 8	+20	− 0	+ 19
42.5°	+134	+148	+141	+ 94	+179	+269	+ 58	+128	+ 43	+ 53	+ 28	+ 23	+53	+ 44	+28	+ 8	+ 52
	− 14	− 68	− 44	− 27	− 38	+121	+ 17	+ 18	− 11	+ 30	+ 22	+ 37	+27	+ 54	+49	− 17	+ 10
47.5°	+196	+157	+154	+133	+102	+162	+107	+103	+109	+132	+117	+101	+64	+138	+61	+116	+104
	− 64	− 87	− 27	− 56	− 40	− 40	− 13	+ 31	+ 43	+ 8	+ 50	+ 61	+26	+ 30	+ 1	+ 37	+ 51
52.5°																	
S 57.5°																	

Table 5. (continued)

	152.5°	147.5°	142.5°	137.5°	W 132.5°	W 127.5°	122.5°	117.5°	112.5°	107.5°	102.5°	97.5°	92.5°	87.5°	82.5°	77.5°	W 72.5°
S	−61	− 80	− 3	− 73	−118	−109	−112	− 90	−103	− 92	− 81	− 92	− 25	− 30	− 15		
7.5°	−12	− 18	− 1	− 2	+ 18	+ 41	+ 52	− 4	+ 45	+ 45	+ 22	+ 74	+ 31	+ 25	+ 17		
12.5°	−44	− 47	− 5	− 72	−80	−116	− 97	− 84	−107	−111	−105	− 74	− 81	− 49	− 33	− 18	
	+12	− 5	+ 1	+ 15	+13	+ 12	+ 15	+ 9	+ 19	+ 19	+ 19	+ 29	+ 40	+ 25	+ 31	+ 18	
17.5°	−43	− 38	− 4	− 71	−65	− 64	− 65	− 66	− 57	− 79	− 94	− 75	− 76	− 64	− 91	− 28	− 10
	+ 3	+ 3	− 0	+ 6	− 3	+ 5	− 3	+ 3	+ 6	+ 11	+ 1	+ 18	+ 25	+ 31	+ 76	+ 22	+ 17
22.5°	−40	− 34	− 6	− 49	−59	− 49	− 67	− 25	− 55	− 34	− 49	− 60	− 55	− 41	− 45	− 32	− 3
	− 1	− 12	+ 3	+ 12	+11	+ 14	+ 1	+ 3	+ 2	− 8	+ 0	+ 7	+ 24	+ 11	+ 39	+ 41	+ 8
27.5°	− 0	− 20	− 3	− 42	−65	− 22	− 24	− 3	− 32	− 2	− 27	− 4	− 14	− 32	− 34	− 17	− 1
	+ 8	− 2	+ 0	+ 11	+14	+ 4	+ 19	+ 5	− 3	− 35	+ 2	− 6	− 0	+ 22	+ 32	+ 44	+ 19
32.5°	+ 8	+ 27	− 1	− 24	−30	− 0	+ 20	+ 17	+ 10	+ 11	+ 16	+ 12	+ 21	+ 5	− 23	− 2	− 6
	+ 7	+ 14	+ 3	− 11	− 6	+ 0	− 5	− 3	+ 1	+ 12	+ 11	− 6	− 9	+ 8	+ 37	+ 33	+ 39
37.5°	− 0	+ 50	+ 5	+ 42	− 7	− 9	− 43	+ 93	+ 62	+ 23	+ 62	+ 42	+ 46	+ 44	+ 46	+ 27	+ 13
	+27	+ 34	+ 3	+ 20	−19	− 40	+ 7	+ 47	+ 17	− 9	− 2	− 10	+ 10	+ 2	+ 19	+ 37	+ 33
42.5°	+ 1	+ 61	+ 9	+ 89	+35	+ 12	+ 24	+ 95	+133	+ 94	+ 78	+ 57	+106	+ 85	+117	+ 96	
	+24	− 12	+ 4	− 5	− 9	+ 1	− 1	+ 19	+ 24	+ 48	+ 47	+ 27	+ 31	+ 6	+ 46	+ 24	
47.5°	+83	+127	+18	+ 91	+49	+ 54	+ 66	+146	+176	+ 64	+178	+127	+ 78	+140	+187	+148	
	+27	− 19	− 5	− 60	− 3	− 3	+ 6	− 23	+ 11	+ 44	+ 68	+ 66	+ 72	+ 17	+ 5	− 25	
52.5°				+121	+46	+100	+137	+108	+149	+135	+111	+197	+181	+ 48	+188	+259	+169
				+ 16	−36	+ 50	− 9	− 15	+ 5	+ 31	+ 15	+ 34	+ 24	+ 50	+ 3	− 30	+ 2
S												+ 89	+137	+163	+178	+206	+246
57.5°												+ 24	− 57	− 41	− 31	− 12	− 25

Table 6. Computed Wind Stresses over the Indian Ocean—January.

(τ_x and τ_y are given by the upper and lower figures, respectively, of each compartment, the unit being 10^{-2} dynes/cm^2).

	E 32.5°	37.5°	42.5°	47.5°	52.5°	57.5°	62.5°	67.5°	72.5°	77.5°	82.5°	87.5°	92.5°	97.5°	102.5°	107.5°	112.5°	117.5°	E 122.5°
N 22.5°							− 36 − 28	+ 3 − 7											
17.5°						− 6 − 24	− 14 − 12	− 5 − 12	+ 1 − 8			− 7 − 11	− 17 − 13						
12.5°				− 16 − 4	− 11 − 11	− 50 − 79	− 46 − 83	− 6 − 15	+ 10 − 10		− 12 − 10	− 52 − 52	− 8 − 11	− 4 − 12					
7.5°					− 45 − 87	− 49 −133	− 45 − 82	− 7 − 15	− 5 − 14	− 27 − 61	− 35 − 60	− 35 − 62	− 39 − 38	− 11 − 6					
N 2.5°				− 61 − 98	− 38 − 80	− 6 − 11	− 4 − 13	− 4 − 10	− 8 − 9	− 4 − 28	− 1 − 39	− 1 − 10	− 7 − 12						
S 2.5°			− 51 − 49	− 4 − 14	+ 12 − 24	+ 1 − 6	− 2 − 8	+ 5 − 5	+ 28 − 11	+ 4 − 6	+ 10 − 6	+ 44 + 7	+ 26 − 1	+ 21 − 17					
7.5°			− 3 − 12	− 6 + 0	+ 10 − 23	+ 60 − 7	− 2 − 1	+ 16 − 15	− 5 − 12	+ 25 − 23	+ 18 + 9	+ 19 + 3	+ 6 + 13	+ 3 + 6	+ 4 + 2	+ 17 + 8			
12.5°			− 2 − 25	+ 13 − 21	+ 13 + 1	+ 30 − 18	− 14 + 10	+ 12 + 9	− 0 − 18	−125 + 71	− 34 + 33	− 71 + 2	− 68 + 43	− 46 + 55	− 22 + 24	− 1 + 12	+ 28 + 25	+ 24 + 4	+ 55 + 23
17.5°		− 43 + 23	+ 7 − 17		− 22 + 19	− 33 + 50	− 68 − 21	−205 + 34	− 77 + 17	− 78 + 39	−141 + 98	−207 + 75	− 76 + 38	− 72 + 39	− 55 + 97	− 12 + 52	+ 36 + 56	+ 88 + 48	− 6 + 12
22.5°		− 69 + 57	− 77 + 53	− 25 − 26	− 13 − 19	− 41 − 10	− 68 − 1	− 75 + 11	− 88 + 4	− 88 + 12	− 75 + 6	−163 + 3	− 85 + 32	−123 + 47	− 73 + 54	− 99 +152	− 20 + 87		
27.5°	− 36 + 7	− 6 + 77	− 82 + 59	− 74 + 10	− 60 + 17	− 61 + 24	− 56 − 3	−110 − 65	− 15 − 7	− 72 + 70	− 38 + 17	− 64 + 21	− 22 + 17	− 37 + 46	− 60 + 58	−102 +140	− 20 +160		
32.5°	− 4 + 47	− 34 + 14	− 40 + 20	− 72 + 72	− 64 + 12	− 35 − 12	− 25 + 14	− 10 − 2	− 41 + 7	− 14 + 7	− 27 + 8	− 8 + 18	− 22 + 17	+ 16 + 47	+ 15 + 99	+ 28 +130	− 3 +224		
37.5°	+ 11 − 29	+ 24 − 15	+ 16 +136	+ 82 + 38	+ 16 + 10	+ 89 − 56	+ 91 − 49	+127 −115	+127 − 35	+ 82 − 96	+ 68 − 7	+ 41 − 3	+ 77 + 48	+ 86 + 1	+ 41 + 4	− 0 + 44	− 16 + 56	− 4 + 19	+ 21 + 22
42.5°	+101 − 53	+ 95 + 5	+ 70 + 12	+ 95 − 95	+125 + 27	+185 − 0	+180 − 2	+114 − 16	+139 − 31	+186 − 6	+162 − 33	+267 +147	+223 + 20	+204 + 82	+206 + 93	+243 + 88	+168 + 40	+126 − 47	+135 − 80
47.5°	+299 − 64	+274 − 21	+264 −133	+171 − 48	+103 − 33	+270 −122	+134 + 9	+172 − 89	+197 + 13	+177 − 13	+261 − 90	+211 + 45	+111 − 8	+300 −205	+265 + 63	+150 + 37	+201 − 82	+307 − 32	+146 − 12

Table 7. Computed Wind Stresses over the Indian Ocean—April.

(τ_x and τ_y are given by the upper and lower figures, respectively, of each compartment, the unit being 10^{-2} dynes/cm^2).

	E 32.5°	37.5°	42.5°	47.5°	52.5°	57.5°	62.5°	67.5°	72.5°	77.5°	82.5°	87.5°	92.5°	97.5°	102.5°	107.5°	112.5°	117.5°	122.5°
N 22.5°							+ 5	+ 34											
							+ 2	+ 5											
17.5°						+ 1	+ 6	+ 5	+ 8			+ 5	+ 6						
						+ 8	− 4	− 9	− 6			+ 11	+ 4						
12.5°				− 12	− 6	− 1	+ 1	− 4	+ 7		− 2	− 1	0	+ 2					
				− 6	+ 3	− 1	− 4	− 4	− 4		+ 4	+ 2	− 1	− 1					
7.5°					− 10	+ 10	− 5	+ 4	+ 8	+ 10	+ 4	+ 4	+ 4	+ 2					
					+ 5	− 4	− 2	− 6	− 4	+ 1	+ 6	+ 4	+ 2	− 2					
N 2.5°				− 5	− 9	− 1	+ 4	+ 7	+ 60	+ 23	+ 10	+ 20	+ 6	0					
				+ 5	− 5	− 3	− 2	− 4	+ 15	− 10	+ 4	+ 17	+ 1	− 1					
S 2.5°			− 5	− 10	− 1	+ 6	+ 24	+ 11	+ 6	+ 29	+ 34	+ 1	+ 25	+ 18					
			+ 11	0	+ 2	+ 2	+ 2	− 9	+ 1	+ 5	− 1	+ 6	+ 1	+ 3					
7.5°			− 12	− 40	+ 2	+ 7	+ 11	+ 29	− 10	− 2	− 41	− 31	+ 3	− 7	− 1	− 2			
			+ 7	+ 7	+ 4	+ 13	− 4	+ 23	+ 5	+ 1	+ 40	+ 43	+ 1	+ 8	− 7	+ 2			
12.5°			− 47	− 42	− 44	− 68	− 71	− 56	−105	− 66	−107	− 74	− 83	−137	−181	− 79	− 32	− 13	− 17
			+ 61	+ 22	+ 76	− 14	+ 20	0	+ 47	+ 34	+ 51	+ 39	+ 30	+ 9	+ 52	+ 21	+ 2	+ 1	− 18
17.5°		− 2	+ 4		− 18	− 78	−131	−201	−196	−118	−277	−225	−204	−129	−302	− 91	− 11	− 3	
		+ 46	+ 18		+ 8	+ 33	+ 54	+173	+ 66	+ 53	+105	+ 67	+ 87	+ 98	+ 84	+ 50	+ 2	− 1	
22.5°		− 31	− 76		− 68	− 73	−182	−148	−162	−154	−172	−200	−156	− 81	−162	− 64	− 27		
		+ 81	+ 82		− 1	+ 27	+ 57	+ 42	+ 67	+ 17	+ 11	+ 49	+ 2	+ 19	+ 44	+ 49	+ 46		
27.5°		− 15	− 30	−104	− 55	− 39	− 55	− 74	− 45	+ 2	− 7	− 39	−102	− 40	−111	− 57	− 34		
		+ 68	+ 42	− 8	+ 5	+ 29	+ 34	+ 55	+ 28	− 31	+ 18	+ 1	+ 67	+ 37	+ 39	+115	+ 70		
32.5°	+ 5	− 11	− 46	+ 11	− 14	− 1	− 7	+ 30	+ 6	− 50	− 42	+ 12	− 6	+ 47	+ 26	+ 16	− 13		
	+ 15	− 24	+ 20	− 61	− 47	− 26	+ 3	+ 86	− 7	+ 50	− 46	+ 2	− 7	− 7	+ 19	+ 29	+ 81		
37.5°	+ 75	+104	+ 92	+ 89	+152	+238	+ 41	+139	+ 97	+ 92	−132	+ 28	+107	+100	+ 54	+ 81	+ 55	+ 47	+ 52
	+ 18	− 27	− 36	− 48	+ 29	+113	+145	− 37	+ 56	− 11	− 29	− 87	− 29	+ 34	+ 12	+ 98	− 5	+137	+ 22
42.5°	+ 96	+ 10	+107	+126	+110	+208	+123	+129	+ 87	+277	+159	+142	+286	+211	+341	+376	+236	+268	+172
	+ 52	−105	+ 21	− 38	− 81	+ 2	− 23	− 18	−198	− 24	− 5	− 27	+152	+ 28	− 82	−152	− 70	+ 15	+ 50
47.5°	+270	+183	+292	+197	+170	+168	+203	+195	+107	+149	+204	+162	+270	+123	+129	+190	+139	+145	+192
	− 43	+ 23	−136	+ 19	− 83	+ 32	+ 8	+ 42	− 6	− 39	− 33	− 59	− 80	− 33	+ 10	+ 29	+ 30	+ 5	+ 9

Table 8. Computed Wind Stresses over the Indian Ocean—July.

(τ_x and τ_y are given by the upper and lower figures, respectively, of each compartment, the unit being 10^{-2} dynes/cm^2).

	E 32.5°	37.5°	42.5°	47.5°	52.5°	57.5°	62.5°	67.5°	72.5°	77.5°	82.5°	87.5°	92.5°	97.5°	102.5°	107.5°	112.5°	117.5°	E 122.5°
N 22.5°							+ 3 + 16	+ 81 + 36											
17.5°						+251 +304	+313 +324	+337 +260	+154 +131			+143 +153	+120 +152						
12.5°				+ 46 + 58	+ 43 +292	+395 +545	+300 +320	+194 +159	+187 + 32		+167 +115	+152 +149	+ 72 + 64	+102 + 58					
7.5°					+243 +355	+295 +301	+192 +175	+149 +107	+ 85 + 24	+ 88 + 19	− 54 + 46	− 54 + 59	+ 52 + 68	+ 64 + 61					
N 2.5°				+ 52 +143	+137 +200	+ 61 + 74	+ 35 + 41	+ 11 + 6	+ 8 + 2	+ 48 + 6	+ 74 + 51	+ 69 + 59	+ 47 + 42	+ 1 + 1					
S 2.5°			− 56 +123	+ 32 + 41	− 38 + 56	− 21 + 81	− 13 + 44	+ 2 + 11	− 31 + 28	+ 39 + 11	− 10 + 23	+ 2 + 43	− 5 + 8	+ 1 + 2					
7.5°			− 7 + 20	− 42 + 75	−131 +149	− 53 + 77	− 86 + 68	− 63 + 51	− 85 + 68	− 66 + 62	− 58 + 46	− 55 + 40	− 46 + 25	− 40 + 33	− 45 + 34	− 43 + 3			
12.5°			− 73 + 70	− 30 + 33	− 46 +103	− 71 + 56	− 44 + 59	−141 +131	− 70 + 65	−192 +134	− 70 + 59	−108 +121	− 93 +156	−125 + 87	−220 + 13	−213 + 30	− 39 + 25	− 17 + 2	− 54 + 1
17.5°		− 33 + 29	− 19 + 30		− 81 + 34	− 74 + 53	−126 + 34	−220 + 99	−148 +110	−147 +103	−191 +117	−176 +136	−127 +191	+ 51 + 65	−163 + 45	−174 + 31	− 28 + 51	− 47 − 5	
22.5°		− 19 + 26	− 46 + 44		− 54 + 22	− 67 + 21	−139 + 98	−150 + 61	−182 + 66	−188 + 79	−147 +115	− 65 +168	−146 + 92	−130 + 29	−123 + 19	− 73 + 88	− 30 + 43		
27.5°		+ 14 + 67	− 21 − 13	− 67 − 27	− 29 + 49	− 73 + 16	− 83 + 60	+ 27 − 6	− 12 − 19	−102 +112	+ 3 + 33	+ 13 + 58	− 83 +107	− 2 + 36	− 16 + 45	+ 35 + 29	− 10 + 38		
32.5°	+ 11 + 58	+ 37 − 8	+ 35 − 57	+ 67 +146	+ 42 + 48	+ 29 − 32	+105 + 91	+ 87 − 30	+ 29 + 23	+ 76 − 44	+ 1 − 18	+138 + 95	+ 90 + 71	+ 76 + 26	+ 48 − 14	+135 − 21	+ 99 + 33		
37.5°	+240 − 24	+261 − 7	+183 + 65	+200 + 17	+209 + 74	+263 + 27	+297 − 13	+233 − 2	+200 − 9	+284 − 29	+213 + 40	+226 + 21	+175 − 48	+154 + 71	+ 97 + 65	+ 12 − 32	+ 81 + 50	+136 − 30	+ 53 − 23
42.5°	+181 − 60	+129 − 33	+116 − 53	+136 + 24	+194 + 12	+260 + 7	+504 +143	+207 − 34	+367 + 9	+367 − 1	+309 −119	+432 + 59	+317 − 41	+108 +109	+375 + 35	+241 + 1	+320 +104	+185 − 96	+ 22 − 23
47.5°	+ 75 −186	+ 33 −258	+270 −161	+348 − 95	+106 − 18	+213 − 91	+183 − 34	+197 −114	+261 + 50	+184 + 75	+208 − 95	+287 + 62	+304 + 51	+257 −111	+262 −116	+228 − 79	+234 − 44	+164 − 52	+141 −186

Table 9. Computed Wind Stresses over the Indian Ocean—October.

(τ_x and τ_y are given by the upper and lower figures, respectively, of each compartment, the unit being 10^{-2} dynes/cm^2).

	E 32.5°	37.5°	42.5°	47.5°	52.5°	57.5°	62.5°	67.5°	72.5°	77.5°	82.5°	87.5°	92.5°	97.5°	102.5°	107.5°	112.5°	117.5°	E 122.5°
N 22.5°							+ 0	+ 6											
							− 1	− 5											
17.5°						+ 5	+ 4	+ 7	+ 3			− 2	− 3						
						+ 5	− 15	− 28	− 3			+ 2	− 14						
12.5°				− 11	− 2	+ 2	+ 7	+ 24	− 9		− 1	− 7	− 41	+ 0					
				− 3	+ 1	− 3	− 0	+ 2	+ 11		+ 4	− 3	+ 12	+ 8					
7.5°					− 0	+ 6	+ 5	+ 12	− 18	+ 12	+ 61	+ 45	+ 33	− 11					
					+ 5	+ 1	− 7	+ 1	+ 5	− 6	+ 34	+ 41	+ 29	− 0					
S 2.5°				− 5	− 0	+ 3	+ 11	+ 22	+ 25	+ 80	+ 74	+ 97	+ 39	− 0					
				+ 10	+ 21	+ 1	+ 3	+ 15	+ 18	+ 18	+ 39	+ 67	+ 4	− 9					
N 2.5°			− 9	− 11	− 8	− 6	+ 1	+ 15	+ 17	+ 45	+ 31	+ 26	+ 4	+ 5					
			+ 4	+ 11	+ 10	+ 9	+ 8	+ 4	+ 12	+ 8	+ 16	+ 5	+ 2	+ 1					
7.5°			− 9	−151	− 53	− 86	−109	− 44	− 23	+ 12	− 8	− 22	− 61	−116	− 47				
			+ 5	+121	+ 52	+ 37	+ 60	+ 46	+ 12	+ 21	+ 35	+ 19	+ 24	+ 65	+ 36				
12.5°			− 5	− 36	− 35	− 43	−196	−145	−199	−207	−315	−186	−146	−139	− 64	− 49	− 33	− 29	+ 1
			+ 11	− 1	+ 8	− 7	+105	+129	+130	+100	+312	+190	+115	+ 99	+ 44	+ 86	+ 59	+ 36	+ 8
17.5°		− 53	− 7		− 14	− 68	− 81	−153	− 64	−160	−205	−214	−149	−139	−151	− 55	− 7	+ 12	+ 9
		− 17	− 2		+ 4	− 7	+ 41	+135	+ 54	+115	+104	+ 98	+ 67	+ 99	+111	+ 44	+ 54	− 4	+ 7
22.5°		− 28	− 14	− 40	− 25	− 39	− 77	− 21	− 93	−122	−174	−166	−164	− 62	− 69	− 57	− 27		
		+ 19	+ 92	− 4	+ 4	+ 4	+ 33	+ 26	+ 34	− 62	+ 77	+ 18	+ 14	+ 42	+ 30	+ 50	+ 80		
27.5°	− 21	− 23	− 41	− 28	− 41	+ 14	− 43	+ 5	− 10	+ 4	− 48	− 9	+ 1	− 42	+ 22	− 5	− 15		
	+ 38	+ 11	+ 13	− 5	− 4	− 5	− 40	+ 5	− 46	− 21	+ 45	+ 39	− 19	+ 77	+ 37	+ 36	+ 65		
32.5°	− 31	− 60	− 9	+ 52	− 16	+ 44	+ 29	+ 35	− 23	+ 68	+ 65	+ 32	+ 21	+ 78	+ 53	+ 67	+ 86		
	+ 35	− 52	+ 7	+ 14	−133	− 1	− 14	− 30	− 39	− 0	− 54	− 33	+ 13	+ 5	+ 25	+ 9	+ 40		
37.5°	+ 69	+101	+128	+121	+202	+105	+143	+111	+145	+130	+147	+145	+101	+186	+275	+141	+ 78	+123	+ 75
	+ 65	+ 4	−103	− 41	+ 11	+ 13	+ 44	− 60	− 94	+ 2	− 51	− 92	− 34	+ 6	+ 84	− 21	− 35	+ 11	− 5
42.5°	+138	+120	+144	+155	+217	+311	+231	+276	+223	+209	+222	+318	+281	+373	+310	+227	+165	+173	+142
	+ 78	+ 59	+ 27	− 10	+ 79	− 42	+ 38	− 72	+ 21	− 61	− 22	− 27	− 32	−105	+ 2	+ 34	−130	− 88	− 14
S 47.5°	− 20	+138	+131	+179	+175	+179	+272	+221	+316	+269	+305	+263	+180	+177	+178	+289	+193	+133	+190
	− 45	−116	− 23	− 47	− 45	+ 13	− 59	− 2	+ 12	− 60	− 91	− 61	− 41	− 21	− 84	− 64	− 90	− 9	+ 66

Table 10. Computed Wind Stresses over the Indian Ocean—Annual Mean.

(τ_x and τ_y are given by the upper and lower figures, respectively, of each compartment, the unit being 10^{-2} dynes/cm^2).

	E 32.5°	37.5°	42.5°	47.5°	52.5°	57.5°	62.5°	67.5°	72.5°	77.5°	82.5°	87.5°	92.5°	97.5°	102.5°	107.5°	112.5°	117.5°	E 122.5°
N 22.5°							− 7	+ 31											
							− 2	+ 7											
17.5°						+ 63	+ 78	+ 86	+ 41			+ 47	+ 26						
						+ 73	+ 73	+ 53	+ 28			+ 39	+ 32						
12.5°				+ 2	+ 6	+ 86	+ 66	+ 52	+ 49		+ 38	+ 23	+ 6	+ 25					
				+ 11	+ 71	+116	+ 58	+ 36	+ 7		+ 28	+ 24	+ 16	+ 13					
7.5°					+ 47	+ 66	+ 37	+ 40	+ 18	+ 21	− 6	− 10	+ 13	+ 11					
					+ 69	+ 41	+ 21	+ 22	+ 3	− 12	+ 6	+ 10	+ 15	+ 13					
N 2.5°				− 5	+ 22	+ 17	+ 12	+ 9	+ 21	+ 37	+ 39	+ 46	+ 21						
				+ 15	+ 34	+ 15	+ 7	+ 2	+ 7	− 4	+ 14	+ 33	+ 9						
S 2.5°			− 30	+ 2	− 9	− 5	+ 3	+ 8	+ 5	+ 29	+ 16	+ 18	+ 12	+ 11					
			+ 22	+ 9	+ 11	+ 22	+ 12	+ 0	+ 7	+ 45	+ 8	+ 15	+ 3	− 3					
7.5°			− 8	− 60	− 43	− 18	− 47	− 16	− 31	− 8	− 22	− 22	−245	− 40	− 22				
			+ 5	+ 51	+ 45	+ 30	+ 31	+ 26	+ 18	+ 15	+ 32	+ 26	+ 16	+ 28	+ 16				
12.5°			− 32	− 24	− 28	− 38	− 81	− 83	− 94	−148	−132	−110	− 98	−112	−122	− 85	− 19	− 9	− 4
			+ 29	+ 8	+ 47	+ 4	+ 48	+ 67	+ 56	+ 85	+114	+ 88	+ 86	+ 63	+ 33	+ 37	+ 28	+ 10	+ 4
17.5°		− 33	− 3		− 34	− 63	−101	−194	−121	−126	−204	−205	−139	− 72	−168	− 83	− 3	+ 12	
		+ 20	+ 7		+ 16	+ 32	+ 27	+110	+ 62	+ 78	+106	+ 56	+ 96	+ 75	+ 84	+ 44	+ 41	+ 10	
22.5°		− 36	− 54		− 40	− 55	−116	− 98	−131	−138	−142	−149	−138	− 99	−107	− 7	− 26		
		+ 41	+ 68		+ 0	+ 11	+ 47	+ 35	+ 43	+ 11	+ 52	+ 59	+ 35	+ 34	+ 37	+ 85	+ 64		
27.5°		− 7	− 44	− 68	− 46	− 40	− 59	− 38	− 21	− 42	− 23	− 25	− 51	− 31	− 41	− 32	− 20		
		+ 56	+ 25	− 7	+ 17	+ 16	+ 13	− 3	− 11	+ 32	+ 28	+ 30	+ 43	+ 49	+ 45	+ 80	+ 83		
32.5°	− 5	− 17	+ 15	+ 15	+ 5	+ 9	+ 26	+ 35	− 7	+ 20	− 1	+ 44	+ 21	+ 54	+ 35	+ 62	+ 42		
	+ 39	− 18	− 3	+ 43	− 30	− 18	+ 24	+ 6	− 4	− 12	− 28	+ 20	+ 23	+ 18	+ 32	+ 37	+ 94		
37.5°	+ 99	+123	+105	+123	+145	+174	+143	+152	+142	+147	+140	+110	+115	+131	+117	+ 58	+ 49	+ 76	+ 50
	+ 7	− 11	+ 15	+ 29	+ 32	+ 24	+ 32	− 54	− 20	− 33	− 12	− 40	− 16	+ 28	+ 41	+ 22	+ 16	+ 34	+ 4
42.5°	+129	+ 89	+109	+128	+161	+241	+260	+182	+ 20	+260	+213	+290	+277	+224	+308	+272	+222	+188	+118
	+ 4	− 19	− 1	− 30	+ 92	− 8	+ 39	− 35	− 50	− 23	− 45	+ 38	+ 25	+ 29	+ 12	− 7	− 14	− 54	− 17
S 47.5°	+181	+155	+239	+224	+138	+208	+198	+196	+220	+195	+245	+231	+216	+214	+209	+214	+192	+187	+167
	−109	− 93	−113	− 43	− 45	− 42	− 19	− 41	+ 17	− 9	− 77	− 3	− 20	− 92	− 32	− 19	− 47	− 22	− 31

Table 11. Computed Wind Stresses over the Atlantic Ocean – Dec., Jan. and Feb.

(τ_x and τ_y are given by the upper and lower figures, respectively, of each compartment, the unit being 10^{-2} dynes/cm^2).

	82.5°W	77.5°	72.5°	67.5°	62.5°	57.5°	52.5°	47.5°	42.5°	37.5°	32.5°	27.05°
57.5°N											+240 **+106**	+298 **+ 89**
52.5°						+146 **− 31**		+325 **+ 12**	+217 **+ 14**	+236 **+ 25**	+213 **+ 51**	+219 **+ 75**
47.5°				+ 94 **− 61**	+154 **− 79**	+153 **− 69**	+ 92 **− 1**	+172 **− 20**	+228 **− 4**	+207 **+ 35**	+226 **+ 30**	+199 **+ 71**
42.5°				+165 **− 87**	+181 **− 56**	+196 **− 29**	+111 **− 40**	+125 **− 54**	+189 **− 17**	+176 **− 11**	+172 **+ 30**	+126 **+ 49**
37.5°			+ 68 **− 60**	+103 **− 16**	+ 92 **− 22**	+ 99 **− 7**	+175 **− 3**	+153 **+ 13**	+104 **+ 23**	+105 **+ 31**	+ 93 **+ 24**	+ 58 **+ 13**
32.5°		+ 40 **− 34**	+ 74 **− 31**	− 5 **− 20**	+ 12 **− 12**	− 2 **− 14**	+ 72 **+ 5**	+ 62 **+ 1**	+ 41 **− 6**	+ 43 **+ 9**	+ 23 **+ 4**	+ 9 **+ 4**
27.5°	−30 **−26**	− 5 **− 23**	− 8 **− 19**	− 59 **− 21**	− 59 **− 28**	− 56 **− 18**	− 10 **− 7**	− 7 **− 14**	− 18 **− 6**	− 18 **− 6**	− 7 **− 9**	− 21 **− 14**
22.5°	−42 **−35**	− 56 **− 30**	− 64 **− 27**	− 80 **− 26**	− 85 **− 25**	− 83 **− 24**	− 62 **− 19**	− 56 **− 12**	− 60 **− 21**	− 62 **− 15**	− 49 **− 16**	− 68 **− 24**
17.5°	−64 **−43**	− 73 **− 33**	− 73 **− 32**	− 86 **− 25**	− 80 **− 24**	− 90 **− 35**	− 79 **− 22**	− 80 **− 19**	− 72 **− 18**	− 83 **− 33**	− 97 **− 32**	− 71 **− 38**
12.5°	−57 **−43**	−118 **− 80**	−151 **− 45**			− 80 **− 40**	−105 **− 50**	−145 **− 71**	−106 **− 51**	−102 **− 64**	−123 **− 53**	− 73 **− 48**
7.5°							− 76 **− 43**	−107 **− 65**	−113 **− 67**	− 78 **− 55**	− 85 **− 39**	− 63 **− 49**
2.5°N								− 63 **− 45**	− 66 **− 24**	− 39 **− 7**	− 16 **− 6**	− 14 **− 5**

Table 11. (continued)

	82.5°W	77.5°	72.5°	67.5°	62.5°	57.5°	52.5°	47.5°	42.5°	37.5°	32.5°	27.5°
2.5°S									− 70 + **2**	− 67 + **34**	− 57 + **44**	− 53 + **46**
7.5°											− 72 + **36**	− 75 + **32**
12.5°										− 64 + **3**	−104 + **23**	−111 + **11**
17.5°										− 45 − **34**	− 68 − **16**	− 70 − **18**
22.5°										− 37 − **47**	− 40 − **37**	− 30 − **18**
27.5°								− 24 − **9**	− 40 − **55**	− 34 − **62**	− 11 − **15**	− 10 − **26**
32.5°							− 19 **0**	− 19 − **15**	− 8 − **10**	− 24 − **27**	+ 12 − **26**	− 1 − **39**
37.5°						− 5 − **28**	+ 24 − **20**	+ 79 + **1**	+ 27 + **4**	+ 15 − **18**	+ 36 − **21**	− 24 − **40**
42.5°					+ 49 − **22**	+ 60 − **7**	+133 − **52**	+ 84 + **8**	+ 62 − **31**	+ 59 − **96**	+102 − **77**	+ 76 − **75**
47.5°					+111 + **26**	+ 78 − **21**	+107 − **12**	+102 − **72**	+177 − **39**	+133 − **70**		
52.5°				+ 88 + **39**	+123 + **21**	+109 − **51**	+118 − **60**	+ 91 − **87**				
57.5°S			+134 − **48**	+114 − **71**	+ 85 − **18**	+149 − **28**	+164 + **98**					

Table 11. (continued)

	22.5°	17.5°	12.5°	7.5°	2.5°W	2.5°E	7.5°	12.5°	17.5°	22.5°	27.5°	32.5°E
57.5°N	+249 + **86**	+281 + **78**	+214 +**108**	+179 + **85**								
52.5°	+207 + **87**	+212 + **67**	+183 + **38**									
47.5°	+191 + **41**	+141 + **24**	+131 + **25**	+101 + **22**	+ 74 + **19**							
42.5°	+126 + **42**	+116 + **14**	+ 74 − **12**									
37.5°	+ 41 − **9**	+ 17 − **18**	+ 20 − **21**									
32.5°	+ 13 − **17**	− 6 − **19**	+ 4 − **30**									
27.5°	− 39 − **25**	− 40 − **33**										
22.5°	− 61 − **40**	− 51 − **39**										
17.5°	− 63 − **51**	− 58 − **53**										
12.5°	− 61 − **53**	− 28 − **37**										
7.5°	− 22 − **17**	− 4 − **5**	− 4 + **2**									
2.5°N	− 9 + **1**	− 5 + **6**	− 5 + **19**	+ 2 + **9**	− 5 + 8	− 5 +**13**	+ 3 +**10**					

Table 11. (continued)

	22.5°	17.5°	12.5°	7.5°	2.5°W	2.5°E	7.5°	12.5°	17.5°	22.5°	27.5°	32.5°E
2.5°S	− 39 + **47**	−41 +**64**	− 30 + **71**	− 2 + **50**	+ 17 + **68**	− 36 + **41**	+ 29 + **51**					
7.5°	− 71 +**114**	−61 +**61**	− 56 + **48**	− 53 + **59**	− 68 + **95**	− 34 + **61**						
12.5°	− 76 + **12**	−73 +**42**	− 61 + **51**	− 57 + **52**	− 54 + **64**	− 98 +**141**	− 31 + **68**					
17.5°	− 77 − **9**	−81 +**10**	− 63 + **51**	− 23 + **14**	− 59 + **42**	− 61 + **49**	− 62 +**104**					
22.5°	− 34 − **6**	−43 + 8	− 39 + **32**	− 63 + **49**	− 37 + **28**	− **70** + **36**	− 94 +**131**	− 40 +**183**				
27.5°	− 9 − **33**	− 6 −**31**	− 15 + **19**	− 13 + **28**	− 25 + **28**	− 28 + **58**	− 46 + **91**	− 57 +**152**				
32.5°	− 1 − **24**	+14 −**19**	− 4 − **21**	+ 11 − **1**	+ 43 + **34**	+ 53 + **16**	− 7 + **53**	+ 3 + **65**	− 20 + **65**	+ 83 + **34**	+86 + 8	+ 85 + **22**
37.5°	+ 33 − **82**	+32 −**19**	+ 28 − **25**	+ 78 − **44**	+ 69 + **24**	+ 94 + **14**	+ 47 − **12**	+133 + **44**	+ 74 + **39**	+129 − **15**	+91 −**22**	+ 89 − **72**
42.5°	+101 − **13**	+95 −**81**	+125 − **68**	+145 − **46**	+120 − **57**	+140 − **27**	+123 − **29**	+107 − **14**	+188 − **11**			+193 − **75**
47.5°												
52.5°												
57.5°S												

Table 12. Computed Wind Stresses over the Atlantic Ocean—Mar., Apr. and May.

(τ_x and τ_y are given by the upper and lower figures, respectively, of each compartment, the unit being 10^{-2} dynes/cm^2).

	82.5°W	77.5°	72.5°	67.5°	62.5°	57.5°	52.5°	47.5°	42.5°	37.5°	32.5°	27.5°
57.5°N											+112 − 50	+158 + 18
52.5°									+165 − 22	+132 + 8	+120 + 5	+131 − 5
47.5°							+ 27 + 6	+ 59 − 3	+142 − 2	+123 + 18	+110 0	+108 − 5
42.5°				+33 −28	+53 −29	+ 57 − 26	+ 40 − 18	+ 55 − 16	+105 − 16	+ 97 0	+ 85 + 11	+ 67 + 9
37.5°			+ 28 − 29	+59 −47	+86 −31	+ 89 − 18	+ 75 − 9	+ 67 + 7	+ 55 + 18	+ 47 + 15	+ 49 + 4	+ 24 − 6
32.5°		+21 −22	+ 31 − 9	+45 −10	+43 − 3	+ 46 + 5	+ 34 + 7	+ 41 + 2	+ 37 + 10	+ 32 + 6	+ 23 0	+ 14 − 15
27.5°	−21 −12	−14 − 7	− 13 − 13	− 8 −13	+ 2 − 4	+ 3 − 6	+ 3 0	− 6 − 2	− 28 − 2	− 16 0	− 17 − 7	− 13 − 24
22.5°	−34 −11	−39 −20	− 48 − 12	−58 − 1	−62 − 1	− 44 − 1	− 58 − 3	− 40 − 8	− 61 − 23	− 60 − 19	− 74 − 28	− 56 − 38
17.5°	−22 − 5	−68 −21	− 62 − 16	−71 − 9	−84 − 6	− 77 − 12	− 79 − 14	− 84 − 14	− 82 − 30	− 77 − 30	− 82 − 30	− 70 − 59
12.5°	−32 −27	−73 −49	−102 − 29	−94 − 9	−82 −10	−117 − 34	−136 − 58	−140 − 77	−131 − 70	− 99 − 75	−147 − 87	− 73 − 61
7.5°						− 81 − 39	− 85 − 50	−188 −120	−139 −100	−102 − 96	− 66 − 56	− 65 − 59
2.5°N								− 59 − 45	− 58 − 30	− 51 − 18	− 23 − 24	− 8 − 3

Table 12. (continued)

	82.5°W	77.5°	72.5°	67.5°	62.5°	57.5°	52.5°	47.5°	42.5°	37.5°	32.5°	27.5°
2.5°S									− 44 + **6**	− 29 + **48**	− 25 + **48**	−37 +**28**
7.5°											− 58 + **42**	−97 +**68**
12.5°										− 43 + **28**	− 67 + **25**	−39 +**30**
17.5°										− **30** + **21**	− 51 + **3**	−53 −**12**
22.5°										− 26 − **9**	− 36 − **8**	−33 −**13**
27.5°								− 19 − **7**	− 20 − **2**	− 21 − **20**	− 24 − **17**	−12 − **9**
32.5°							+ 8 **0**	+ 4 − **43**	+ 45 + **1**	+ 23 − **16**	+ 5 − **16**	0 −**36**
37.5°						+ 6 − **4**	+ 34 − **1**	+136 + **41**	+ 27 − **18**	+ 56 − **12**	+ 59 − **24**	+73 −**27**
42.5°					+106 + **8**	+ 51 − **9**	+193 + **51**	+106 + **70**	+ 96 − **46**	+123 − **44**	+123 − **70**	+72 +**26**
47.5°					+130 + **5**	+136 − **1**	+136 + **57**	+130 − **2**	+157 − **55**	+203 − **34**	+156 − **19**	
52.5°				+179 + **9**	+113 + **43**	+133 − **3**	+210 − **86**	+ 94 −**102**				
57.5°S			+186 − **15**	+202 − **39**	+138 + **38**	+ 94 − **42**	+ 55 − **96**					

Table 12. (continued)

	22.5°	17.5°	12.5°	7.5°	2.5°W	2.5°E	7.5°	12.5°	17.5°	22.5°	27.5°	32.5°E
57.5°N	+148 + **18**	+113 + **18**	+103 + **28**	+70 +**16**								
52.5°	+122 **0**	+ 99 − **12**	+ 70 − **6**									
47.5°	+ 85 − **13**	+ 64 − **13**	+ 55 − **19**	+41 − **1**	+24 − **4**							
42.5°	+ 61 − **11**	+ 48 − **31**	+ 24 − **41**									
37.5°	+ 27 − **23**	+ 13 − **39**	+ 11 − **42**									
32.5°	+ 6 − **24**	− 2 − **40**	− 2 − **50**									
27.5°	− 34 − **51**	− 32 − **49**	− 14 − **45**									
22.5°	− 53 − **54**	− 47 − **70**										
17.5°	− 55 − **76**	− 21 − **84**										
12.5°	− 53 − **79**	− 2 − **21**										
7.5°	− 14 − **18**	0 − **7**	− 1 − **1**									
2.5°N	− 4 **0**	− 3 + **6**	− 24 + **37**	−17 +**36**	− 2 +**54**	+ 2 + **6**	+ 4 +**12**					

Table 12. (continued)

	22.5°	17.5°	12.5°	7.5°	2.5°W	2.5°E	7.5°	12.5°	17.5°	22.5°	27.5°	32.5°E
2.5°S	−43 +34	− 47 + 39	−37 +58	−44 +56	− 19 + 63	+ 4 + 32	+ 5 + 41					
7.5°	−66 +41	− 62 + 56	−59 +60	−56 +55	− 34 + 50	− 32 + 61	+ 1 + 52	+ 20 + 44				
12.5°	−63 +12	− 69 + 32	−58 +56	−59 +58	− 43 + 52	− 37 + 66	− 26 + 75	+ 27 + 30				
17.5°	−40 − 3	− 65 + 15	−68 + 8	−55 +42	− 55 + 54	− 97 +103	− 86 + 97					
22.5°	−29 −19	− 17 + 10	−31 +10	−49 +40	− 47 + 41	− 35 + 49	− 31 + 58	− 22 + 61				
27.5°	− 7 −30	− 16 − 19	+ 1 − 8	− 5 +24	− 29 − 16	− 23 + 43	− 22 + 50	− 39 + 74				+ 8 + 21
32.5°	− 1 −67	0 − 20	− 2 + 3	+52 +18	+ 25 + 21	− 30 + 28	+ 9 + 44	− 35 +119	+ 7 + 38	+ 51 + 9	+ 27 − 18	+ 17 − 9
37.5°	+32 −23	+ 55 − 51	+50 −30	+54 −31	+ 69 − 10	+ 76 + 32	+ 51 − 9	+ 91 + 26	+ 68 + 7	+ 17 − 29	+102 + 11	+ 29 − 34
42.5°	+74 −21	+ 48 −111	+45 −13	+87 −49	+112 − 11	+135 − 35	+163 − 59	+151 − 51	+170 − 83	+200 −126	+201 −131	+125 − 85
47.5°												
52.5°												
57.5.S												

Table 13. Computed Wind Stresses over the Atlantic Ocean—Jun., Jul. and Aug.

(τ_x and τ_y are given by the upper and lower figures, respectively, of each compartment, the unit being 10 dynes/cm).

	82.5°W	77.5°	72.5°	67.5°	62.5°	57.5°	52.5°	47.5°	42.5°	37.5°	32.5°	27.5°
57.5°N								+ 22 − 45	+ 21 + 15	+59 − 2	+ 67 + 7	+96 + 7
52.5°							+ 20 + 4	+ 30 + 4	+ 55 + 5	+67 + 7	+ 73 + 2	+90 + 1
47.5°							+ 30 + 19	+ 38 + 18	+ 60 + 11	+65 +16	+ 40 + 10	+42 + 6
42.5°				+ 6 + 2	+27 +11	+27 +14	+ 27 + 22	+ 31 + 17	+ 43 + 12	+44 +13	+ 45 + 11	+43 + 9
37.5°			+ 3 + 1	+18 +16	+29 +18	+38 +27	+ 41 + 35	+ 39 + 23	+ 26 + 22	+28 +21	+ 13 + 8	+ 7 − 2
32.5°		+11 +12	+ 26 + 29	+27 +28	+20 +20	+10 +13	+ 13 + 12	+ 8 + 12	+ 2 + 3	0 + 2	+ 1 0	0 − 6
27.5°	− 8 + 4	− 4 + 5	− 5 + 8	− 3 + 7	− 9 + 8	− 8 + 7	− 9 + 4	− 9 + 3	− 10 0	−10 − 2	− 28 − 12	−40 −31
22.5°	−13 + 3 −42	−41 + 3	− 68 + 8	−65 +15	−78 + 5	−64 + 1	− 70 − 2	− 71 − 8	− 76 − 16	−77 −32	− 82 − 35	−67 −45
17.5°	+ 4 −50 −18	−83 −13	− 67 − 3	−87 0	−92 − 5	−90 − 9	− 92 − 18	−102 − 24	− 77 − 27	−76 −25	−117 − 51	−71 −55
12.5°		−92 −44	−175 − 35	−94 + 1	−81 −21	−81 −16	−119 − 34	−107 − 36	−108 − 47	−73 −29	− 51 − 31	−26 −19
7.5°						−32 − 8	− 31 − 9	− 34 − 8	− 24 − 6	−17 2	− 24 + 25	+ 7 +30
2.5°N								− 12 + 3	− 23 + 24	−52 +45	− 56 + 56	−45 +57

Table 13. (continued)

	82.5°W	77.5°	72.5°	67.5°	62.5°	57.5°	52.5°	47.5°	42.5°	37.5°	32.5°	27.5°
2.5°S								− 77 + **10**	− 61 + **34**	− 66 + **53**	− 67 + **55**	− 65 + **49**
7.5°											−133 +**125**	−107 + **43**
12.5°										− 67 + **37**	−174 +**105**	−189 + **66**
17.5°										− 46 + **22**	− 61 + **30**	− 96 + **21**
22.5°									− 25 − **11**	− 32 − **7**	− 49 + **3**	− 28 + **2**
27.5°								+ 5 + **5**	− 5 − **29**	− 9 − **6**	− 12 − **17**	− 11 − **28**
32.5°							+ 49 + **18**	+ 55 + **10**	+ 64 − **29**	+ 58 **0**	+ 63 − **49**	+ 40 −**100**
37.5°						+ 6 − **6**	+ 62 + **46**	+103 − **18**	+121 − **13**	+ 93 − **32**	+ 84 −**118**	+184 - **101**
42.5°					+ 16 − **12**	+ 54 − **16**	+210 + **77**	+125 − **24**	+128 + **14**	+142 − **10**	+120 − **81**	+236 −**185**
47.5°				+ 21 − **15**	+ 91 − **10**	+142 − **65**	+105 + **5**	+210 + **23**	+146 − **27**			
52.5°			+ 82 − **9**	+145 + **13**	+142 + **49**	− 7 + **48**	+ 89 + **3**	+141 − **80**				
57.5°			+169 − **30**	+175 + **6**	+150 − **36**	+ 22 − **64**	+ 95 −**190**					

Table 13. (Continued)

	22.5°	17.5°	12.5°	7.5°	2.5°W	2.5°E	7.5°	12.5°	17.5°	22.5°	27.5°	32.5°E
57·5°N	+60 **+10**	+55 **+ 8**	+32 **− 0**	+29 **− 1**								
52.5°	+77 **0**	+64 **− 2**	+59 **+ 3**									
47.5°	+41 **+ 3**	+44 **− 1**	+44 **− 1**	+43 **− 3**	+30 **+ 3**							
42.5°	+43 **+ 6**	+29 **−13**	+ 5 **−41**									
37.5°	+ 7 **− 3**	−13 **−38**	− 7 **−60**									
32.5°	−20 **−25**	−35 **−51**	−24 **−72**									
27.5°	−39 **−44**	−46 **−63**	−30 **−66**									
22.5°	−55 **−66**	−42 **−75**										
17.5°	−39 **−52**	− 5 **−38**										
12.5°	0 **− 5**	+11 **+ 5**										
7.5°	+16 **+53**	+26 **+57**	+29 **+47**									
2.5°N	−24 **+69**	− 9 **+78**	− 4 **+71**	+13 **+68**	+ 4 **+44**	+18 **+78**	+14 **+67**					

Table 13. (continued)

	22.5°	17.5°	12.5°	7.5°	2.5°W	2.5°E	7.5°	12.5°	17.5°	22.5°	27.5°	32.5°E
2.5°S	− 66 + **47**	− 53 + **60**	− 18 + **32**	− 50 + **61**	− 8 + **44**	+ 16 + **41**	+ 4 + **11**					
7.5°	− 74 + **41**	− 67 + **57**	−126 +**120**	− 71 +**129**	− 56 + **71**	−142 +**122**	+ 3 + **13**					
12.5°	−176 +**139**	−119 +**108**	− 88 + **52**	−111 +**110**	− 61 + **67**	− 56 + **71**	− 13 + **80**					
17.5°	−131 + **48**	− 70 + **22**	− 96 + **71**	− 60 + **59**	− 56 + **60**	−111 +**119**	−114 +**115**					
22.5°	− 30 **0**	− 54 + **33**	− 83 + **62**	−103 + **95**	− 57 + **49**	− 79 + **98**	− 93 +**131**	− 21 +**112**				
27.5°	− 5 − **23**	+ 8 − **2**	− 9 + **40**	+ 43 + **55**	− 29 + **50**	− 40 + **49**	− 31 + **60**	− 40 + **72**				
32.5°	+ 33 − **66**	+ 35 − **28**	+ 38 + **18**	+ 33 + **44**	+ 35 + **73**	+ 62 − **6**	+ 15 + **22**	+ 42 + **28**	+ 25 + **14**	+ 78 + **3**	+132 + **8**	+27 + **4**
37.5°	+137 −**126**	+144 −**109**	+103 − **68**	+134 −**108**	+157 − **87**	+122 − **74**	+162 + **8**	+ 95 − **12**	+107 − **35**	+ 70 + **6**	+ 12 + **68**	+49 +**25**
42.5°	+140 + **14**	+219 − **97**	+184 − **67**	+254 − **89**	+ 85 − **99**	+ 77 −**128**	+131 −**144**	+203 − **95**	+268 − **17**	+140 − **12**	+104 − **9**	+75 −**11**
47.5°										+125 − **31**	+113 − **30**	+75 −**84**
52.5°												
57.5°												

Table 14. Computed Wind Stresses over the Atlantic Ocean—Sept., Oct. and Nov.

(τ_x and τ_y are given by the upper and lower figures, respectively, of each compartment, the unit being 10^{-2} dynes/cm^2).

	82.5°W	77.5°	72.5°	67.5°	62.5°	57.5°	52.5°	47.5°	42.5°	37.5°	32.5°	27.5°
57.5°N									+117 − 47	+134 − 2	+170 + 19	+194 + 31
52.5°							+63 −41	+151 − 32	+149 − 30	+155 − 16	+156 + 1	+161 + 2
47.5°							+58 −17	+ 65 − 18	+142 − 35	+144 + 10	+130 − 5	+106 − 22
42.5°				+24 −31	+50 −48	+53 −41	+25 −17	+ 34 − 35	+ 94 − 36	+ 81 − 9	+ 62 − 24	+ 63 − 9
37.5°			+19 −46	+38 −47	+45 −39	+48 + 1	+51 +12	+ 34 + 2	+ 20 + 18	+ 16 + 3	+ 9 − 11	+ 17 − 8
32.5°		−11 −43	− 6 −27	+ 8 −18	− 2 − 3	+ 1 − 1	+ 8 + 2	+ 4 + 10	+ 1 + 1	− 2 − 0	+ 4 − 7	− 2 − 18
27.5°	−36 −25	−29 −30	−30 −13	−27 −10	−23 − 4	−17 + 1	−15 + 3	− 22 + 1	− 29 0	− 26 − 6	− 22 − 10	− 22 − 10
22.5°	−41 −29	−43 −26	−43 −15	−45 − 3	−49 − 1	−33 + 2	−53 − 3	− 74 + 1	− 62 − 1	− 58 − 16	− 66 − 18	− 57 − 17
17.5°	−24 −17	−31 −12	−30 −13	−41 − 6	−64 − 7	−58 − 4	−76 −12	− 84 − 3	− 73 − 9	− 77 − 11	− 74 − 22	− 74 − 35
12.5°	−11 −16	−33 −16	−68 −13	−57 − 3	−19 − 4	−38 −11	−65 − 7	− 76 − 16	− 65 − 17	− 55 − 12	− 65 − 23	− 42 − 15
7.5°						−15 − 2	−14 − 1	− 24 − 1	− 36 − 4	− 34 + 2	− 27 + 7	− 5 + 5
2.5°N								− 13 + 1	− 69 + 24	− 51 + 56	− 52 + 60	− 38 + 65

Table 14. (continued)

	82.5°W	77.5°	72.5°	67.5°	62.5°	57.5°	52.5°	47.5°	42.5°	37.5°	32°5°	27.5°
2.5°S								− 80 + **5**	−94 +**39**	−114 + **91**	− 69 + **50**	− 64 + **55**
7.5°											− 72 + **28**	−106 + **64**
12.5°										− 68 + **3**	−110 + **37**	−110 + **30**
17.5°										− 44 − **18**	− 66 − **4**	− 67 − **14**
22.5°									−30 −**25**	− 32 − **44**	− 50 + **4**	− 25 − **13**
27.5°								− 20 − **18**	−43 − **2**	− 21 − **7**	− 29 − **22**	− 15 − **35**
32.5°							− 13 + **2**	− 23 − **33**	−16 −**17**	− 37 − **22**	+ 10 − **27**	+ 7 − **30**
37.5°						−22 −**43**	+ 13 − **4**	+ 49 + **12**	+70 +**28**	+112 + **51**	+ 46 − **34**	+ 88 − **50**
42.5°					+ 40 − **20**	+99 −**38**	+ 91 − **10**	+ 61 + **17**	+50 +**20**	+151 − **68**	+ 24 − **27**	
47.5°					+131 − **8**	+76 −**26**	+127 − **15**	+121 − **94**	+69 −**35**	+ 20 + **1**		
52.5°			+108 + **23**	+ 53 − **10**	+182 − **31**	+76 + **5**	+142 − **34**	+ 94 + **6**				
57.5°			+325 −**106**	+297 −**104**	+141 − **43**	+55 − **1**						

Table 14. (continued)

	22.5°	17.5°	12.5°	7.5°	2.5°W	2.5°E	7.5°	12.5°	17.5°	22.5°	27.5°	32.5°E
57.5°N	+169 + **25**	+141 + **51**	+109 + **43**	+110 + **29**								
52.5°	+155 + **14**	+137 − **2**	+113 + **2**									
47.5°	+103 − **20**	+ 81 − **18**	+ 86 − **14**	+ 67 − **3**	+59 + **7**							
42.5°	+ 75 − **32**	+ 60 − **26**	+ 33 − **28**									
37.5°	+ 12 − **20**	+ 8 − **36**	+ 9 − **37**									
32.5°	− 2 − **26**	− 3 − **21**	− 3 − **43**									
27.5°	− 29 − **24**	− 26 − **28**										
22.5°	− 52 − **39**	− 44 − **53**										
17.5°	− 51 − **51**	− 29 − **49**										
12.5°	− 12 − **13**	− 2 − **5**										
7.5°	− 2 + **5**	+ 6 + **5**	+ 6 + **9**									
2.5°N	− 26 + **61**	− 12 + **78**	+ 1 + **51**	+ 2 + **14**	+13 +**15**	+ 3 +**14**	+ 4 +**10**					

Table 14. (continued)

	22.5°	17.5°	12.5°	7.5°	2.5°W	2.5°E	7.5°	12.5°	17.5°	22.5°	27.5°	32.5°E
2.5°S	− 58 + **62**	− 42 + **57**	− 33 + **78**	− 42 + **58**	+ 20 + **57**	+ 44 + **46**	+ 42 + **53**					
7.5°	− 62 + **62**	− 66 + **62**	− 59 + **64**	− 57 + **70**	− 74 +**114**	+ 17 + **71**	+ 48 + **55**					
12.5°	−144 +**119**	− 62 + **47**	− 68 + **66**	− 58 + **58**	− 58 + **66**	− 63 +**104**	+ 7 + **27**	+ 10 + **9**				
17.5°	− 82 + **38**	− 77 + **20**	− 62 + **54**	− 55 + **62**	− 53 + **62**	− 51 + **64**	− 32 + **31**					
22.5°	− 16 + **15**	− 25 + **1**	− 31 + **26**	− 43 + **41**	− 54 + **65**	− 58 +**110**	− 60 +**100**	− 46 + **50**				
27.5°	− 25 + **18**	− 16 + **15**	− 7 + **35**	− 16 + **34**	− 22 − **3**	− 37 + **52**	− 10 + **66**	− 28 + **91**				
32.5°	− 7 − **28**	+ 21 − **5**	− 6 − **1**	+ 17 − **15**	+ 21 − **3**	+ 1 + **16**	− 9 + **37**	+ 15 +**101**	− 3 + **74**	+ 80 + **18**	+ 84 + **78**	+ 38 + **29**
37.5°	+ 36 − **2**	+100 − **88**	+124 − **47**	+ 68 − **21**	+ 52 + **1**	+ 26 − **23**	+ 17 + **6**	+ 41 + **17**	+125 + **95**	+ 57 + **48**	+ 16 + **12**	+133 + **7**
42.5°			+ 52 − **14**	+154 − **68**	+ 70 −**150**	+107 − **58**	+148 −**116**	+143 − **43**	+248 − **35**	+107 + **33**	+ 92 + **60**	+199 − **3**
47.5°								+105 − **71**	+113 − **75**	+163 − **29**	+157 − **42**	+216 − **60**
52.5°												
57.°5												

Table 15. Computation Wind Stresses over the Atlantic Ocean—Annual Mean.

(τ_x and τ_y are given by the upper and lower figures, respectively, of each compartment, the unit being 10^{-2} dynes/cm^2).

	82.5°W	77.5°	72.5°	67.5°	62.5°	57.5°	52.5°	47.5°	42.5°	37.5°	32.5°	27.5°
57.5°N											+147 + 20	+187 + 36
52.5°									−146 − 8	+148 + 6	+141 + 14	+150 + 18
47.5°							+ 52 + 2	+ 83 − 6	+143 − 8	+135 + 20	+126 + 9	+114 + 11
42.5°				+39 −29	+71 −36	+72 −30	+ 51 − 13	+ 61 − 22	+108 − 15	+100 − 2	+ 91 + 7	+ 75 + 15
37.5°			− 30 − 34	+70 −42	+85 −27	+93 − 5	+ 85 + 9	+ 73 + 12	+ 51 + 20	+ 49 + 18	+ 41 + 6	+ 26 − 1
32.5°		+15 −22	+ 31 − 10	+45 − 4	+38 − 2	+39 + 3	+ 32 + 6	+ 29 + 6	+ 20 + 2	+ 18 + 4	+ 13 − 1	+ 5 − 9
27.5°	−24 −15	−13 −14	− 14 − 9	−11 − 9	− 5 − 3	− 6 − 3	− 8 0	− 11 − 3	− 21 − 2	− 17 − 3	− 19 − 9	− 24 − 20
22.5°	−32 −18	−45 −18	− 56 − 11	−57 − 3	− 2 − 6	−49 − 4	− 60 − 7	− 60 − 7	− 65 − 15	− 64 − 20	− 68 − 24	− 62 − 31
17.5°	−38 −15	−63 −20	− 58 − 16	−70 −10	−81 −11	−77 −12	− 82 − 17	− 87 − 15	− 76 − 21	− 78 − 25	− 93 − 34	− 72 − 47
12.5°	−38 −26	−79 −47	−124 − 30	−83 − 9	−65 −15	−82 −24	−107 − 37	−117 − 50	−103 − 46	− 82 − 45	− 97 − 49	− 53 − 36
7.5°						−52 −22	− 51 − 26	− 88 − 49	− 78 − 42	− 58 − 37	− 50 − 16	− 31 − 18
2.5°N								− 37 − 22	− 54 − 2	− 48 + 19	− 37 + 22	− 26 + 29

Table 15. (Contieued)

	82.5°W	77.5°	72.5°	67.5°	62.5°	57.5°	52.5°	47.5°	42.5°	37.5°	32.5°	27.5°
									− 67	− 69	− 54	− 55
2.5°S									+ **20**	+ **56**	+ **49**	+ **44**
											− 84	− 96
7.5°											+ **58**	+ **52**
										− 60	−114	−112
12.5°										+ **18**	+ **48**	+ **34**
										− 41	− 61	− 71
17.5°										− **2**	+ **3**	− **6**
										− 32	− 44	− 29
22.5°										− **27**	− **10**	− **10**
								− 15	− 27	− 21	− 19	− 12
27.5°								− **7**	− **22**	− **24**	− **18**	− **24**
							+ 6	+ 4	+ 21	+ 5	+ 22	+ 11
32.5°							+ **5**	− **21**	− **14**	− **16**	− **30**	− **51**
						− 4	+ 33	+ 92	+ 61	+ 69	+ 57	+ 92
37.5°						− **20**	+ **5**	+ **9**	**0**	− **3**	− **49**	− **55**
					+ 53	+ 66	+157	+ 94	+ 84	+119	+ 92	
42.5°					− **11**	+ **17**	+ **16**	+ **18**	− **11**	− **54**	− **64**	
					+116	+108	+118	+141	+137			
47.5°					+ **3**	− **28**	+ **9**	− **37**	− **39**			
				+116	+140	+ 78	+140	+105				
52.5°				+ **13**	+ **21**	**0**	− **44**	− **66**				
			+204	+197	+128	+ 80						
57.5°S			− **50**	− **52**	− **15**	− **34**						

Table 15. (continued)

	22.5°	17.5°	12.5°	7.5°	2.5°W	2.5°E	7.5°	12.5°	17.5°	22.5°	27.5°	32.5°E
57.5°N	+157 + **35**	+147 + **39**	+114 + **45**	+97 +**33**								
52.5°	+139 + **25**	+128 + **13**	+106 + **9**									
47.5°	+105 + **3**	+ 82 − **2**	+ 79 − **2**	+63 + **4**	+47 + **6**							
42.5°	+ 76 + **1**	+ 63 − **14**	+ 34 − **31**									
37.5°	+ 22 − **14**	+ 6 − **33**	+ 8 − **40**									
32.5°	0 − **23**	− 11 − **33**	− 6 − **49**									
27.5°	− 35 − **36**	− 36 − **43**										
22.5°	− 56 − **50**	− 46 − **60**										
17.5°	− 52 − **57**	− 28 − **56**										
12.5°	− 32 − **38**	− 5 − **15**										
7.5°	− 6 + **6**	+ 7 + **13**	+ 8 + **14**									
2.5°N	− 15 + **33**	− 7 + **42**	− 8 + **45**	0 +**32**	0 +**30**	+ 4 +**28**	+ 6 +**25**					

Table 15. (continued)

	22.5°	17.5°	12.5°	7.5°	2.5°W	2.5°E	7.5°	12.5°	17.5°	22.5°	27.5°	32.5°E
2.5°S	− 52 + **47**	−46 +**55**	− 29 + **60**	− 35 + **56**	+ 3 +**58**	+ 7 + **40**	+ 20 + **39**					
7.5°	− 68 + **64**	−64 +**59**	− 75 + **73**	− 59 + **78**	−58 +**82**	− 48 + **79**						
12.5°	−115 + **70**	−81 +**57**	− 69 + **56**	− 71 + **70**	−54 +**62**	− 63 + **95**	− 16 + **62**					
17.5°	− 83 + **19**	−73 +**17**	− 72 + **46**	− 48 + **44**	−56 +**55**	− 80 + **84**	− 73 + **86**					
22.5°	− 27 − **2**	−35 +**13**	− 46 + **33**	− 64 + **56**	−49 +**46**	− 61 + **73**	− 70 +**105**	− 32 +**102**				
27.5°	− 12 − **17**	− 8 − **9**	− 8 + **22**	+ 2 + **35**	−26 +**15**	− 32 + **51**	− 27 + **67**	− 41 + **97**				
32.5°	+ 6 − **46**	+18 −**18**	+ 7 **0**	+ 28 + **12**	+31 +**31**	+ 22 + **13**	+ 2 + **39**	+ 6 + **78**	+ 2 + **48**			
37.5°	+ 60 − **58**	+82 −**67**	+ 76 − **42**	+ 83 − **51**	+87 −**18**	+ 79 − **13**	+ 69 − **2**	+ 90 + **19**	+ 93 + **27**	+65 +**25**	+35 +**17**	+ 71 + **11**
42.5°			+102 − **41**	+160 − **63**	+97 −**79**	+115 − **62**	+142 − **87**	+151 − **51**	+218 − **36**	+98 − **6**	+97 +**10**	+ 98 − **30**
47.5°												+152 − **76**
52.5°												
57.5°S												

Reco ds of Oceanographic Works
in Japan Vol. 4, No. 2,
March 1958

On the Seasonal Variations of Surface Divergence of the Ocean Currents in Terms of Wind Stresses over the Oceans

By
Koji Hidaka and Kiheiji Ogawa
(Geophysical Institute, University of Tokyo)

Abstract

Seasonal variations of divergence of the surface currents are discussed in terms of wind stresses after the method employed by one of the authors, a complementary note being added.

1. Introduction

The transport of water due to the prevailing wind system over the North Atlantic was computed by R. B. Montgomery (1936a, b) use being made of C.-G. Rossby's theory of air-sea boundary. This problem lead necessarily to the computation of upwelling and sinking of water in the surface layer of the sea. In a previous paper, one of the authors (Hidaka, 1955) derived a relation representing the divergence of surface drift vectors in terms of wind stresses with a simple assumption, and obtained the chart of divergence areas for the whole Pacific Ocean. Here it must be mentioned that the chart he got will be correct in the most part of the ocean, although some point to correct was found concerning sign in his final expressions.

In this paper, the authors extend the computation to the three oceans and discuss the seasonal changes of surface divergence patterns, use being made of the data of wind stresses partly complied at the Scripps Institution af Oceanography for the North Pacific and partly computed by Hidaka for the remaining oceans from the Pilot Charts of U. S. Navy Hydrographic Office which provide us with sufficient data of monthly and quarterly wind roses. (Hidaka, 1958)

2. Relation between the wind stresses and the divergence of surface water of the sea

As previously stated, Hidaka has derived a relation between the wind stresses and the divergence of surface water of the sea with a simple assumption. He assumes an ocean of uniform density and uniform depth, and starts with the following dynamical equations:

$$\frac{\mu}{\rho}\frac{\partial^2 u}{\partial z^2}+2\omega\sin\varphi v-g\frac{\partial\zeta}{\partial x}=0\,,\qquad \frac{\partial u}{\partial x}+\frac{\partial v}{\partial y}+\frac{\partial w}{\partial z}=0 \tag{1}$$

$$\frac{\mu}{\rho}\frac{\partial^2 v}{\partial z^2}-2\omega\sin\varphi u-g\frac{\partial\zeta}{\partial y}=0\,,$$

where x is eastward positive, y northward positive, z downward positive and u and v are horizontal components of current velocity in x and y directions respectively, ζ the elevation of the sea surface, μ the coefficient of vertical eddy viscosity, ω the angular velocity of the earth's rotation and ρ the geographic latitude. Further we have the following boundary conditions

$$z=0:\ -\mu\frac{\partial u}{\partial z}=\tau_x\,;\ -\mu\frac{\partial v}{\partial z}=\tau_y\,,\ w=0\,;\ z=h:\ u=v=w=0\,,$$

where τ_x and τ_y are the wind stress components in x and y directions, w the vertical component of current velocity.

Then, after some reductions he obtains the following expression:

$$\left(\frac{\partial u}{\partial x}+\frac{\partial v}{\partial y}\right)_{z=0}=\frac{\mathrm{div}\,\tau+\mathrm{curl}_z\,\tau}{2\sqrt{\rho\omega\sin\varphi\mu}}+\frac{\tau_x-\tau_y}{4\sqrt{\rho\omega\sin\varphi\mu}}\cdot\frac{\cot\varphi}{R}$$
$$+\frac{\mathrm{curl}_z\,\tau}{2\rho\omega\sin\varphi h}-\frac{\tau_x}{4\rho\omega\sin\varphi h}\cdot\frac{\cot\varphi}{R}\,.$$

Since the depth of the sea h is sufficiently large, we can neglect the last two terms in the right hand side of the above equation except at or close to the Equator. Thus we have for the northern hemisphere the following expression:

$$\left(\frac{\partial u}{\partial x}+\frac{\partial v}{\partial y}\right)_{z=0}=\frac{\mathrm{div}\,\tau+\mathrm{curl}_z\,\tau}{2\sqrt{\rho\omega\sin\varphi\mu}}+\frac{\tau_x-\tau_y}{4\sqrt{\rho\omega\sin\varphi\mu}}\cdot\frac{\cot\varphi}{R}\,. \tag{2}$$

Likewise, for the southern hemisphere we have the following one:

$$\left(\frac{\partial u}{\partial x}+\frac{\partial v}{\partial y}\right)_{z=0}=\frac{\mathrm{div}\,\sigma-\mathrm{curl}_z\,\tau}{2\sqrt{\sigma\omega\sin|\varphi|\mu}}+\frac{\tau_x+\tau_y}{4\sqrt{\rho\omega\sin|\varphi|\mu}}\cdot\frac{\cot|\varphi|}{R}\,. \tag{3}$$

These relations (2, 3) are the results obtained by him. Of course, these expressions cannot be used at or close to the Equator. For the variation of a long period like seasonal, accerelation terms in the dynamical equations may be neglected; hence we can use these relations for the discussion of the seasonal variation.

3. Application to the three oceans

In order to determine the distribution of monthly and quarterly wind stresses over the entire oceans except one for the North Pacific the computation of which was already made at the Scripps Institution of Oceanography, the pilot charts published by the U. S. Navy Hydrographic Office have been available which provide us with necessary and sufficient data for the oceans at an interval of 5 degrees

in both latitudes and longitudes. Further, the formula by W. MUNK has been adopted for the determination of the wind stresses. (HIDAKA, 1958)

For the application of the results to the oceans let the four points at which the wind stresses are given be denoted by 1, 2, 3 and 4, and the center of the rectangular area with these four points at its corners be given by (λ, φ) and let these coordinates be given, respectively, by

$$\begin{array}{llll} ① & |\varphi|\pm 2.5°, & |\lambda|\mp 2.5° & ② \quad |\varphi|\pm 2.5°, \quad |\lambda|\pm 2.5° \\ ③ & |\varphi|\mp 2.5°, & |\lambda|\pm 2.5° & ④ \quad |\varphi|\mp 2.5°, \quad |\lambda|\mp 2.5° \end{array}$$

Then, the expressions (2, 3) are reduced to the following:

$$\begin{aligned} \left(\frac{\partial u}{\partial x}+\frac{\partial v}{\partial y}\right)_{z=0} = \Bigg[& \left\{ \frac{\tau_x②+\tau_x③}{2} - \frac{\tau_x①+\tau_x④}{2} + \frac{\tau_y①+\tau_y②}{2} \cos(|\varphi|\pm 2.5°) \right. \\ & - \frac{\tau_y③+\tau_y④}{2} \cos(|\varphi|\mp 2.5°) \pm \frac{\tau_y②+\tau_y③}{2} \mp \frac{\tau_y①+\tau_y④}{2} \mp \frac{\tau_x①+\tau_x②}{2} \\ & \left. \times \cos(|\varphi|\pm 2.5°) \pm \frac{\tau_x③+\tau_x④}{2} \cos(|\varphi|\mp 2.5°) \right\} \frac{36}{\pi \cos\varphi} \\ & + \frac{1}{2} \left\{ \frac{\tau_x①+\tau_x②+\tau_x③+\tau_x④}{4} \mp \frac{\tau_y①+\tau_y②+\tau_y③+\tau_y④}{4} \right\} \frac{\cot|\varphi|}{R} \Bigg] \\ & \times \frac{1}{2\sqrt{\rho\omega \sin|\varphi|\mu}} . \end{aligned} \qquad (2', 3')$$

where the upper and lower signs refer to the northern hemisphere and the southern hemisphere respectively.

The value of the eddy viscosity μ was taken to be 400 (in c.g.s. unit) throughout all the computation.

Thus, quarterly and annual values as well as figures are obtained of divergence of surface water for the Pacific, the Indian and the Atlantic Oceans, use being made of the equations (2′, 3′).

The results are shown at the end of this paper in the Tables 1–15 and Figures 1–15.

For the computation of these values, however, it must be remarked that we regarded the distribution of monthly wind stresses in the middle of a season (January, April, July and October) as representatives of the season for the **North Pacific** and the **Indian Oceans**.

4. Seasonal variations of surface divergence and convergence induced by ocean currents

When we consider the general features of the wind system, we can expect a zone of convergence of surface water near 20° to 30°N, and divergence at lower and higher latitudes.

Now, let us see the variations of the divergence and convergence of the surface wind driven currents.

(1) The Pacific Ocean (Refer to **Figs. 1 to 5**)

(A) The North Pacific

Generally speaking, the distribution of divergence and convergence are as follows: The central part of the ocean is an area of weak convergence containing divergence areas in it. The intensity of convergence increases greatly towards the south and is much stronger in the eastern part of the ocean in a belt centered at 5°N. Strong divergences also exist in the same belt. In the northern part 40°N to 50°N, there appear sometimes wide divergence areas, convergence again existing north of them.

Now let us describe briefly their seasonal variation below.

In the belt of about 5°N, in autumn strong convergences exist, being much stronger in the eastern part (max. int. −700 at 5°N125°W) and weaker in the western part (max. int. 50). In winter, strong convergences exist as before in the eastern part (max. int. −600 at 5°N145°W) and divergences appear in the western part (max. int. −250). In spring, convergence exists almost in all the region (max. int. −150 at 5°N135°W). In summer, convergences exists almost in all the region and is stronger in the eastern part (max. int. −500 at 5°N145°W, 5°N125°W and 5°N115°W).

In the wide area centered at 25°N, there is a weak convergence which contains relatively small divergence areas varying with seasons.

In the northern part 40°N to 50°N, in autumn divergence area exists (max. int. 50) in the eastern part and in the sea off Japan. In winter a belt of divergence is formed across the ocean (max. int. 100 at 40°N, 155°E). In spring it disappears, and in summer weak and considerably wide divergence areas appear in a state cut into pieces.

Thus, it may be said that the activity of surface divergence due to the Ekman drift currents is more intense in autumn and winter in the North Pacific.

(B) The South Pacific

Here, a more detailed study will be made for the variation of surface divergence. Taking the distribution of wind velocities into account.

Of course, the discussions must be made under consideration of the correspondence to the seasonal variation of wind distribution. So, first the main features are given here concerning the seasonal variation of wind distribution briefly.

Generally speaking, patterns of wind vectors show fluctuations in northsouth direction, deviating farthest to the north in southern winter and to the south in southern summer respectively.

Next, some main characteristics in them are shown for every seasons.

March, April, May: Region of doldrum is seen in lat. 5° to 10°S, long. 120°E

to 140°W, where very weak east wind blows. Trade wind is found in belts of lat. 15° to 30°S, long. 145°E to 140°W and of lat. 5° to 25°S, long. 145°W to 75°W, where east wind blows. Westerlies exist in a belt of lat. 45° to 50°S, where very strong west wind blows, strongest in a region near long. 135°W. Subtropical anticyclones which have very complicated patterns of very weak wind vectors are seen between the trade winds and westerlies.

June, July, August: Total patterns have the tendency to shift to the north. Trade winds stronger than in the former season exist in a belt near 10°S, where east-south wind blows. Westerlies seem to exist near the band centering at 45°S, stronger in the region of long. 125°E to 170°W, where north-west winds turn to west winds as a longitude increases. They deviate northward to 30°S in a region of long. 170°W to 145°W. They become weak in long. 140°W to 80°W and, very complicated patterns appear there. Subtropical anticyclones exist between them where wind vectors are very weak.

September, October, November: The patterns in this season are mostly manifest among the figures representing wind vectors in every season. The patterns have much similarity to those in the season March, April and May.

December, January- February: Most extraordinaries appear in wind distribution. These are seen in the regions near the eastern coast of Australia; i.e., trades in the region of lat. 5° to 10°, long. 145°E to 160°E consists of very strong east winds. Westerlies in the region of lat. 35° to 45°S, long. 140°E to 160°E are also very strong ones which blow from south-west, the direction of the wind deflecting from the mean westerlies blowing to the east. Also, in this season general patterns shift farthest to the south.

Next, local character as well as general will be considered concerning to the seasonal variations of divergence of surface currents in the South Pacific.

General characters: First, we see that in the South Pacific the patterns of divergence and convergence areas are not so manifest as those in the North Pacific as to the construction of equatorial divergence, subtropical convergence, divergence in sub-arctic region and convergence in arctic region. This is due to the wind action such as doldrum, trade winds, subtropical anticyclones, westerlies and others. From the Figs. 1, 2, 3, 4 and 5, it may be concluded that divergence and convergence regions can be traced in their changes of intensity and location from season to season, and divergences as well as convergences seem to begin their shift to the north in southern autumn in the eastern half of the ocean, to lie farthest to the north in southern winter, to begin their return in southern spring, and to recover their original disposition once more in southern summer, thus completing one cycle in a year.

Local characters: Comparison of the figures representing surface divergence in each season with the annual mean shows that the seasonal variation is very re-

markable in the ocean considered. Below, some descriptions concerning the shifting, appearance, and disappearance of strong divergences, will be made.

From southern summer to southern autumn: Extraordinary strong divergence near 160°E, 15°S in southern summer decreases its intensity and moves to the region neor 155°E, 15°S in southern autumn, its original position being occupied by relatively strong convergence. Very strong convergence near 155°E, 20°S in southern summer vanishes in southern autumn. Strong divergence near 160°E, 30°S shifts to the region near 160°E, 25°S, decreasing its intensity, and its original position is replaced by convergence. Strong divergence near 155°E, 40°S vanishes. Relatively strong divergence near 135°E to 155°E, 45°S changes to weak convergence, leaving weak divergence in the region 140°E, 40°S. Large weak divergence zone near 175°E to 145°W, 20°S increases its intensity generally. Strong divergence near 165°E to 180°E, 50°S vanishes, being left only in the region near 180°W, 45°S. Strong convergence near 170°W, 45°S approximately holds its position and intensity. Convergence in about 160°W, 45°S nearly holds its position increasing its intensity. Weak divergences near 165°W, 35°S and near 160°W, 50°S change into strong divergence near 165°W, 40°S. Two strong convergences near 145°W to 130°W, 50°S increase their intensities and shift slightly eastward. Divergence near 140°W, 45°S holds its position increasing its intensity. Strong convergence near 135°W, 10°S much weakens its intensity. Wide divergence area near 125°W to 80°W, 10°S disintegrates to pieces, decreasing its intensity. Weak divergence near 130°W, 35°S changes into a comparatively strong one. Strong divergence near 125°W, 50°S seems to move to the region of 120°W, 45°S. Strong convergence pattern near 110°W to 95°W, 40°S to 50°S, moves to the north to the region near 120°W to 95°W, 30°S to 45°S. Also strong divergence region near 110°W to 80°W, 45°S to 55°S shifts to the north to the region 110°W to 80°W, 45°S to 55°S.

Generally speaking, in the sea off eastern, north-eastern and south-eastern coasts of Australia, divergence and convergence are very active in southern summer, but in the central portion of the ocean activities of divergence and convergence in southern autumn are comparable to or greater than in southern summer.

From southern autumn to southern winter: Generally speaking, modification of patterns is remarkable. Wide weak divergence area near 165°E to 145°W, 15°S seems to shift to the north, to disintegrate into strips of divergence and convergence. Convergence near 170°W, 30°S seems to move to the region near 170°W, 25°S. Convergence region near 155°E to 180°E, 35°S changes to divergence. Convergence near 165°E, 45°S seems to move to the region 170°E, 40°S, its original position being occupied by relatively strong divergence. Strong divergence near 165°W, 40°S holds its position and intensity. Convergence strip extending in the north-south direction along 135°W, having its stronger intensity about 45°S, seems

to remove to the north-west to the location near 150°W, 30°S. Divergence near 120°W, 45°S holds its position increasing its intensity and area. Convergence near 100°W, 10°S seems to shift to the region of 115°W, 10°S, increasing its intensity and extending to the south, its original position being occupied by strong divergence. Convergence area near 120°W to 100°W, 30°S to 45°S holds nearly its position changing its pattern slightly. Divergence area near 105°W to 80°W, 50°S shifts to the north, and large convergence zone near 95°W, 30°S shrinks into a relatively small one.

From southern winter to southern spring: Generally the change of patterns from southern winter to southern spring shows a shift to the south. Remarkable similarities can not be seen between the patterns in southern spring and those in southern autumn. Divergence near 160°E, 15° to 30°S changes to convergence. Convergence near 165°E to 175°W, 40°S removes to the region near 170°E, 45°S. Divergence near 165°W, 40°S and convergence near 155°W, 45°S seem to shift to the south-west. Divergence near 150°W, 45°S holds its position decreasing its intensity. Again in southern spring the convergence strip can be seen at the longitudes 140°W to 145°W, and is stronger near 45°S. Divergence strips near 165°E to 165°W, 15°S and divergence near 145°W, 15°S expands to the south. Strong convergence near 115°W, 10°S and strong divergence near 105°W, 10°S vanish. Strong convergence near 110°W, 40°S seems to remove to the south to the region near 110°W to 95°W, 45°S. Relatively large divergence area near 110°W 80°W, 40°S to 55°S is seen to shift to the south.

From southern spring to southern summer: A general shift of the pattern to the south is seen. In the region of weak convergence near 155°E to 160°E, 15°S to 40°S, there appear very strong divergences and convergences, and these are most remarkable in their seasonal variation. Removal of divergence area near 165°E to 160°W, 15°S to the south is remarkable. Convergence near 170°E, 45°S varies to weaker one near 175°E, 45°S. Divergence near 180°W, 50°S holds its position. Convergence near 170°W, 50°S becomes stronger, deviating slightly to the north. Convergence near 140°W, 10°S extends its intensity and area to the south. Wide divergence area in the sea near the western coast of South America at about 10°S elongates to the west to 130°W in southern summer. Strong convergences near 145°W, 45°S and near 130°W, 40°S seem to change into a more active one near 145°W to 135°W, 50°S. Convergence near 110°W to 90°W, 45°S seems to deviate to the north slightly, becoming more active.

Other more complicated changes in seasonal variation are to be seen from the figures.

(2) **The Indian Ocean** (Refer to Figs. 6 to 10)

The main features of the patterns are as follows: There are a convergence

belt centering at about 30°S, and divergence belts to its north and south, shifting to north and south, farthest to the north in summer, farthest to the south in winter.

Considerable variations in their patterns and intensities can be perceived in the annual cycle. Below we will describe these briefly.

The divergence region in spring (max. int. 50) near the station 55°E10°N off Arabia becomes much stronger in summer (max. int. 500), becomes convergent in autumn and becomes stronger in winter (max. int. −200). The strong divergence in spring (max. int. −350) near the station 7°E, 5°N south-east off the Decan Highland varies to strong convergence in summer (max. int. −750), becomes divergent again in autumn, its maximum locating off the south end of the Decan Highland (max. int. +500) and becomes divided into two parts, the strong divergence near the station 65°E, 50°N (max. int. 200) and the strong convergence near the station 75°E, 5°N (int. −200) in winter. The divergence around the station 85°E, 5°N south-east off the Decan Highland in spring (int. 50∼100) becomes strongest in summer (max. int. 600), is located off the south end of the Decan Highland (max. int. 500) in autumn, and recovers its original position, becoming weaker in intensity (max. int. 100) in winter.

For the southern hemisphere, we have several strong divergences in a divergence belt around lat. 10°S. Here, the strongest divergences appear in summer at two locations 55°E, 5°S (500), and 75°E, 5°S (500), the activity being apparently weakest in winter. They move somewhat a little in duration season to season. Convergences in the same belt are a few at all the seasons with maximum −700 at about 45°E, 5°S in autumn.

A large area around lat. 30°S is dominated by weak convergence, which involves several relatively strong divergence vortices varying in a rather complicated way. It is seen that the activity is more intense (max. 200) in summer and autumn.

In a divergence zone around lat. 45°S, we have several relatively strong divergences with maximum 250 in summer, the activity being more intense in the same season. Their movements are relatively small throughout all the seasons.

(3) **The Atrantic Ocean** (Refer to Figs. 11 to 15)

Let us will first describe the general feature. There are a divergence belt of weak intensity in the western part of the ocean near 40°N to 50°N, a weak convergence zone (max. int. -75×10^{-9}) on the south of it to about lat. 15°N, a divergence belt near lat. 10°N varying considerably in its intensity (max. int. $50\sim100\times10^{-9}$) according to the season, a strong convergence belt near 5°N, a convergence region near 5°S (max. int. -50×10^{-9}) which disappears from time to time, a strong divergence belt in 5°S to 20°S (max. int. $250\sim300\times10^{-9}$), a wide convergence belt to the south of it about lat. 40°S containing many divergence vortices, and there

seems to be a divergence belt to its south.

As for their seasonal variations, we may say that the patterns are not likely to vary strongly at all the seasons on the whole, but there are considerable variations concerning their intensity and location. We shall now briefly describe these main features.

The divergence belt near 50°N to 40°N (max. int. 25×10^{-9}) converges in autumn to the neighbourhood of about 50°N, 40°W, showing maximum intensity of about 75×10^{-9}.

The convergence belt near 30°N is relatively weak (max. int. -25×10^{-9}), but becomes stronger in spring and autumn (max. int. -75×10^{-9}).

The divergence belt near 10°N is stronger in winter (max. int. 75×10^{-9}) spring (max. int. 100×10^{-9}).

The convergence region near 5°N is very strong at all seasons, and is strongest in summer (max. int. -300×10^{-9}) and autumn (max. int. -400×10^{-9}).

In the divergence belt near 10°S, there is a strong divergence (max. int. 250×10^{-9}) at all the seasons off the western coast of Africa close to the Equator, and it moves a little to the west in the winter.

In the region near 20°W, 10°S, there appears a relatively strong divergence vortex in summer and autumn (max. int. 100×10^{-9}). Also off the eastern coast of South America in about 5°S to 10°S, there appears a strong divergence (max. int. 150×10^{-9}) in summer and autumn which moves a little to the north in the latter season.

The convergence belt near 30°S is relatively weak most of the seasons, but there appear strong convergences (max. int. $-75\sim-100\times10^{-9}$) in summer, autumn and winter, in the regions near 10°W to 20°W, 40°S and 0°EW, 20°S.

A permanent strong divergence in the region near 40°S to 50°S, 50°W becomes strongest in summer (max. int.200×10^{-9}).

A permanent convergence south of the south end of Africa becomes stronger in summer and autumn (max. int. -100×10^{-9}).

5. Supplementary Notes

So far, we have discussed the seasonal variation of divergence of surface drift currents, or the Ekman currents. Hence and also, it would be misleading to say much of the detailed patterns of divergence in the discussion, partly because of the rough distribution of wind stresses at an interval of 5 degrees and partly because of the neglect of pressure gradients for the formation of which thermodynamical processes, meridional boundaries and the β effect are responsible. To our regret, we have little understanding of the problem: What would be the situation in case when these pressure field is taken into account? Apart from the obscure character

of mixing and diffusion in the ocean at present, it is essentially due to the non-linear character of the problem that we have been hindered from the better understanding of it. Moreover, even if making compromise with it, we are still bothered by the existence of both the meridional boundaries peculiar to the ocean and the β effect. (Leneykin 1955, Stommel and Veronis 1957).

The current fashion to avoid this difficulty for convenience sake, is to accept the density field as it really is in a theoretical computation. In spite of this compromise, however, we shall necessarily encounter with the difficulty in determining the pressure gradients (Hidaka 1955, Stommel 1956a). But now, the resent works carried by Stommel *et al* have revealed fairly intense baroclinicity in the ocean current in the central ocean for a long period variation. Thus, the usual dynamic computation will be justified for our discussion.

Now, the annual or quarterly pressure gradients *in situ* being included, it is easy to derive an expression for the surface divergence in the same dynamical system as (1) as follows

$$\left(\frac{\partial u}{\partial x}+\frac{\partial v}{\partial y}\right)_{z=0}=\text{Expression (2)}-\frac{1}{2\sqrt{\rho\omega\sin\varphi\mu}}\left[\int_0^a \nabla_H{}^2 p\cdot e^{-a\xi}(\cos a\xi-\sin a\xi)\,d\xi\right.$$
$$\left.+\frac{\cot\varphi}{2R}\int_0^a\left(\left[\frac{\partial p}{\partial x}-(2a\eta+1)\frac{\partial p}{\partial y}\right]\cos a\eta+\left[(2a\eta+1)\frac{\partial p}{\partial x}+\frac{\partial p}{\partial y}\right]\sin a\eta\right)e^{-a\eta}d\eta\right], \tag{4}$$

where

$$a=\sqrt{\frac{\rho\omega\sin\varphi}{\mu}} \qquad \text{and} \qquad \nabla_H{}^2=\frac{\partial^2}{\partial x^2}+\frac{\partial^2}{\partial y^2},$$

and it is assumed that the depth of the sea is many times as large as the Ekman's depth.

The last term in the right-hand side of the expression (4) is certainly capable of computation from observational data in the ocean and is nothing but the correction terms to the expression (2), which include all the thermodynamical effects such as evaporation and precipitation at the sea surface.

Now, it will be especially convenient for the present purpose if there is any relationship between the actual density structure and the wind stress at that place throughout the ocean. In this connection, we remind ourselves of the model proposed by R. O. Reid (1948). We may well apply this model in the Pacific at least in case when the region considered is from close to the Equator to the North Equator and it is regarded as nearly steady.

The application of this model with adequate approximation to our problem leads for the surface divergence to the expression

$$\left(\frac{\partial u}{\partial x}+\frac{\partial v}{\partial y}\right)_{z=0}=\text{Expression (2)}-\frac{1}{\rho\omega\sin\varphi}\cdot\frac{\cot\varphi}{R}\cdot\frac{1}{5h}(\tau_x+R\tan\varphi\,\text{curl}\,\tau), \tag{5}$$

and for the vertical velocity at the interface $z=h$ to the expression

$$w_h \approx -\frac{3\beta}{5\rho f^2}\left(\tau_x + \frac{f}{\beta}\mathrm{curl}_z\tau\right). \qquad (6)$$

These results, of course, agree well with that by ICHIYE (1955). In usual circumstances, referred to the eqs. (2) and (5), this model leads to the error of about 50% for τ_x and 25% for $\mathrm{curl}_z\tau$ at the largest. We shall arrive at the similar result when we adopt the two-layered complete baroclinic ocean as the model.

In larger part of the oceans, $\mathrm{curl}_z\tau$ is most responsible among the wind actions involved in (5) and (6). Hence, surface divergence necessarily and sufficiently will induce upwelling at the internal boundary in general at least so long as we adopt this model.

Generally, however, there will be no doubt that we should not expect such a simple model for describing relation between the wind and the pressure fields in the actual oceans.

The problem to examine the effect of pressure field to the surface divergence is left unsolved in the future study.

6. Conclusions

From the preceding discussions following conclusions are obtained.

(1) The expressions (2, 3) which represent the relation between surface divergence of ocean current and wind stress distribution seem to be reliable for the discussion of seasonal variation of surface divergence from the wind stress distribution. But, of course a more detailed analysis is left for consideration of correction terms to the expressions (2, 3).

(2) Surface divergence induced by wind seems to be mainly caused by the effect of wind stress vorticity. Hence, strong surface divergence may necessarily and sufficiently induce upwelling at the interface in the oceans, at least in the equatorial region of the Pacific.

(3) The seasonal variation of surface divergence and convergence is generally remarkable.

(4) On the whole, some regularity is seen in the seasonal variation of surface divergence, in other word, approximately in the wind stresses vorticity. Of course, this is due to the regular fluctuation in the distribution of wind velocity in the north-south direction in its annual cycle.

Acknowledgements

This research has been partly financed by the funds of the Japanese National Commission for Unesco, to which the authors wish to express their sincerest thanks,

References

ICHIYE, Takashi (1955) A short note on the vertical current in the ocean. Oceanogr. Magazine, **7** (1): 49–54.

HIDAKA, Koji (1955) Divergence of surface drift currents in terms of wind stresses, with special application to the location of upwelling and sinking. Japanese Journal of Geophysics, **1** (2): 47–56.

HIDAKA, Koji (1957) Influence of Friction on Geostrophic Flow: Sources of Errors in Dynamic Computation of Ocean Currents. Journ. Oceanogr. Soc. Japan, **13** (2): 1–3.

HIDAKA, Koji (1958) Computation of Wind Stresses over the Oceans. Records of Oceanographic Works in Japan **4** (2):

LENEYKIN, P. C. (1955) DOKLADY SSSR AKAD. Nauk, 101, pp. 461.

MONTGOMERY, R. B. (1936a) Transport of surface water due to the wind system over the North Atlantic. Pap. in Phys. Oceanogr. and Meterology, **4** (3): 23–30.

——— (1936b) Computation of the transport of surface water due to the wind-system over the North Atlantic. Amer. Geophys. Union Trans. Seventeenth Annual Meeting; 225–229.

STOMMEL, Henry (1956) On the determination of the depth of no meridional motion. Deep Sea Res., **3**, pp. 273–278.

——— (1957) A Survey of Ocean Current Theory. Deep-sea Research **4** (3): 149–184.

STOMMEL, Henry and G. VERONIS (1956) The action of variable wind stresses on a stratified Ocean. J.M.R., **15** (1): 43–75.

——— (1957) Steady convective motion in a horizontal layer of fluid heated uniformly from above and cooled non-uniformly from below. Tellus **9** (3): 401–407.

YOSHIDA, Kozo (1955) Coastal upwelling off the California coast. Records of Oceanogr. Works in Japan, **2** (2): 1–13.

Fig. 1. Distribution of Divergence and Convergence Areas in the Pacific Ocean (Unit: mg/m³/sec).
Northern Winter (Shaded Areas show the Divergence Zones).

Fig. 2. Distribution of Divergence and Convergence Areas in the Pacific Ocean (Unit: mg/m³/sec).
Northern Spring (Shaded Areas show the Divergence Zones).

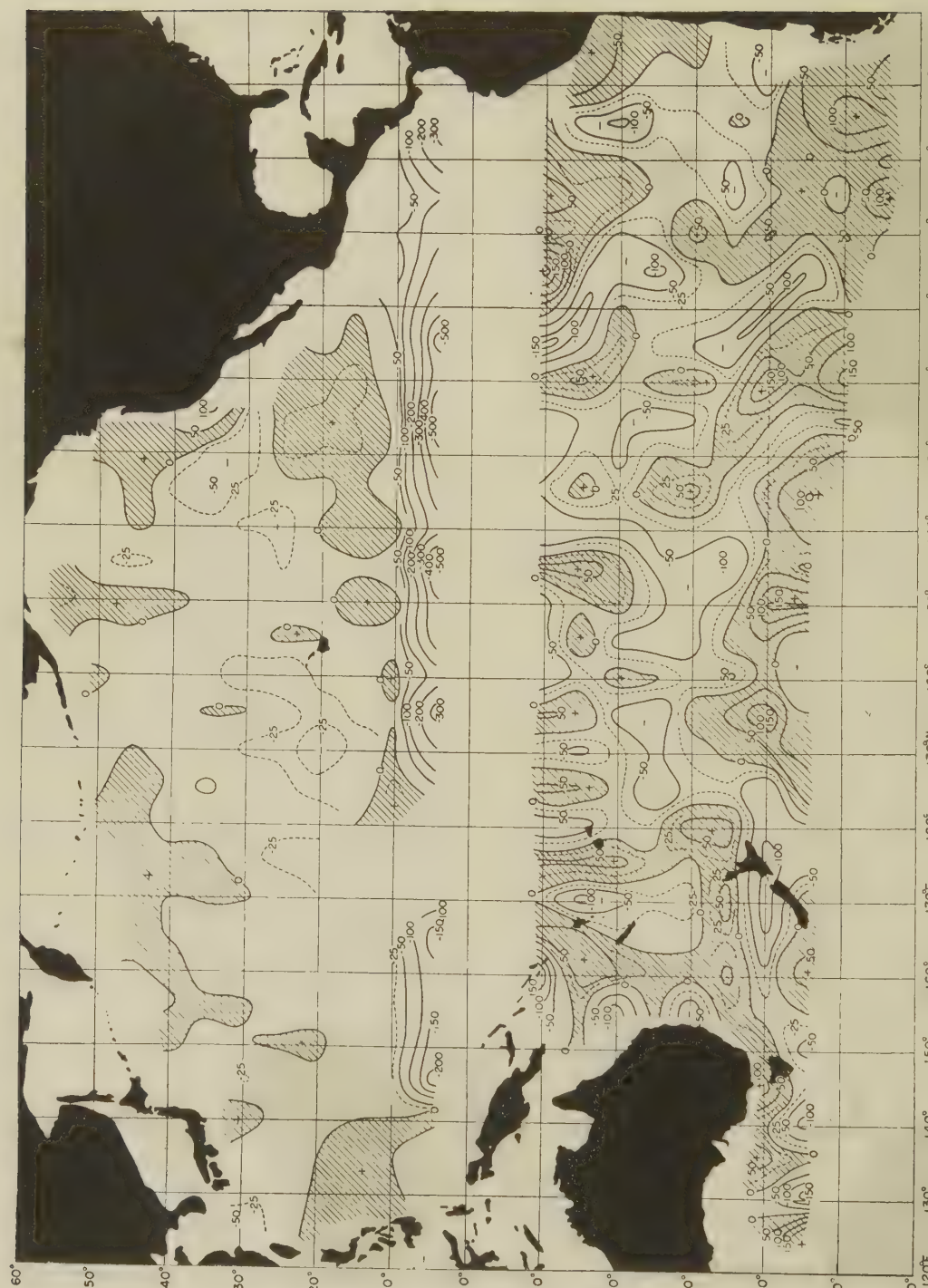

Fig. 3. Distribution of Divergence and Convergence Areas in the Pacific Ocean (Unit: mg/m³/sec).
Northern Summer (Shaded Areas show the Divergence Zones).

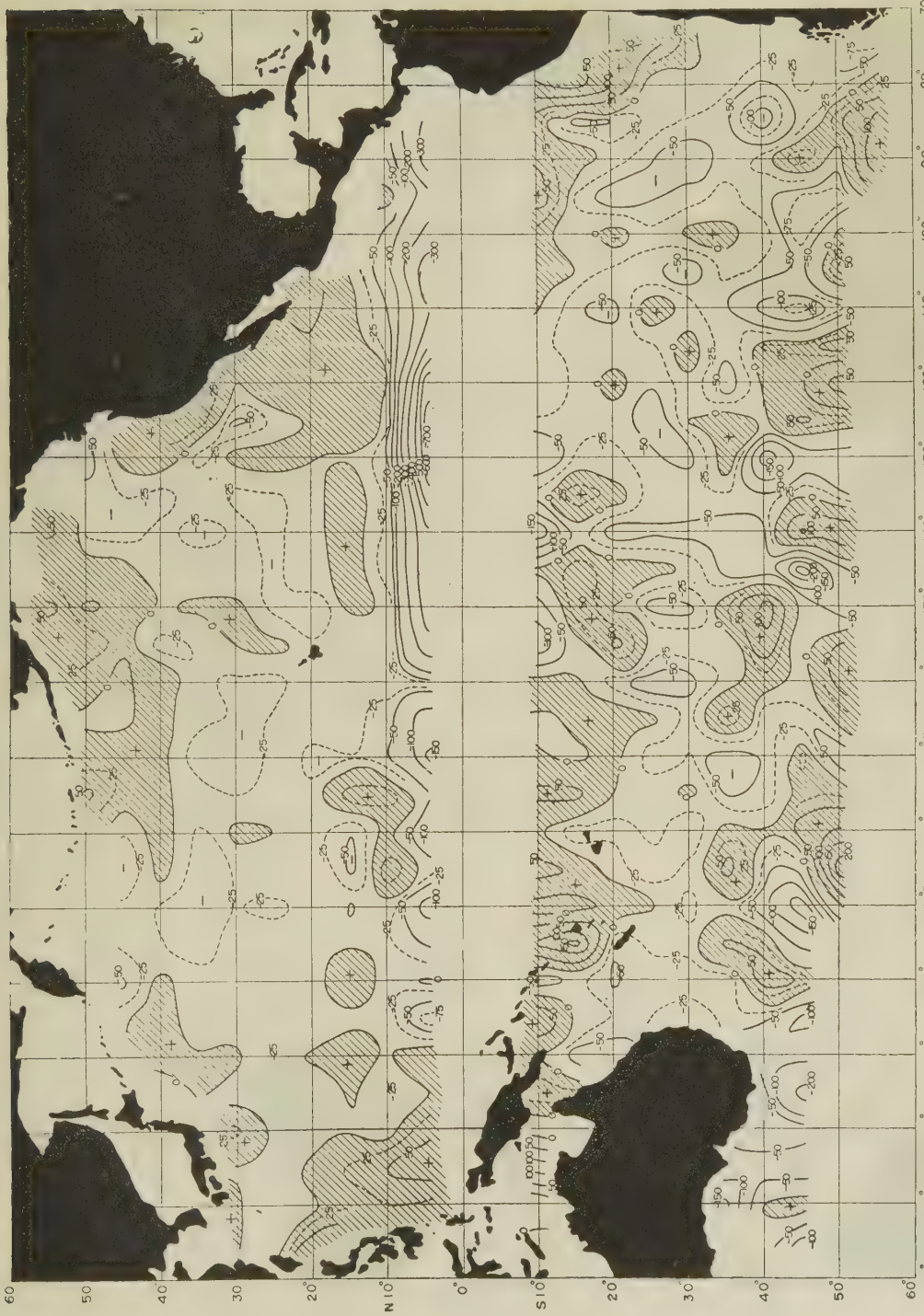

Fig. 4. Distribution of Divergence and Convergence Areas in the Pacific Ocean (Unit: mg/m³/sec).
Northern Autumn (Shaded Areas show the Divergence Zones).

Fig. 5. Distribution of Divergence and Convergence Areas in the Pacific Ocean (Unit: mg/m³/sec).
Annual Mean (Shaded Areas show the Divergence Zones).

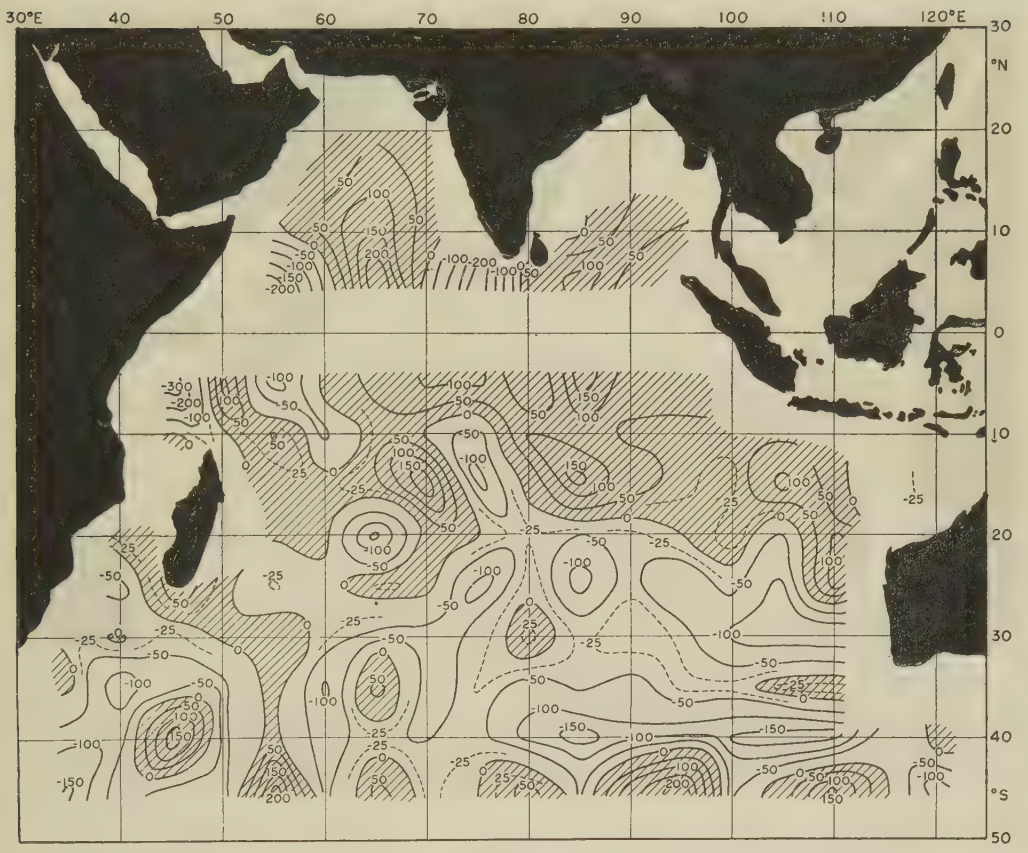

Fig. 6. Distribution of Divergence and Convergence Areas in the Indian Ocean (Unit: mg/m³/sec). Northern Winter (Shaded Areas show the Divergence Zones).

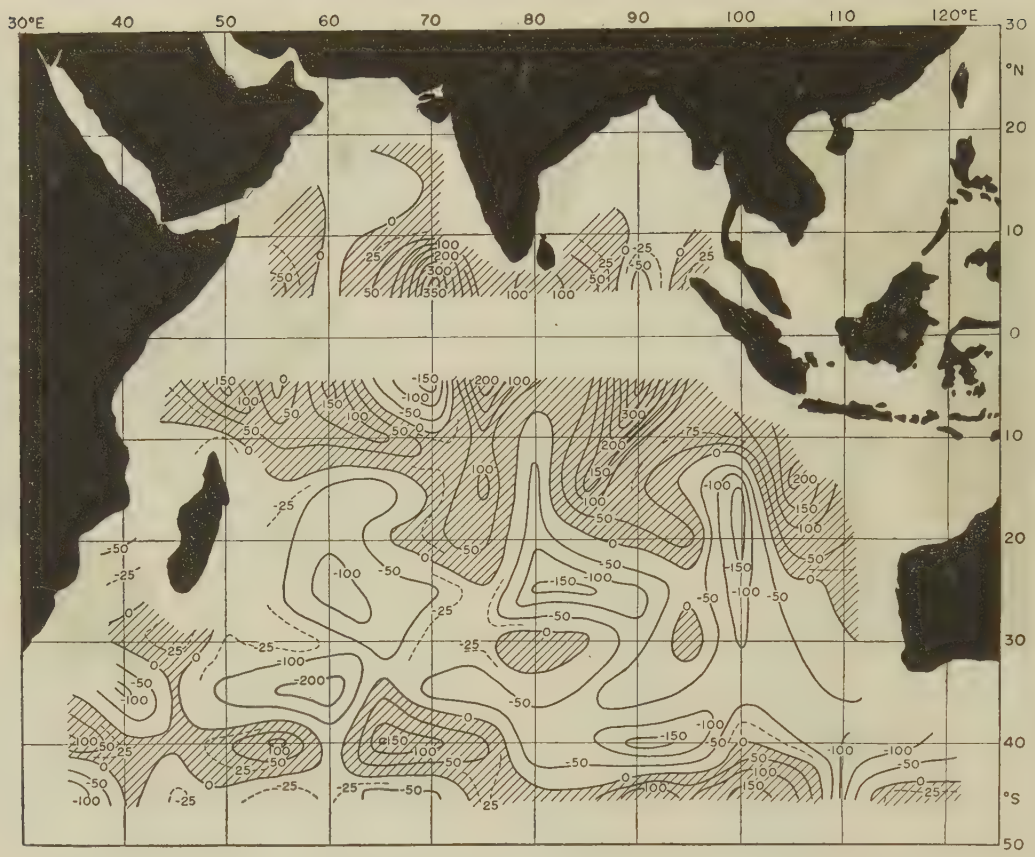

Fig. 7. Distribution of Divergence and Convergence Areas in the Indian Ocean (Unit: mg/m³/sec). Northern Spring (Shaded Areas show the Divergence Zones).

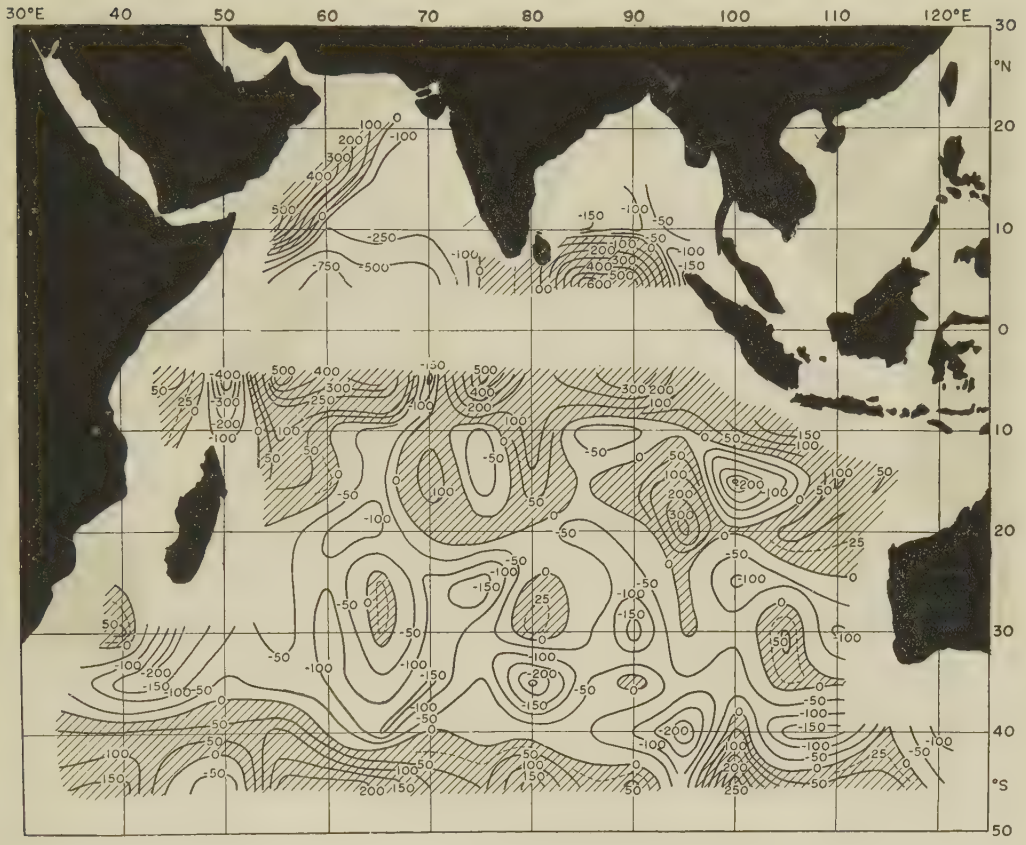

Fig. 8. Distribution of Divergence and Convergence Areas in the Indian Ocean (Unit: mg/m³/sec). Northern Summer (Shaded Areas show the Divergence Zones).

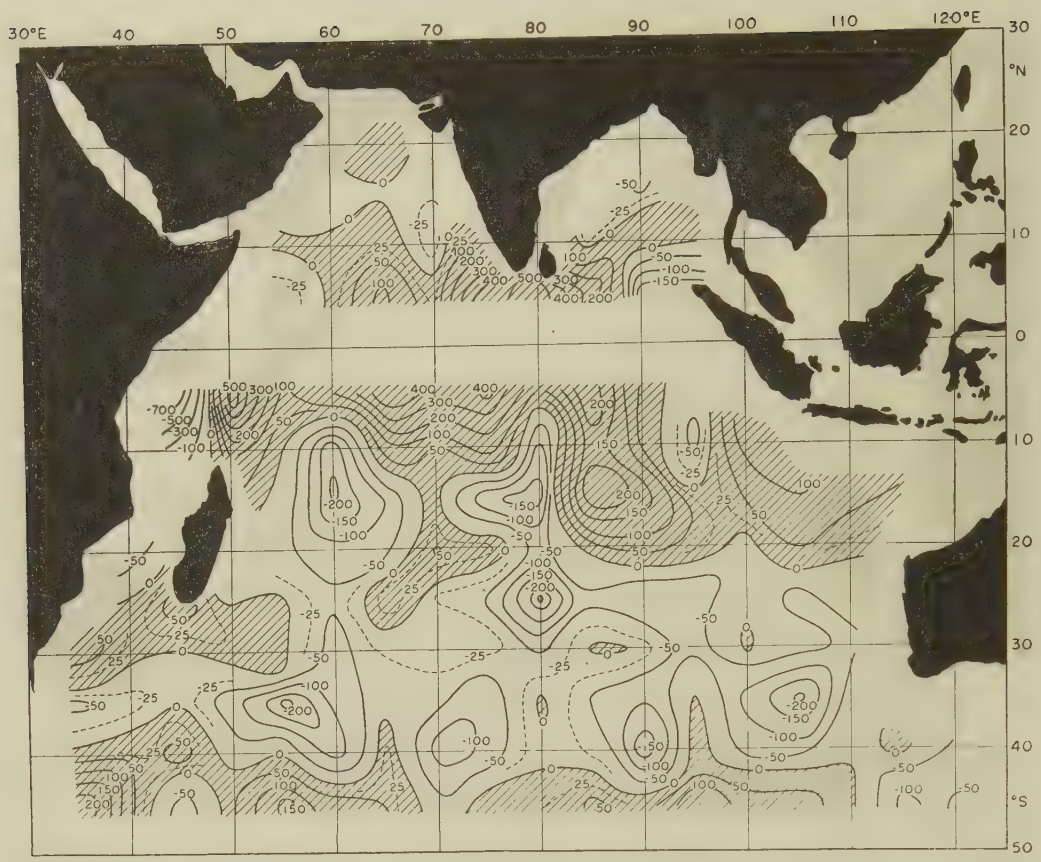

Fig. 9. Distribution of Divergence and Convergence Areas in the Indian Ocean (Unit: mg/m³/sec). Northern Autumn (Shaded Areas show the Divergence Zones).

Fig. 10. Distribution of Divergence and Convergence Areas in the Indian Ocean (Unit: mg/m³/sec). Annual Mean (Shaded Areas show the Divergence Zones).

Fig. 11. Distribution of Divergence and Convergence Areas in the Atlantic Ocean (Unit: mg/m³/sec). Northern Winter (Shaded Areas show the Divergence Zones)

Fig. 12. Distribution of Divergence and Convergence Areas in the Atlantic Ocean (Unit: mg/m³/sec). Northern Spring (Shaded Areas show the Divergence Zones).

Fig. 13. Distribution of Divergence and Convergence Areas in the Atlantic Ocean (Unit: mg/m³/sec). Northern Summer (Shaded Areas show the Divergence Zones).

Fig. 14. Distribution of Divergence and Convergence Areas in the Atlantic Ocean (Unit: mg/m³/sec). Northern Autumn (Shaded Areas show the Divergence Zones).

Fig. 15. Distribution of Divergence and Convergence Areas in the Atlantic Ocean (Unit: mg/m³/sec). Annual Mean (Shaded Areas show the Divergence Zones).

Tables 1 ~ 15.

Divergence of the Surface Drift-Vectors in the Pacific, Indian and Atlantic Oceans for Different Seasons and the Year.

Table 1. Divergence of the Surface Drift Vectors for the Pacific Ocean as Computed

	125°E	130	135	140	145	150	155	160	165	170	175°E	E180°W	175°W	170	165	160
55°N																
50													−57	4	7	48
45							−12	−32	−15	−10	32	30	8	73	8	27
40					9	59	102	95	−16	48	−3	75	24	57	51	0
35					14	−6	−40	−8	13	−7	−79	−22	−31	−26	6	4
30	51	74	−26	−52	−50	−23	4	−54	−65	−58	−99	−26	−47	−45	−65	−76
25	31	21	−44	−13	−43	−76	−86	−63	−66	−66	−53	−6	−36	−30	−20	14
20		2	−9	15	35	8	−8	−29	−6	−44	−9	−15	−51	34	−31	−28
15		−21	−18	31	−29	−51	−58	−106	−86	−62	34	−93	−38	13	−18	−80
10		−2	31	6	−44	−65	7	−47	137	−39	−62	−88	43	40	−59	−108
5°N		26	75	−13	206	−69	−13	−42	260	169	−307	236	−60	−33	208	−168
0																
5°S																
10	108	563	272			80	−46	13	−13	−2	3	−5	14	−18	−85	−57
15					−154	210	159	698	48	−21	23	38	15	27	8	16
20						−400	−462	275	18	−9	1	22	10	18	1	14
25							−25	4	−66	16	−6	12	5	8	4	−16
30							99	229	−30	−1	−8	−2	−38	−25	−50	4
35	−88	−85	−99				−400	137	−37	−47	−29	−10	−39	15	25	−7
40	−19	−30	−59	77	−218	−169	270	−353	−58	11	17	57	15	−15	13	−51
45	−52	−3	−14	319	192	188	197	−105	−18	−26	−145	−43	−43	−156	−37	−83
50									229	73	49	177	−52	−121	41	63
55°S																

from the Distribution of Wind Stresses—Northern Winter (in 10^{-9} c.g.s. or mg/m³/sec).

155	150	145	140	135	130	125	120	115	110	105	100	95	90	85	80	75°W
	75	55	85													
19	−21	35	15	−81	−76											
−7	32	11	26	−12	79											
41	−28	−56	−21	−22	−31											
37	−62	−12	−43	2	−25	97										
−6	−33	29	−5	−48	−36	−51	12									
6	−8	−20	−52	−32	−31	10	17									
−39	−5	−36	−44	26	−29	−33	22	70	4							
−32	2	−111	−23	94	−95	−16	25	50	17	7						
81	49	−152	−12	48	−79	53	38	39	−7	−14	−84	28	−44			
−246	−320	−644	−177	−108	−436	−406	−338	−131	−211	58	−149	−207	−258	18		
−11	−61	14	−105	−269	−23	111	63	49	36	7	72	126	101	60	−10	
27	−59	−10	−70	−47	−162	−18	−49	−62	−64	−10	51	−55	62	1	40	
78	28	35	−100	−16	−9	−3	−5	−6	−53	−87	−37	−59	26	−37	53	5
−47	−23	46	−74	4	6	−7	36	−36	38	−34	−4	−25	−19	−49	42	34
−29	9	−22	−40	−54	−8	−7	7	−129	2	−5	−63	−27	−48	−34	−41	1
−15	10	−54	−2	−30	4	−2	−31	−48	50	35	−55	−16	−21	−55	−69	−6
−50	27	−22	55	−41	17	20	−38	−41	−143	−103	−122	−114	−71	−86	−90	−51
22	−32	−112	76	−112	−31	14	37	−31	−130	78	−132	8	69	116	−53	
−54	77	−271	−49	−105	0	107	23	−42	14	−127	−62	−200	−23	49	−43	
								67	132	149	−23	185	−13	42	179	−75

Table 2. Divergence of the Surface Drift Vectors for the Pacific Ocean as Computed

	125°E	130	135	140	145	150	155	160	165	170	175°E	E180°W	175°W	170	165	160
55°N																
50													7	−29	−39	−38
45							44	−40	−37	−1	11	−72	−36	−13	−17	−40
40					40	−29	−52	−49	−62	−51	2	−80	−5	−49	−26	−82
35					−11	−9	−62	−27	−51	−17	−18	−46	−6	−25	−9	−36
30	−14	−46	−24	−12	−22	4	9	10	1	−39	−21	−23	−11	−9	−10	−28
25	25	−6	5	−12	−6	−30	20	−19	17	−13	−12	−2	−9	−1	−20	68
20	16	−12	0	−12	−8	−33	−11	−3	−15	−22	−35	−37	−15	−23	−18	−1
15		−22	0	−20	−54	−17	−68	−14	−50	−40	−59	−97	−64	−74	−95	−121
10		−43	−21	−11	−51	−122	46	−236	−51	−125	−67	−60	−160	−69	−64	−143
5°N		−9	−18	−30	−35	−36	−38	−62	−67	−115	−119	−135	−149	−136	−87	−84
0																
5°S																
10	−21	36	−68	77	17	81	4	−16	20	23	2	15	−2	−3	−5	−5
15						−19	68	−63	8	−12	−6	18	28	16	11	12
20						131	−12	−18	16	−7	−9	14	20	11	4	64
25							−30	71	5	37	4	1	−8	−2	15	22
30							−67	−23	−51	4	−30	−23	−43	−92	−109	5
35							−43	22	−37	−21	−19	−7	3	−23	58	−32
40	−6	−125	−52	36	−16	−51	−34	57	−55	−7	−15	31	−144	−99	193	87
45	190	−37	−89	−18	−26	−22	−60	−132	−96	−155	−76	52	−107	−63	17	−153
50															44	−26
55°S																

from the Distribution of Wind Stresses—Northern Spring (in 10^{-9} c.g.s. or mg/m³/sec).

155	150	145	140	135	130	125	120	115	110	105	100	95	90	85	80	75°W
−22	−38	−22	−1													
−51	−35	−8	−9	−29	−22											
−67	−39	−37	−54	−62	−30											
−13	−38	−50	−43	−48	−54											
24	−16	−33	−23	−64	−77	−54										
−17	−11	−11	−7	−44	−47	−55	−30									
−1	−25	4	−16	18	5	−40	−35									
−48	−49	−57	−41	12	5	−14	11	33								
−45	28	−120	3	−38	−46	5	23	85	33	0						
−117	−1	−118	−3	−114	−30	20	−29	72	50	−1	13	−14	29			
−51	−82	−78	−66	−155	−135	−78	−90	−62	−50	−45	−33	−17	−11	−4		
35	33	6	−49	−97	−14	35	63	−69	60	−72	−101	50	95	28	−7	
−39	10	3	−65	−24	−33	−24	−46	−44	−13	−32	−23	6	45	33	43	
17	−4	27	−66	−40	−14	17	−37	−63	43	−12	−70	−18	−39	−29	50	48
−59	5	3	−29	−67	23	−9	−23	−58	59	−17	−33	−41	−20	−27	5	48
−28	31	1	17	−63	48	19	−24	22	−54	−162	−48	−5	−49	−71	−56	−2
−144	8	92	5	−97	80	6	−89	−70	−97	−1	−16	−0	−36	−12	−27	−11
−143	−12	40	144	−151	51	−44	56	11	−31	−80	−54	19	−64	−1	−58	16
−225	48	−80	215	−235	−39	−123	133	−18	−30	−31	−127	−79	8	−39	−8	
−80	29	−26	−106	−224	−146	−89	48	−23	27	97	70	26	48	9	65	
										83	65	228	24	82	103	−120

Table 3. Divergence of the Surface Drift Vectors for the Pacific Ocean as Computed

	125°E	130	135	140	145	150	155	160	165	170	175°E	E180°W	175°W	170	165	160
55°N																
50													−3	−8	−1	1
45							−9	−3	23	2	7	6	9	0	0	−3
40					−10	5	−1	6	−4	0	11	−17	−3	−18	−5	0
35					−7	−6	3	−6	−15	3	4	−6	2	−16	2	−17
30	−50	−4	−13	21	−26	−1	2	−8	−10	2	−17	4	−12	−27	1	−49
25	−14	−10	−16	−17	−15	3	−9	−18	−21	−12	−32	−19	−19	−36	−15	−41
20	10	2	−3	−14	−3	4	−7	−7	−18	−24	−49	−11	−36	−3	−35	−15
15		22	22	−1	−1	−14	−8	−1					−45	−38	−19	−18
10		10	0	0	−5	−5	−16	−10					36	6	−4	7
5°N		−44	−99	50	−214	−165	−137	−139	−166	−46			−21	−181	−329	−134
0																
5°S																
10	−16	−26	−46				−80	−197	62	−11	56	−86	63	−41	54	−90
15						9	18	90	92	−120	58	−78	51	−58	45	−38
20							−135	55	−22	−61	76	−3	−20	−10	−68	31
25							16	21	−19	−28	14	−20	−79	−53	−93	4
30							−83	4	−4	−38	−10	81	−37	−20	27	−38
35							22	64	20	75	23	74	−30	13	57	−54
40	7	−8	62	1	130	−33	−14	−43	−96	−127	−111	−94	−115	48	160	18
45	173	−169	24	−113	−4	−60	−6	73	22	38	−77	−88	105	23	10	−63
50																
55°S																

from the Distribution of Wind Stresses—Northern Summer (in 10^{-9} c.g.s. or mg/m³/sec).

155	150	145	140	135	130	125	120	115	110	105	100	95	90	85	80	75°W
5	31															
−9	10	−22	−7	−22	8											
−3	10	−30	4	21	9											
−9	6	−19	−5	−32	21											
−6	−7	−18	−13	−51	−41	106										
−9	11	−7	−29	−17	−44	−47										
6	−17	−28	−31	−18	31	25	11									
0	−6	−3	2	−9	24	29	16	−8	−5							
−4	7	−4	21	15	25	24	38	11	−6	1						
−8	7	−24	13	−40	−10	−10	−38	−64	−90	−29	−52	0	−27			
−373	−388	−513	−249	−340	−490	−597	−444	−520	−320	−255	−151	−90	−257	−314		
−65	−64	54	−140	−30	−92	−71	40	−187	21	237	−19	91	28	10		
28	−6	71	−88	17	−16	−49	56	−55	−121	−47	38	34	9	−80	95	
−68	26	27	−67	−27	−65	−49	−24	−32	5	−81	−57	46	3	−117	3	45
−83	−34	−56	−40	27	−1	−85	20	−36	−9	−116	−35	−25	−4	−27	−20	1
−60	−86	−76	−29	64	−19	−58	31	−55	3	−31	79	−2	−37	−29	−14	16
16	−16	−102	−49	−39	15	45	−20	−99	−26	16	−10	−66	−50	6	−21	−40
50	157	41	7	36	−35	8	163	11	−101	−10	54	−15	19	−7	−63	
−90	162	−7	68	102	27	−47	51	37	1	−100	−7	21	−2	50	86	
				68	62	−52	162	101	−11	12	55	−37	28	145	88	
											−5	118	−17	100	22	58

Table 4. Divergence of the Surface Drift Vectors for the Pacific Ocean as Computed

	125°E	130	135	140	145	150	155	160	165	170	175°E	E180°W	175°W	170	165	160
55°N																
50													59	17	−5	11
45							−5	−55	−21	−14	−45	−23	11	11	−3	−9
40					−18	9	20	6	−24	−29	11	22	4	4	7	23
35					2	5	−21	−9	−46	−42	−40	−27	−10	−40	−14	−23
30	2	3	−2	27	−11	5	−14	−8	−1	−24	−21	11	−25	−40	−35	−28
25	−17	−13	−23	−3	−1	−25	−1	−15	−12	−31	−13	−1	−19	−12	−21	−31
20	78	−4	8	−15	−18	4	−19	−15	−10	−15	−4	−20	−14	−39	−2	−5
15		21	28	−1	2	15	−8	31	−3	1	−57	−49	42	−25	−17	−11
10		25	50	−16	−25	−2	−10	−23	−22	−4	40	15	44	−51	−48	4
5°N		23	67	44	−1	22	−91	8	−57	−121	−17	−114	−40	−151	−137	−20
0																
5°S																
10	14	−25	125	−34	40	−6	97	−82	103	−28	78	5	60	3	−9	36
15					28	−67	−8	−20	169	−14	29	−50	57	−6	8	3
20						−69	−28	−56	−45	14	−11	−36	−4	8	26	−38
25							−24	−38	−17	0	−46	−18	−16	−32	4	−76
30							−5	−46	−19	−30	−16	−55	8	−24	−34	−61
35		−157	−70				−36	−42	54	−12	62	16	−50	−78	47	−10
40	−10	5	−70	−37	−42	−80	−43	85	25	−98	−44	6	−35	−46	−41	13
45	−113	22	−96	−13	231	−71	−111	44	−67	−195	−49	80	18	33	−47	−8
50										46	228	114	24	−99	13	76
55°S																

from the Distribution of Wind Stresses—Northern Autumn (in 10^{-9} c.g.s. or mg/m³/sec).

155	150	145	140	135	130	125	120	115	110	105	100	95	90	85	80	75°W
25	58	13	58													
45	−5	19	−29	−38	−69											
6	9	5	−39	−24	13											
−38	−1	−18	−19	−33	20											
−18	4	−13	−35	−4	−38	48										
0	2	−7	−19	−30	10	−55	0									
9	−32	−31	−31	−28	10	−11	21									
−21	−46	−8	−6	−10	0	3	2	4	−6							
−12	3	14	21	18	−2	27	14	27	19	−3						
−10	−2	−46	−35	−31	−62	−16	−1	−38	−51	−95	−67	22	−50			
−268	−352	−365	−370	−549	−671	−754	−646	−359	−289	−357	−216	−151	−370	−309		
−135	−72	15	−186	−10	−89	−28	−6	−15	0	23	12	74	45	31	143	
−12	52	41	−11	47	−21	−36	−37	−40	−47	−1	−20	−28	12	−58	173	
61	−1	18	−75	16	−16	−33	28	−34	−57	−28	17	−71	−11	−49	100	45
−11	−61	15	−53	−44	46	−70	−43	−30	28	−40	−21	−57	−46	−18	−28	58
−6	−57	−7	−57	−33	56	3	−8	17	−21	−67	7	−38	−70	−28	−11	17
−17	22	−67	−77	−27	26	22	−67	−40	−43	−12	7	−14	−39	−40	−11	−35
70	124	−83	−49	−46	−181	−5	6	28	−116	−35	−14	−43	−15	−118	−52	−15
−33	−11	−217	104	−1	−71	58	3	29	−141	−59	−95	−77	49	−48	−18	
53	−76	−69	97	−49	−71	36	−87	85	−89	52	14	−90	−36	43	−40	
													146	111	24	−84

Table 5. Divergence of the Surface Drift Vectors for the Pacific Ocean as Computed

	125°E	130	135	140	145	150	155	160	165	170	175°E	E180°W	175°W	170	165	160
55°N																
50													−1	−4	−9	6
45							4	−33	−128	−6	1	−15	−2	18	−3	−6
40					5	11	17	14	−27	−8	5	0	5	−1	7	15
35					−1	−4	−30	−12	−25	−16	−33	−25	−12	−27	−4	−18
30	0	13	−16	−40	−272	5	0	−15	−21	−30	−39	−9	−24	−30	−27	−45
25	11	−2	−194	−11	−20	−32	−22	−29	−20	−30	−28	−7	−12	−20	−19	−5
20		2	−1	−5	2	−4	−11	−13	−12	−26	−24	−21	−29	−30	−27	−25
15		0	9	2	−22	−14	−36	−24				−33	−26	−31	−37	−58
10		−24	15	−5	−31	−49	7	−100					−9	−19	−44	−46
5°N		−1	6	13	−14	−60	−70	−59	5	−28			−68	−125	−12	−102
0																
5°S																
10	22	137	71				−6	−71	43	−4	35	−18	34	−15	−11	−29
15							59	176	79	−42	26	−18	38	−5	18	−2
20							−159	64	−8	−16	14	−1	2	7	−9	18
25							−16	23	−24	6	−8	−7	−25	−20	−18	−17
30							−14	41	−26	−17	−16	0	−28	−40	−41	−23
35							−115	45	0	−1	9	18	−29	−18	47	−26
40	−7	−39	−30	19	−37	−83	45	−63	−46	−54	−38	0	−70	−28	81	15
45	49	−48	−44	44	98	9	5	−30	−40	−85	−87	0	−7	−41	−14	−77
50																
55°S																

from the Distribution of Wind Stresses—Annual Mean (in 10^{-9} c.g.s. or mg/m³/sec).

155	150	145	140	135	130	125	120	115	110	105	100	95	90	85	80	75°W
	32															
10	13	6	−7	−43	−40											
−18	3	12	−16	−19	18											
−5	−153	−36	−22	−34	−11											
9	−20	−19	−28	−39	−45	50										
−6	−8	1	−15	−35	−29	−52										
−5	−21	−19	−32	−15	3	−4	4									
−27	−27	−26	−22	5	0	−4	13	25								
−23	10	−55	5	22	−29	10	25	43	16	1						
−14	−13	−85	−9	−34	−45	12	−8	3	−25	−35	−48	9	2			
−235	−286	−400	−216	−288	−433	−459	−379	−268	−165	−150	−138	−116	−224	−152		
−44	−41	22	−120	−102	−55	12	40	−56	29	49	−9	85	67	32		
1	−1	26	−59	−2	−58	−32	−19	−50	−61	−23	11	−11	32	−26	88	
22	12	27	−77	−17	−26	−17	−10	−34	−15	−52	−37	−26	−6	−58	51	36
−50	−28	2	−49	−20	18	−43	−3	−40	29	−52	−23	−37	−22	−30	−1	35
−31	−26	−26	−27	−22	19	−11	2	−36	−18	−66	−6	−18	−51	−41	−30	8
−40	6	−33	−31	−48	31	18	−52	−64	−29	10	−19	−24	−36	−25	−32	−23
−18	74	−6	39	−51	−37	−5	47	2	−98	−57	−34	−38	−33	−53	−66	
−81	42	−79	116	−61	−28	−25	56	4	−75	−28	−90	−32	31	20	2	
				−79	−39	−10	36	31	−15	40	19	−75	4	62	17	
													35	84	32	−55

Table 6. Divergence of the Surface Drift Vectors for the Indian Ocean as Computed from the Distribution of Wind Stresses—Northern Winter (in 10^{-9} c.g.s. or mg/m³/sec).

	35°E	40	45	50	55	60	65	70	75	80	85	90	95	100	105	110	115	120	125°E
20°N							+41												
15						+32	+86	+22				+41							
10					−26	+86	+144	+13			−16	+89	+30						
5°N					−238	−48	+267	−9	−242	+52	+131	+27							
0																			
5°S			−376	+119	−131	+13	+72	+105	+116	+4	+174	+85	+91						
10			+1	−6	+59	−59	+27	−19	−80	+108	+74	+41	+38	+43	+40				
15					+6	+18	+43	+196	−122	+11	+168	+86	+32	+10	+118	+6	−20	−30	
20		+42			+4	+16	−162	+17	+4	−27	−52	−34	−5	+46	−70	+105			
25		−62	+84	+11	−26	−17	+26	+24	−124	−9	−125	−31	−100	−40	−111	+116			
30	−7	+3	−39	+9	+21	−11	−69	−63	−42	+32	−31	−6	−35	−102	−142	−143			
35	+11	−141	−62	−54	+26	−112	+80	−89	−23	−75	−45	−63	−21	−21	+30	+48			
40	−77	−83	+197	−52	+14	−89	−45	−58	−45	−122	−178	−117	−100	−159	−181	−161	−30	+6	
45°S	−152	−20	−68	−82	+201	−84	+64	−33	−1	+78	−60	+130	+256	−67	+38	+153	+26	−137	

Table 7. Divergence of the Surface Drift Vectors for the Indian Ocean as Computed from the Distribution of Wind Stresses—Northern Spring (in 10^{-9} c.g.s. or mg/m³/sec).

	35°E	40	45	50	55	60	65	70	75	80	85	90	95	100	105	110	115	120	125°E
20°N							+12												
15						−3	−15	+1				−7							
10					+12	−4	+3	+20			+2	0	−1						
5°N					+59	−18	+61	+368	+72	+118	+82	−71	+37						
0																			
5°S			+26	+165	−13	+172	−53	−171	+245	+49	+24	+387	+84						
10			−14	−33	+87	+81	+118	+36	+76	−40	+91	+109	+71	+92	+177				
15					−13	−78	−95	+18	+118	−83	+176	+54	−16	−160	+220	+77			
20		−58			−36	−90	−22	+42	+74	−97	−18	+38	+77	−173	+92	+54			
25		−16			−45	−133	−81	−66	−10	−153	−161	−122	−12	−130	−20	+15			
30		+17	+37	−27	0	−26	−93	−1	−21	+43	+11	−89	+38	−111	−55	−9			
35	−19	−102	+3	−138	−208	−299	+47	−86	−98	−23	−59	−1	−66	−63	−81	−35			
40	+106	+22	+5	+48	+119	−33	+156	+127	+72	−95	−85	−171	−144	+10	−44	−102	−144	−70	
45°S	−145	+11	−28	−5	−49	−17	−78	−56	+26	+15	+4	+141	+79	+190	+121	−105	+46	+26	

Table 8. Divergence of the Surface Drift Vectors for the Indian Ocean as Computed from the Distribution of Wind Stresses—Northern Summer (in 10^{-9} c g.s. or mg/m³/sec).

	35°E	40	45	50	55	60	65	70	75	80	85	90	95	100	105	110	115	120	125°E
20°N							+45												
15						+384	−188	−178				−76							
10					+522	−251	−157	−211			−161	−129	−19						
5°N					−594	−901	−602	−619	+5	+37	+613	+538	−183						
0																			
5°S			+623	−490	+583	+374	+468	−161	+527	+153	+257	+392	+107						
10			+27	−156	+115	+4	−107	+50	−86	+168	−86	−65	−12	+106	+193				
15					+62	+48	−95	+171	−95	+81	0	+17	+113	−252	−102	+109	+41		
20		−16			−12	−107	−112	+19	+49	−25	−73	−14	+335	0	+78	+33			
25		−15			−30	−98	+36	−114	−196	+5	−4	−83	+14	−115	−52	−7			
30		+56	−205	−119	−23	−142	+31	−102	−83	+49	−29	−173	+10	−33	+54	−111			
35	−76	−200	−133	−41	−82	−105	−63	−156	−47	−267	−55	+20	−65	−93	+47	+12			
40	+65	+65	+73	+72	+129	−3	−158	+18	−24	−29	−49	−105	−240	+67	−190	−183	+10	−120	
45°S	+150	+152	−32	−88	+208	+236	+195	+75	+41	+190	+33	+56	−95	+280	+56	+86	+73	−45	

Table 9. Divergence of the Surface Drift Vectors for the Indian Ocean as Computed from the Distribution of Wind Stresses—Northern Autumn (in 10^{-9} c.g.s. or mg/m³/sec).

	35°E	40	45	50	55	60	65	70	75	80	85	90	95	100	105	100	115	120	125°E
20°N							+16												
15						−8	−4	−21				−54							
10					+1	+4	+23	−42			−30	+65	+5						
5°N					−47	+8	+116	+22	+461	+544	+279	−193	−188						
0																			
5°S			−704	+555	+83	+144	+475	+336	+406	+70	+249	+37	−37						
10			−184	+116	0	−193	+92	+39	+142	−117	+179	+33	−70	+136					
15					−26	−201	−109	+27	−146	−189	+236	+190	+17	+60	+107	+62	+48	+22	
20		−80			−43	−84	−61	+52	+31	−61	+27	+77	+37	−24	+68	+16			
25		+9	+83	−1	+8	−45	+40	−26	−52	−252	−66	−110	−101	−11	−69	−28			
30	+76	+11	−8	+25	+16	−60	−25	−4	−13	−64	+3	−2	−66	+7	−17	−60			
35	−54	−30	−17	−81	−220	−77	−30	−46	−80	+6	−52	−95	+6	−120	−201	−4			
40	+2	+22	+70	−33	−8	−126	+35	−136	−76	−9	−39	−182	+22	−70	−71	−11	+10	−52	
45°S	+232	+57	−81	+55	+166	+63	+45	−32	+17	+11	+55	+20	+149	+73	+88	+17	−107	−50	

Table 10. Divergence of the Surface Drift Vectors for the Indian Ocean as Computed from the Distribution of Wind Stresses—Annual Mean (in 10^{-9} c.g.s. or mg/m^3/sec).

	35°E	40	45	50	55	60	65	70	75	80	85	90	95	100	105	110	115	120	125°E
20°N							+28												
15						+101	−30	−44				−24							
10					+128	−41	+3	−55			−51	+6	+4						
5°N					−205	−240	−39	−59	+74	+188	+276	+75							
0																			
5°S			−108	+88	+131	+176	+241	+27	+323	+69	+176	+225	+61						
10			−43	−20	+65	−42	+33	+27	+13	+30	+65	+30	+7	+94					
15					+7	−53	−64	+103	−61	−45	+145	+87	+37	−86	+86	+63			
20		−28			−21	−66	−89	+33	+40	−53	−29	+17	+111	−38	+42	+52			
25		−21			−23	−74	+5	−45	−96	−102	−89	−87	−50	−74	−63	+24			
30		+22	−54	−28	+4	−60	−39	−43	−40	+15	−12	−68	−13	−60	−40	−81			
35	−34	−118	−53	−78	−121	−15	+9	−94	−62	−90	−53	−35	−37	−74	−51	+5			
40	+24	+7	+86	+9	+63	−6	−2	−12	−18	−64	−88	−144	−116	−38	−121	−114	−39	−59	
45°S	+22	+50	−52	−30	+131	+49	+56	−12	+21	+74	+8	+9	+98	+119	+76	+38	+10	−51	

Table 11. Divergence of the Surface Drift Vectors for the Atlantic Ocean as Computed from the Distribution of Wind Stresses—Northern Winter (in 10^{-9} c.g.s. or mg/m³/sec).

	77.5°W	72.5	67.5	62.5	57.5	52.5	47.5	42.5	37.5	32.5	27.5	22.5	17.5	12.5	7.5	2.5°W	2.5°E	7.5	12.5	17.5	22.5	27.5°E
52.5°N										+40	−5	−7	−62									
47.5								+30	+11	+15	−25	−59	−41									
42.5						+26	+45	−4	−16	−35	−41	−50	−72									
37.5			+56	+14	−13	−25	−58	−66	−53	−70	−60	−46	−42									
32.5		+2	−81	−78	−74	−82	−65	−31	−29	−39	−42	−40	−21									
27.5	−25	−60	−46	−49	−63	−43	−43	−37	−29	−22	−44	−38										
22.5	−33	−16	−29	−35	−30	−23	−33	−27	−10	−41	−36	+5										
17.5	−9	−39	−18	−12	−10	−10	−15	−24	−24	−22	+17	+3										
12.5					−28	−57	−4	+27	−5	−10	+43	+34										
7.5							−30	+27	0	+42	+86	+86	+13									
2.5°N								−63	−97	−77	−130	−91	−137	−166								
2.5°S										−2	+32	−73	+24	+213	+211	+115	+34					
7.5											−6	+64	+116	+47	−4	+96						
12.5										−58	+37	+77	+21	+4	+10	−66	+39					
17.5										−30	−47	−51	−40	+34	+15	+17	+13					
22.5										−44	−39	−42	−39	−43	−8	+3	−108	−48				
27.5									−26	−33	+8	0	−42	−22	−11	−54	−78	+100				
32.5							−33	−49	−24	+3	−18	−11	−22	−6	−7	−18	−58	−38	−41			
37.5						−1	−58	−31	+19	−9	+13	−34	−77	+13	−41	+41	−56	−9	−17			
42.5					+24	−15	−30	−3														
47.5					+18	+55	+77															
52.5°S				+88	+19																	

Table 12. Divergence of the Surface Drift Vectors for the Atlantic Ocean as Computed from the Distribution of Wind Stresses—Northern Summer (in 10^{-9} c.g.s. or mg/m^3/sec).

	77.5°W	72.5	67.5	62.5	57.5	52.5	47.5	42.5	37.5	32.5	27.5	22.5	17.5	12.5	7.5	2.5°W	2.5°E	7.5	12.5	17.5	22.5	27.5°E
52.5 N										+3	−16	−19	−1									
47.5								+9	−20	−11	−18	−13	−7	−5								
42.5						+1	+3	−11	−13	−9	−8	−22	−44									
37.5			+17	+8	+9	−2	−19	−15	−22	−33	−13	−36	−39									
32.5		+13	−10	−23	−15	−5	−18	−11	−4	−7	−25	−38	−23									
27.5	−6	−31	−35	−39	−29	−32	−26	−27	−31	−49	−30	−14	+5									
22.5	−59	−30	−47	−48	−36	−42	−46	−37	−36	−29	−7	+2										
17.5	−26	−31	−33	0	−16	−36	+35	−31	−45	−7	+53	+41										
12.5					−13	−14	+17	+32	+62	+42	+46	+8										
7.5							+46	+29	−29	−62	−35	−60										
2.5 N								−223	−378	−330	−313	−252	−301	−185								
2.5 S										−14	+67	+46	+222	+125	+43	+257	+345					
7.5											+173	+12	−115	−34	+152	−35	+121					
12.5										−96	0	+35	+145	−5	+40	+68	−3					
17.5										−40	−119	+5	+9	−31	+46	−55	−56					
22.5										−1	−2	−58	−85	−85	−20	+12	−64	+17				
27.5									−55	−19	+28	+3	−44	−39	−43	−90	−18	0				
32.5							+3	−51	−18	+49	−61	−46	−39	−25	+16	+23	−5	−94	−10			
37.5						−33	+53	−41	+6	+66	−8	−84	−87	−26	+6	+27	+5	−13	−10	−78		
42.5					+20	+47	−70	+2													−82	−23
47.5					−10	+54	+63															
52.5 S				−111	+31	+210																

Table 13. Divergence of the Surface Drift Vectors for the Atlantic Ocean as Computed from the Distribution of Wind Stresses—Northern Spring (in 10^{-9} c.g.s. or mg/m³/sec).

	77.5°W	72.5	67.5	62.5	57.5	52.5	47.5	42.5	37.5	32.5	27.5	22.5	17.5	12.5	7.5	2.5°W	2.5°E	7.5	12.5	17.5	22.5	27.5°E
52.5°N										−20	−2	−26	−31									
47.5								+29	−23	−26	−39	−39	−25	−5								
42.5						+27	+34	−5	−20	−29	−47	−39	−34									
37.5			+29	+23	−5	−8	−4	−36	−31	−34	−28	−31	−26									
32.5		−1	−30	−33	−36	−34	−18	−22	−23	−34	−20	−28	−25									
27.5	−22	−33	−34	−33	−29	−33	−44	−31	−24	−37	−50	−33	+9									
22.5	−27	−20	−36	−36	−35	−35	−43	−27	−26	−29	−12	−10										
17.5	−36	−14	−27	−15	−29	−25	−34	−24	+4	−28	−8	+33										
12.5					−66	−36	−17	+28	−7	+36	+63	+59										
7.5							−80	+109	+81	+99	+72	+78	+6									
2.5°N								−49	−131	−11	−23	−105	−122	−258								
2.5°S										+44	+16	−20	−34	+50	+66	+259	+112					
7.5											−29	+68	+4	+19	+37	+47	+42	+75				
12.5										+1	+36	−22	−1	+29	+21	+19	+8	+103				
17.5										0	+26	−32	−47	−3	−9	−52	−26					
22.5										−9	−18	−11	−21	−60	−37	+30	−9	−6				
27.5									−14	−18	+15	+12	+1	−22	−43	−40	−14	−28				
32.5							−55	−15	−44	−33	0	−27	−58	+1	+13	−90	−18	−49	+22			
37.5						−41	−74	−13	0	+36	−62	−40	+32	−22	+8	−26	−64	−6	+2	−52		
42.5					−21	−66	+21	+36	−13	−95											−84	+1
57.5					−51	+40	+133															
52.5°S				−41	+167	+94																

Table 14. Divergence of the Surface Drift Vectors for the Atlantic Ocean as Computed from the Distribution of Wind Stresses—Northern Autumn (in 10^{-9} c.g.s. or mg/m³/sec).

	77.5°W	72.5	67.5	62.5	57.5	52.5	47.5	42.5	37.5	32.5	27.5	22.5	17.5	12.5	7.5	2.5°W	2.5°E	7.5	12.5	17.5	22.5	27.5°E
52.5°N										+11	+2	−17	−19									
47.5								+90	−66	−56	−43	−17	−20									
42.5						−18	+13	−20	−52	−47	−32	−35	−37									
37.5			−8	−3	−3	−18	−37	−51	−50	−27	−17	−44	−30									
32.5		−10	−34	−36	−17	−14	−26	−8	+6	−16	−21	−9	−24									
27.5	+14	−11	−21	−8	−6	−25	−38	−33	−19	−24	−35	−28										
22.5	−5	+12	−7	−14	−22	−41	−35	−20	−38	−20	−19	−8										
17.5	−2	−18	−26	+6	−10	−29	+4	0	−16	−16	−2	+26										
12.5					−14	−6	+17	+27	+10	+11	+59	+28										
7.5							+18	−57	−52	−46	−49	−64	−59									
2.5°N								−335	−415	−379	−370	−320	−328	−337								
2.5°S										+155	+51	+106	+153	+168	+140	+288	+139					
7.5											−29	+60	+10	+46	−46	+136	+227					
12.5										−40	−71	+46	+122	−11	+16	−26	+125					
17.5										−36	−64	−45	+4	−11	+4	−7	+15					
22.5										−24	−2	−27	−41	−48	−33	−23	+72	+12				
27.5									+18	+5	−23	−6	−12	−5	+17	−22	−9	−1				
32.5							−28	−75	−63	−2	−45	−23	−16	−18	+9	−59	−25	−17	−8			
37.5							−7	−29	−6	+37				−65	−83	+29	−30	−14	+19	−60	−30	+65
42.5					−13	−23	−52	+147											+25	+18	−140	+49
47.5					−3	−82	−24															
52.5°S				+16	−21	+63																

Table 15. Divergence of the Surface Drift Vectors for the Atlantic Ocean as Computed from the Distribution of Wind Stresses—Annual Mean (in 10^{-9} c.g.s. or mg/m³/sec).

	77.5°W	72.5	67.5	62.5	57.5	52.5	47.5	42.5	37.5	32.5	27.5	22.5	17.5	12.5	7.5	2.5°W	2.5°E	7.5	12.5	17.5	22.5	27.5°E
52.5°N										+9	−5	−17	−28									
47.5								+39	−24	−19	−31	−32	−24									
42.5						+9	+24	−10	−25	−30	−32	−37	−47									
37.5			+24	+10	+3	−13	−30	−42	−39	−41	−30	−39	−32									
32.5		−1	−39	−43	−36	−34	−32	−18	−13	−24	−27	−29	−23									
27.5	−10	−34	−34	−32	−32	−33	−38	−32	−26	−33	−40	−28										
22.5	−31	−13	−30	−33	−31	−35	−39	−28	−25	−30	−19	−3										
17.5	−18	−25	−26	−5	−16	−25	−3	−20	−20	−18	+15	+26										
12.5					−30	−28	+3	+28	+15	+20	+53	+32										
7.5							−12	+27	0	+8	+18	+10										
2.5°N								−167	−255	−200	−209	−192	−222	−236								
2.5°S										+46	+41	+15	+91	+139	+115	+230	+158					
7.5											+27	+51	+4	+20	+35	+61						
12.5										−48	0	+34	+71	+5	+22	−1	+42					
17.5										−27	−51	−31	−18	−3	+14	−24	−13					
22.5										−18	−15	−35	−47	−59	−25	+6	−27	−6				
27.5									−20	−16	+7	+2	−24	−22	−20	−51	−30	+18				
32.5							−28	−47	−37	+4	−31	−27	−34	−12	+8	−36	−26	−49	−9			
37.5						−24	−22	−28	+5	+33				−25	−28	+18	−36	−10	−1			
42.5					+3	−29	−33	+46														
47.5					−12	+53	+62															
52.5°S				−12	+49																	

Records of Oceanographic Works
in Japan Vol. 4. No. 2,
March 1958

Depth Determination in Oceanographic Observations

By
Toshihiko Teramoto
(Geophysical Institute, University of Tokyo)

Abstract

The accuracy of the depth determination by thermometric sounding which has been commonly used in oceanographic observations is inquired. In the next step, the author shows that the depths determined by the use of underwater clinometers (wire angle gauges) has the comparable accuracy. Needless to say, the latter method is less expensive and far less troublesome than the former.

1. Introduction

The oceanic phenomena are generally discussed on the scale of several hundred or thousand kilometers in horizontal direction. As the electronic location has developed, it will not be very hard to measure the horizontal distance with the accuracy of less than 1/1000 for investigating the horizontal variation of oceanographical factors. The time variations of the various factors whose periods range from a fraction of a second to almost eternity can be measured with the accuracy comparable to that of the horizontal variations. Consequently, it is quite natural that we should request a similar accuracy in the determination of the vertical changes of these phenomena.

In determining a vertical distance in oceanographic observations, we have the following methods.

(1) measurement of travel time of a messenger descent. (Hirano)
(2) bourdon tube.
(3) thermometric sounding
(4) underwater clinometer method

The first method will not be practical, since the accuracy of this method will not be sufficient for our purposes and there will exist several sources of errors.

In case we use bourbon tubes, the pressure in the sea water can be indicated with the accuracy of about 1/100 of full scale, so that we can get the accurate measurement of depth by dividing it into some suitable ranges. Moreover, this method enables us to record the depth on board ship, and it will appear to be still more useful as the telemetering device in future.

In this paper, we shall discuss thermometric sounding which is an accurate and routine method of depth determination in oceanographic observation of the

present day. And on the basis of this method which has been used for the past thirty years, the new method where the underwater clinometer is used will be investigated.

2. Accuracy of a Protected Reversing Thermometer

(a) Principle of accuracy determination

A series of tests was made chiefly on board a research vessel "Ryofu Maru" with a pair of protected reversing thermometers simultaneously attached on a water bottle lowered into the sea water.

If each of these thermometers has no systematic error, their mean accidental error will be found from the distribution of temperature differences of freely paired thermometers as follows.

Let t_1 and t_2 to be the temperatures measured with the two thermometers mentioned above, with the error ε_1 and ε_2 respectively. Then we may write

$$t_1-t_0=\varepsilon_1 \tag{2.1}$$

and

$$t_2-t_0=\varepsilon_2 \tag{2.2}$$

where t_0 is a true temperature of the sea water.

Thus, we have

$$t_1-t_2=\varepsilon_2-\varepsilon_1\,. \tag{2.3}$$

In case the distributions of ε_1 and ε_2 are both approximated by the same normal curve—in fact, they are expected to be—$(\varepsilon_2-\varepsilon_1)$ will also be represented very closely in a normal curve. Suppose we express the normal curve of $(\varepsilon_2-\varepsilon_1)$ in the following form.

$$y=\frac{h}{\sqrt{\pi}}e^{-h^2x^2}\,. \tag{2.4}$$

On the other hand, we assume the distribution of the error of each thermometer to be uniformly represented by

$$y=\frac{h_1}{\sqrt{\pi}}e^{-h_1^2x^2}\,. \tag{2.5}$$

Then the probability that $(\varepsilon_2-\varepsilon_1)$ is equal to κ can be given by

$$\begin{aligned} y(\kappa)&=\int_{-\infty}^{+\infty}\frac{h_1}{\sqrt{\pi}}e^{-h_1^2x^2}\cdot\frac{h_1}{\sqrt{\pi}}e^{-h_1^2(x-\kappa)^2}\,dx \\ &=\frac{h_1}{\sqrt{2}}\frac{1}{\pi}e^{-(h_1^2\kappa^2/2)}\cdot\Gamma\left(\frac{1}{2}\right) \\ &=\frac{h_1}{\sqrt{2\pi}}e^{-(h_1/\sqrt{2})^2\kappa^2}\,. \end{aligned} \tag{2.6}$$

Thus, the normal curve which represents the distribution of $(\varepsilon_2-\varepsilon_1)$ is given by

$$y(x)=\frac{h_1}{\sqrt{2}}\frac{1}{\sqrt{\pi}}e^{-(h_1/\sqrt{2})^2x^2}. \tag{2.7}$$

Comparing (2.7) with (2.4), we have

$$h_1=\sqrt{2}\,h. \tag{2.8}$$

As h is found from the distribution curve of (t_1-t_2), h_1 may easily be computed.

(b) Results

In Fig. 1 is shown the distribution curve of (t_1-t_2), from which we can obtain the mean value, standard deviation and probable value as follows.

$$\left.\begin{array}{ll} \text{mean value} & M_{t_1-t_2}=0.017°\text{C} \\ \text{standard deviation} & \sigma_{t_1-t_2}=0.022°\text{C} \\ \text{probable value} & P_{t_1-t_2}=0.015°\text{C} \end{array}\right\} \tag{2.9}$$

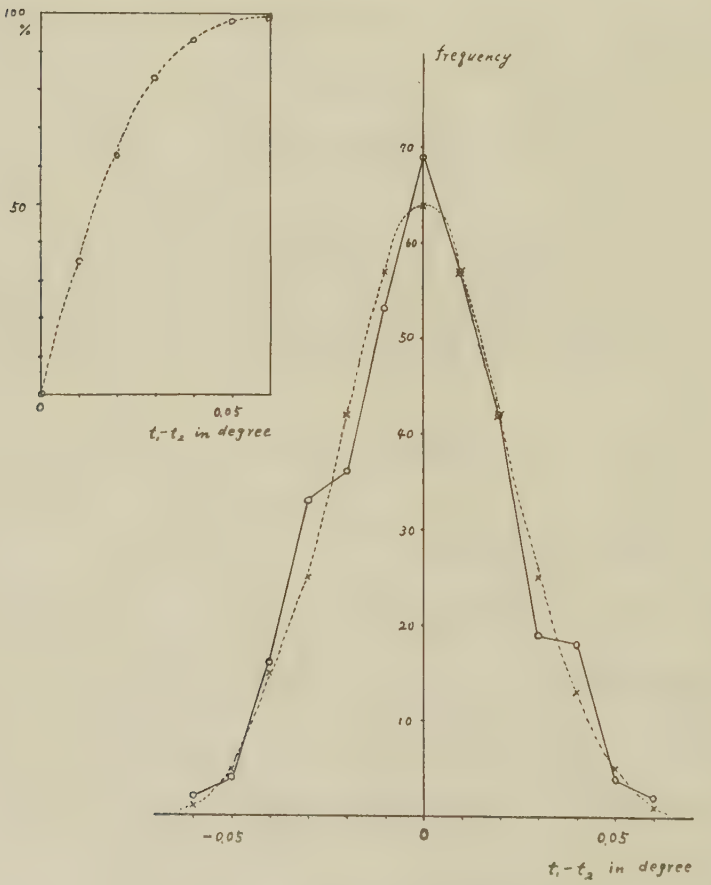

Fig. 1. Distribution Curve of t_1-t_2.

The equation of the normal curve which represents the distribution of (t_1-t_2) is calculated in the following and is shown as a dotted curve in Fig. 1, too.

$$\text{normal curve} \quad y=18.0\,e^{-1030x^2} \quad (h=32.0)\,. \tag{2.10}$$

As the thermometers used are proved to have almost equal accuracy, the normal curve which represents the distribution of the errors of temperature measured with each protected reversing thermometer is obtained in the next form and is plotted in Fig. 2.

$$\text{normal curve} \quad y=25.6\,e^{-2060x^2} \quad (h_1=45.4)\,. \tag{2.11}$$

Thus, the mean value, standard deviation and probable value of the error of each protected reversing thermometer is estimated as

$$\left.\begin{array}{ll} \text{mean error} & M_t=0.012°\text{C} \\ \text{standard deviation of error} & \sigma_t=0.016°\text{C} \\ \text{probable error} & P_t=0.010°\text{C} \end{array}\right\} \tag{2.12}$$

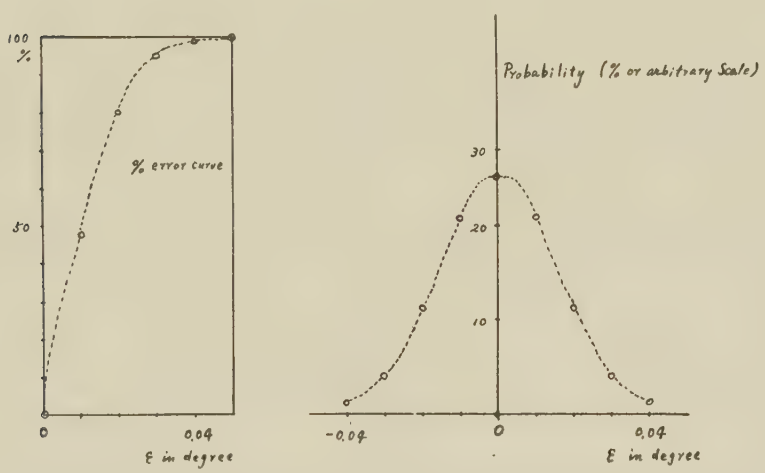

Fig. 2. Distribution curve of error of reversing thermometer (calculated).

3. Accuracy of Thermometric Sounding

(a) Principle

We have sometimes had the cast at which the wire paid out of the research vessel descended vertically in the sea water. We can find such a case easily by drawing the diagram of the relation between the thermometric depth and the wire length to each bottle. In this case, wire length L minus thermometric depth D_0 as to each bottle gives us the error of the thermometric sounding, since it has been proved that there exists scarcely any error in measuring L with the meter wheel.

Moreover, the upper part of the wire can be considered to form a straight line in the sea water as described in chapter 4. Therefore, if we assume α_0 indicates the surface wire angle, $(L\cos\alpha_0 - D_0)$ also represents the error of the thermometric sounding, so long as we treat of the bottles whose depth is less than 200 m.

(b) Results

In Figs. 3 and 4 are shown the distribution curves of $(L-D_0)$ in the depth ranges of 100~500 m and 500~1000 m. In both cases, the wire falls vertically in the sea water. The data are taken from the routine observations on board the "Ryofu-Maru" from the year 1954 to 1956. We find these curves contain the deviation of -2 m.

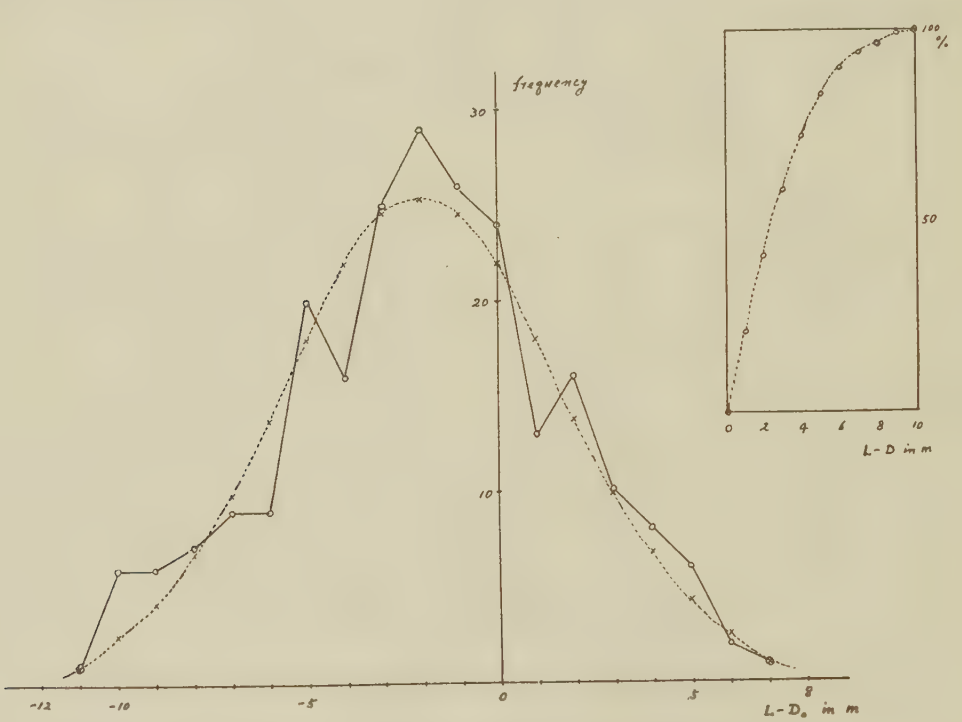

Fig. 3. Distribution curve of $L-D_0$ in the depth range of 100~500 m.

The curves in Fig. 5 show the distribution of $(L\cos\alpha_0 - D_0)$ at the depths which does not exceed 200 m, and here, too, we can see the same deviation as in the former cases.

We investigate the cause of these systematic deviations in detail. As the factors which may produce the error of L, the slip of the wire on the meter wheel, mechanical expansion of the wire and others can be taken into consideration but these must be negligibly small and depend upon the length of the wire paid out. And, since α_0 is determined to be a middle point of the range over which the

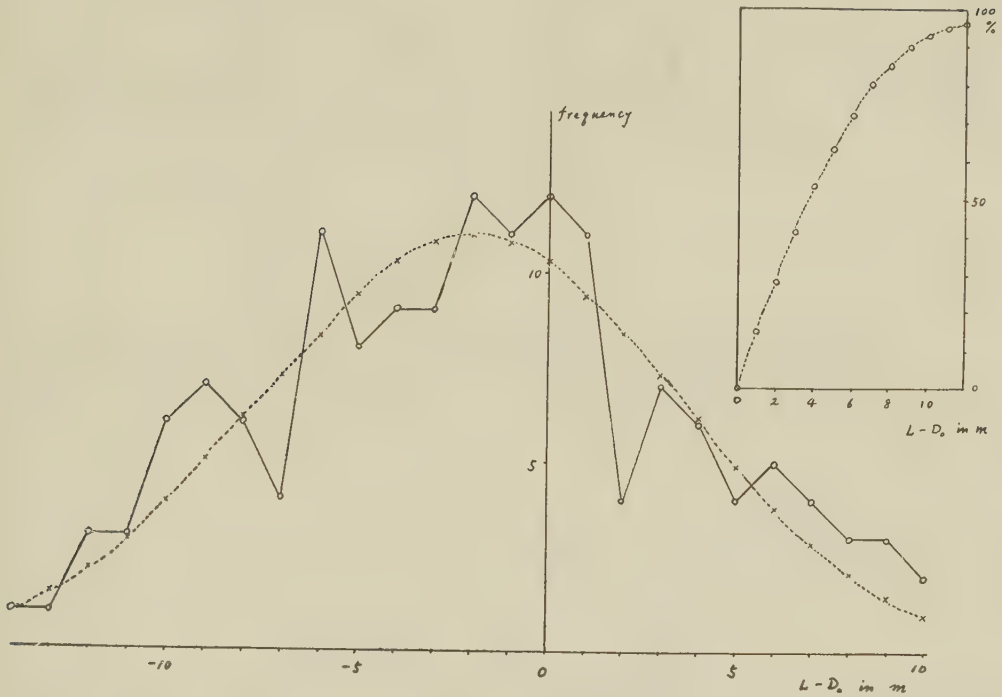

Fig. 4. Distribution curve of $L-D_0$ in the depth range of 500~1000 m.

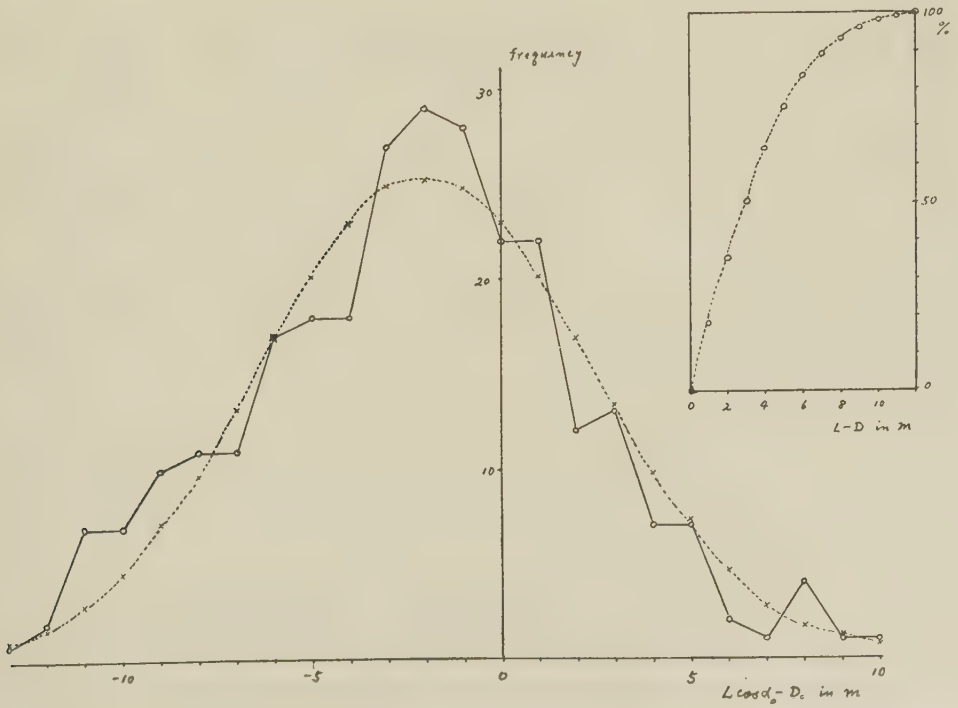

Fig. 5. Distribution curve of $L\cos\alpha_0-D_0$ in the depth range of 100~200 m.

surface wire angle covers, there will be no systematic error in it.

Therefore, L and $\cos\alpha_0$ are supposed not to have any systematic error. Accordingly, the systematic deviations seems to be caused by the thermometric depth D_0. D_0 is given by the following formula.

$$D_0 = 10\frac{\theta - t}{k\bar{\rho}} \tag{3.1}$$

where

k=pressure coefficient of unprotected reversing thermometer
$\bar{\rho}$=vertically averaged density of sea water from surface to sampling layer
t=corrected temperature of sea water measured with protected reversing thermometer
θ=corrected apparent temperature measured with unprotected reversing thermometer.

By taking the differential of the equation, we have

$$dD_0 = \frac{10}{k\bar{\rho}}\,d(\theta - t) - \frac{10(\theta - t)}{k\bar{\rho}^2}\,d\bar{\rho} - \frac{10(\theta - t)}{k^2\bar{\rho}}\,dk\,. \tag{3.2}$$

It is out of the question that the systematic deviation of -2 m in D_0 should be caused by the first term, that is, $(\theta - t)$ can not be thought to have a systematic error.

In the second term, since $|d\bar{\rho}|$ is 0.001~0.002 gr/cm^3 and $|10/k\bar{\rho}^2(\theta - t)|$ is about 10000 cm^4/gr in the depth range of 0~1000 m, $|(10(\theta - t)/k\bar{\rho}^2)\,d\bar{\rho}|$ takes value of 0.1 ~0.2 m at most.

The pressure coefficient k of the unprotected reversing thermometer seems to decrease as the acting pressure increases. However, we have regarded k as a constant at any depth, which, the author supposes, would produce the systematic error in calculating the thermometric depth. As a matter of fact, the examination of k has been carried out under the pressure of 50~200 kg-wt/cm^2, so that a little larger value has come to be used for the depth range of 0~1000 m. That is, for example, dk is thought to be 0.0006°C·cm^2/kg-wt in the depth range of 250~350 m and 0.0003 in the depth range of 600~700 m. Consequently, $-[10(\theta - t)/k^2\bar{\rho}]\,dk$ becomes about -2.0 m which accords with the systematic deviation in the distribution of $(L - D_0)$ and $(L\cos\alpha_0 - D_0)$. Since $10(\theta - t)/k^2\bar{\rho}$ increases and dk decreases with the depth, the third term of (3.2) seems to keep constant irrespective of the depth in the depth range of 0~1000 m.

Thus, we know that the error of the pressure coefficient k adopted is predominant as the cause of the systematic error of D_0.

So, we must correct this systematic error of thermometric depth D_0, according to the above result.

Then we investigate the accidental error of D_0. After the correction of the systematic error of D_0, we have the distribution curves of $(L-D_0)$ in the depth ranges of 0~500 m and 500~1000 m and of $(L\cos\alpha_0-D_0)$. These are shown in Figs. 3, 4 and 5 respectively. The mean value, standard deviation and probable value of these distributions are computed as follows.

(1) as to the distribution of $(L-D_0)$ in the depth range of 100~500 m

$$\left.\begin{array}{ll} \text{mean value} & M_{L-D_0}=2.9\text{ m} \\ \text{standard deviation} & \sigma_{L-D_0}=3.7\text{ m} \\ \text{probable value} & P_{L-D_0}=2.5\text{ m} \end{array}\right\} \tag{3.3}$$

(2) as to the distribution of $(L-D_0)$ in the depth range of 500~1000 m

$$\left.\begin{array}{ll} \text{mean value} & M_{L-D_0}=4.4\text{ m} \\ \text{standard deviation} & \sigma_{L-D_0}=5.5\text{ m} \\ \text{probable value} & P_{L-D_0}=3.7\text{ m} \end{array}\right\} \tag{3.4}$$

(3) as to the distribution of $(L\cos\alpha_0-D_0)$ in the depth range of 100~200 m

$$\left.\begin{array}{ll} \text{mean value} & M_{L\cos\alpha_0-D_0}=3.5\text{ m} \\ \text{standard deviation} & \sigma_{L\cos\alpha_0-D_0}=4.4\text{ m} \\ \text{probable value} & P_{L\cos\alpha_0-D_0}=3.0\text{ m} \end{array}\right\} \tag{3.5}$$

The normal curves which represent these distribution curves are obtained very easily and plotted in the above figures. The fact that M_{L-D_0}, σ_{L-D_0} and P_{L-D_0} in the depth range of 500~1000 m are larger than those in 100~500 m may be caused by the error of $(\theta-t)$. That is, the above mentioned $M_{t_1-t_2}$, $\sigma_{t_1-t_2}$ and $P_{t_1-t_2}$ (mean value, standard deviation and probable value of temperature difference of two paired protected reversing thermometers), too, are slightly larger in the depth range of 500~1000 m than in the depth range of 100~500 m, so that the same tendency must be found as to the errors of t and θ.

The cause for the fact that $M_{L\cos\alpha_0-D_0}$, $\sigma_{L\cos\alpha_0-D_0}$ and $P_{L\cos\alpha_0-D_0}$ in the depth range of 100~200 m are respectively larger than M_{L-D_0}, σ_{L-D_0} and P_{L-D_0} in the depth range of 100~500 m is supposed to be the error of α_0. For, usually, the indicating plumb of the clinometer oscillates with the rolling and pitching of the vessel and we determine the value of α_0 as the center of the oscillating indication.

4. Wire Shape

In order to interpolate and correct the thermometric depth D_0, M. J. Pollak proposed "Depth Difference Method" in 1950. This may be considered as a very effective and proper method when we investigate a fairly deep layer or the unprotected reversing thermometers are insufficient in number. But in case that we treat of the layers whose depth are less than 2000 m and each water bottle has an unprotected thermometer on it as in the routine observation of the Meteorological

Agency in Japan, the "Depth-Wire Length method" where the depth is plotted against the wire length would be simpler, more convenient and more accurate. That is, the former method requires the trouble that first we calculate $(L-D_0)$, then after correction subtract it from L to obtain the corrected depth D_0. Moreover, when $(L-D_0)$ is small, it is difficult to determine the correction curve, as $(L-D_0)$ takes the value comparable to the error of D_0.

The latter method, however, has no these difficulties, and what is better, we can obtain the wire shape and wire angle more easily than by any other method and in many cases the correction curves are in the central part of the coordinates. The author tried to draw the correction curve of D_0 on a scale of one to five thousands and was able to have a sufficient accuracy. The distribution curve of $(D-D_0)$, where D is the depth corrected by the latter method, is shown in Figs. 6 and 7.

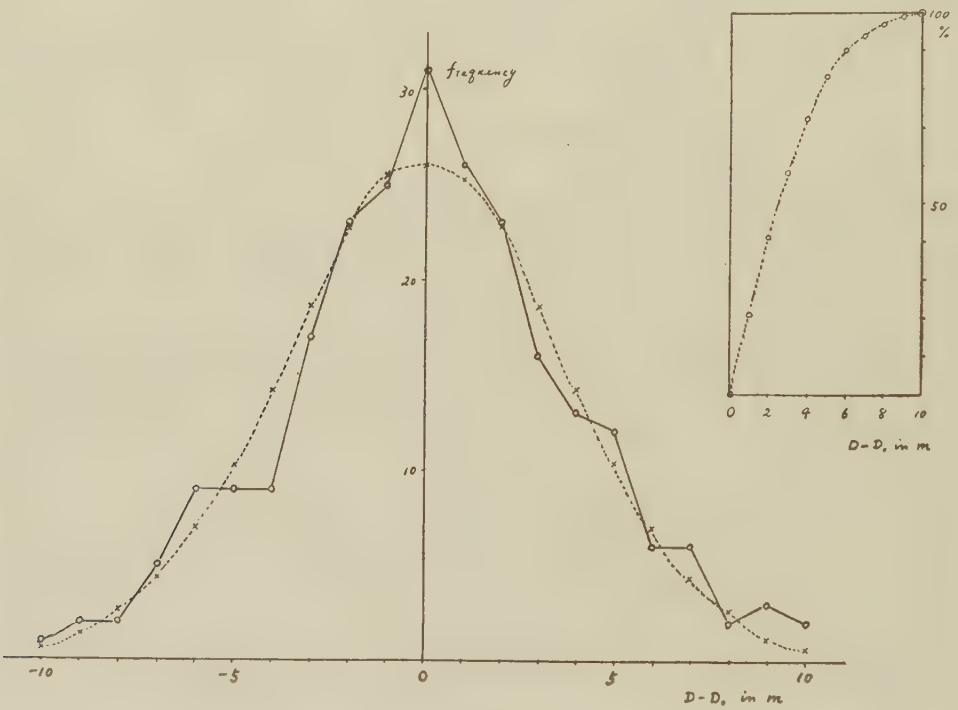

Fig. 6. Distribution curve of $D-D_0$ in the depth range of 100~500 m.

The mean value, standard deviation and probable value are:

(1) in the depth range of 100~500 m

$$\left.\begin{array}{ll} \text{mean value} & M_{D-D_0}=2.9\text{ m} \\ \text{standard deviation} & \sigma_{D-D_0}=3.8\text{ m} \\ \text{probable value} & P_{D-D_0}=2.5\text{ m} \end{array}\right\} \qquad (4.1)$$

(2) in the depth range of 500～1000 m

$$\left.\begin{array}{ll} \text{mean value} & M_{D-D_0}=4.4\text{ m} \\ \text{standard deviation} & \sigma_{D-D_0}=5.5\text{ m} \\ \text{probable value} & P_{D-D_0}=3.8\text{ m} \end{array}\right\} \qquad (4.2)$$

Of course $(D-D_0)$ represents the error of D_0.

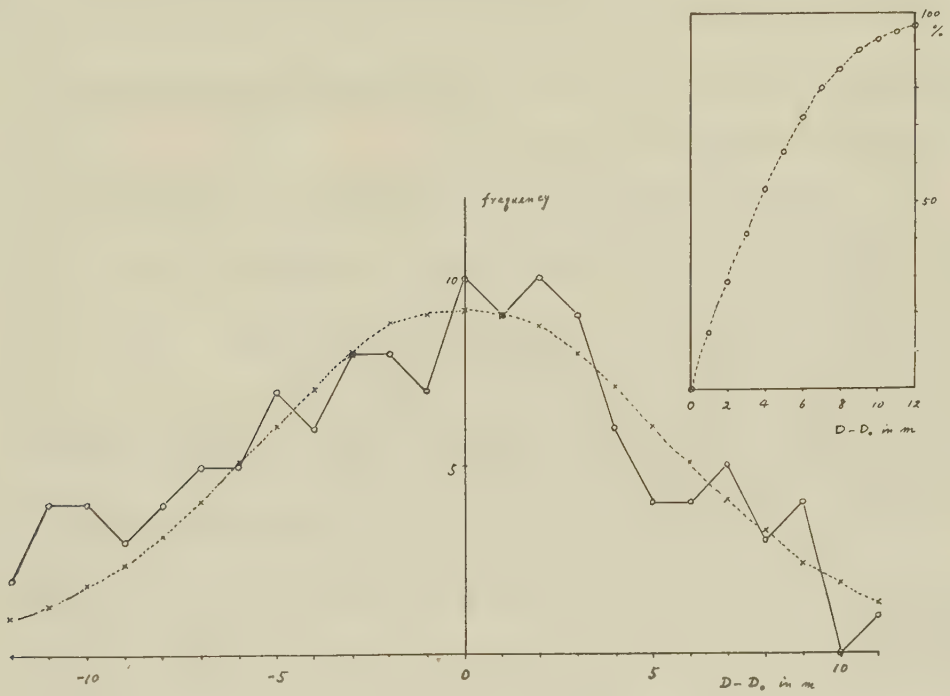

Fig. 7. Distribution curve of $D-D_0$ in the depth range of 500～1000 m.

It must be noticed that these values quite accord with those of the distribution of $(L-D_0)$ in the same depth range.

The corrected depth D is represented accurately by the following function of the wire length L when we attach the water bottles on the wire so as to reach the sampling layers whose depth are proposed by the International Association of Physical Oceanographer in 1936.

$$D=aL+bL^n \qquad (4.3)$$

where a is a positive constant, b is a constant and $1<n\leq 5$.

The author has inquired as to 53 examples where the depth of the lowest bottle ranges from 700 m to 1500 m, and found the wire shape could be regarded as a straight line within the depth of 300 m.

In 26 cases the wire descended wholly vertically and only in 6 cases the wire curved from within the depth of 400 m. And in the remaining cases the wire

seemed to curve either slightly at the lower end or suddenly between the lowest two bottles.

When the depth of the lowest bottle reached only from 350 m to 500 m, the wire forms the straight line in almost all cases.

Needless to say, $b=0$ in (4.3) when the wire is wholly straight.

In case the wire curves suddenly between the lowest two bottles, n takes a value near 5 and b becomes very small.

5. Accuracy of Depth Determined by Means of the Underwater Clinometer

(a) Principle of depth determination

The thermometric sounding has been the only method to measure depth accurately in the oceanographic observation. But it requires a troublesome procedure. The author wishes to ascertain the new method of depth determination by the use of the underwater clinometer.

In 1954, J. N. CARRUTHERS presented a "Wire Angle Gauge" of the pendulum type to use in conjunction with a series of water bottles.

To measure the underwater inclination of the wire, the instruments of water level type and pendulum type are thought to be used. Owing to the facility of the clamping, the latter has been chosen.

The author made the first type of underwater clinometer with the similar idea to that of CARRUTHERS's. The experiments were taken place at sea and the instrument was improved. In Fig. 9, is shown the advanced type (the third type) of the instrument. The instrument was placed at the center of each interval ended with the two neighbouring water bottles. And the depth of a bottle is calculated by adding the products of the wire length and Cosine of the measured wire angle of the intervals successively.

It is supposed that the depth determined by this method has the accuracy of the same degree as the thermometric sounding has as will be shown in the following.

(1) in case the wire forms the straight line

The depth difference between the both end of the i-th interval of the wire, ΔD_i, is given by

$$\Delta D_i=\Delta L_i\cdot\cos\alpha_i \tag{5.1}$$

where ΔL_i is the wire length and α_i is the wire angle of the interval. Taking the differential of (5.1), we have

$$d(\Delta D_i)=\Delta L_i\cdot d(\cos\alpha_i)+d(\Delta L_i)\cdot\cos\alpha_i\,. \tag{5.2}$$

Since the error of ΔL_i is very small, the second term may be negligible compared with the first. So the equation can be reduced to

$$d(\Delta D_i)=\Delta L_i \cdot d(\cos \alpha_i) \ . \tag{5.3}$$

As the wire angle α_i is measured in degree,

$$\begin{aligned} d(\Delta D_i) &= \Delta L_i \cdot \sin \alpha_i \cdot \frac{\pi}{180} \cdot d\alpha_i \\ &= 0.0175 \cdot \Delta L_i \cdot \sin \alpha_i \cdot d\alpha_i \ . \end{aligned} \tag{5.4}$$

With our underwater clinometer, since

$$|d\alpha_i| \leq \pm 1^\circ \tag{5.5}$$

we get

$$d(\Delta D_i) \leq 0.0175 \cdot \Delta L_i \cdot \sin \alpha_i \tag{5.6}$$

if

$$\left.\begin{array}{ll} \alpha_i=15^\circ & d(\Delta D_i) \leq 0.0045 \cdot \Delta L_i \\ \alpha_i=30^\circ & d(\Delta D_i) \leq 0.0087 \cdot \Delta L_i \\ \alpha_i=40^\circ & d(\Delta D_i) \leq 0.011 \cdot \Delta L_i \\ \alpha_i=60^\circ & d(\Delta D_i) \leq 0.015 \cdot \Delta L_i \ . \end{array}\right\} \tag{5.7}$$

Thus, the possible error of the depth determined by this new method does not seem to exceed 10 m, so long as the wire length is less than 1000 m and the wire angle is not extremely large.

(2) in case the wire curves

As stated before, the corrected depth D is given by

$$D=aL+bL^n \ . \tag{5.8}$$

We assume that $OACB$ in Fig. 8 represents (5.8).

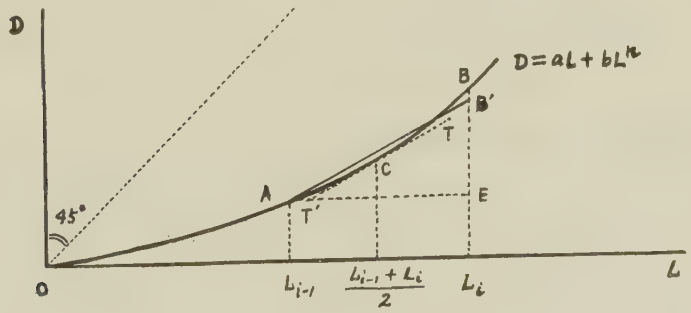

Fig. 8. $D-L$ Diagram.

ΔD_i, the depth difference of the two bottles which were attached on both ends of the i-th interval of the wire, is represented as BE in Fig. 8 and is calculated as follows.

$$\begin{aligned} \Delta D_i &\equiv BE \\ &= D_i - D_{i-1} \\ &= a(L_i - L_{i-1}) + b(L_i^n - L_{i-1}^n) \end{aligned} \tag{5.9}$$

where L_{i-1} and L_i are the wire lengths to the lower and upper end of the i-th interval respectively.

While, BE' in Fig. 8 is equal to the product of ΔL_i and $(dD/dL)_{L=(L_{i-1}+L_i)/2}$ (the differential coefficient of the curve at the center of the i-th interval), and is calculated in the following. Here, we put $BE' \equiv \delta D_i$.

$$\begin{aligned} BE' &\equiv \delta D_i \\ &= (L_i - L_{i-1}) \cdot \left(\frac{dD}{dL}\right)_{L=(L_{i-1}+L_i)/2} \\ &= (L_i - L_{i-1}) \left\{ a + nb \left(\frac{L_{i-1}+L_i}{2} \right)^{n-1} \right\} . \end{aligned} \tag{5.10}$$

As

$$\left(\frac{dD}{dL}\right)_{L=(L_{i-1}+L_i)/2} = (\cos\alpha)_{L=(L_{i-1}+L_i)/2} , \tag{5.11}$$

δD_i is the depth difference between the upper and lower end of the i-th interval which we may obtain by means of the new method.

Thus, $(\Delta D_i - \delta D_i)$ represents the possible error of the depth determined by the new method in which the underwater clinometers are used. This possible error is given by

$$\Delta D_i - \delta D_i = b \left\{ (L_i^n - L_{i-1}^n) - n(L_i - L_{i-1}) \left(\frac{L_{i-1}+L_i}{2} \right)^{n-1} \right\} . \tag{5.12}$$

If

$$\left.\begin{aligned} n=2 \quad & \Delta D_i - \delta D_i = 0 \\ n=3 \quad & \Delta D_i - \delta D_i = b/4\,(L_i - L_{i-1})^3 \\ n=4 \quad & \Delta D_i - \delta D_i = b/2\,(L_i + L_{i-1})(L_i - L_{i-1})^3 \\ n=5 \quad & \Delta D_i - \delta D_i = 11/16\, b(L_i - L_{i-1})(L_i^4 - L_{i-1}^4). \end{aligned}\right\} \tag{5.13}$$

The larger n becomes, the larger the error becomes. But if we let $(L_i - L_{i-1})$ be less than 450 m in case $(L_{i-1}+L_i)/2 > 1000$ m and $(L_i - L_{i-1})$ be less than 300 m in case $(L_{i-1}+L_i)/2 < 1000$ m, we can make this error be within 1 m irrespective of the value of n. There exists the possibility that as the intervals increase in number the error said above accumulates and the error of the determined depth grows larger. In reality, however, when the wire curves from the upper part, n is smaller than 2 and the error is approximately 0. And n is large, the wire shape approaches the straight line on the upper part and the error also decreases. Anyhow, the error is not large. Therefore, the depth error in case of the wire curving can be considered to be comparable to that in case of the wire being straight.

(b) Results

As stated above, the gradient of the curve of D as a function of L is equal to the cosine of the wire angle α. We calculate the gradient dD/dL and compare it with $\cos\alpha$. The mean value and root mean square value of the difference of both must be equal to the mean error and standard deviation of the error in the new method of depth determination and is calculated as follows.

$$\left.\begin{array}{ll} \text{mean value} & M=\dfrac{\sum|dD/dL-\cos\alpha|}{N}=0.0071 \\ \text{root mean square value} & \sigma=\sqrt{\dfrac{\sum(dD/dL-\cos\alpha)^2}{N}}=0.011\ . \end{array}\right\} \quad (5.14)$$

These values well accord with those derived from (5.7).

6. Discussions and Considerations

(**a**) The mean error of the depth determined by the use of the underwater clinometer seems to be proportional to the wire length L and to reach about 7 m at $L=1000$ m as is supposed from the error of $\cos\alpha$ shown in (5.14). Though underwater clinometer used has the allowance error of within $\pm1°$, it is only $\pm1/2°$ with the newly made one (the third type), so that we can expect to make the error nearly half in future experiments.

(**b**) As known widely, we can not apply the thermometric sounding to the measurement of the depth which is less than 100 m, because the error of the reversing thermometers takes the value comparable to the temperature rise of the unprotected thermometer caused by the water pressure. Moreover, in the thermometric sounding at the great depth, either the accuracy becomes low or we must use the very long thermometer. But if we adopt the underwater clinometer method, such inconvenience never happens. The wire seems to approximate to a straight line from a certain depth in case we treat of a very deep layer, and the error of the depth determined by this method does not increase in proportion to the wire length paid out.

(**c**) The procedure to determine the depth by means of the underwater clinometer is far simpler than that of the thermometric sounding.

(**d**) The underwater clinometer costs less than a pair of protected and unprotected reversing thermometers.

(**e**) As shown in already, the cosine of the wire angle measured with the underwater clinometer and that calculated from the results of the thermometric sounding accord very well, hence it is supposed that the wire in the sea is fairly stable against the vibration caused by the rolling and pitching of the ship except the part very near the sea surface and we can use it as a stable platform in various experiments.

(**f**) We stated that the thermometric depth D_0 contained the systematic deviation of -2 m. We calculated the gradient of the curve of $D=f(L)$ which contained the systematic error still and computed the mean value of the difference between this gradient and the cosine of the measured wire angle. The value was 0.011 and was a little larger than that shown in (5.14) in which the systematic error has been corrected. Therefore, we know there exists the systematic deviation in the thermometric depth D_0.

(**g**) As to the wire shape, many have analytically calculated long since, but such calculations seems to be very difficult and unpractical, for the drag force acting on the wire and attached bottles is a function of the relative velocity between the ship and the sea water around them and we can not know about it in detail. Moreover, when we attach the water bottles the wire shape quite changes depending on the number and the position of them, so that such a trial is in fact meaningless in many cases.

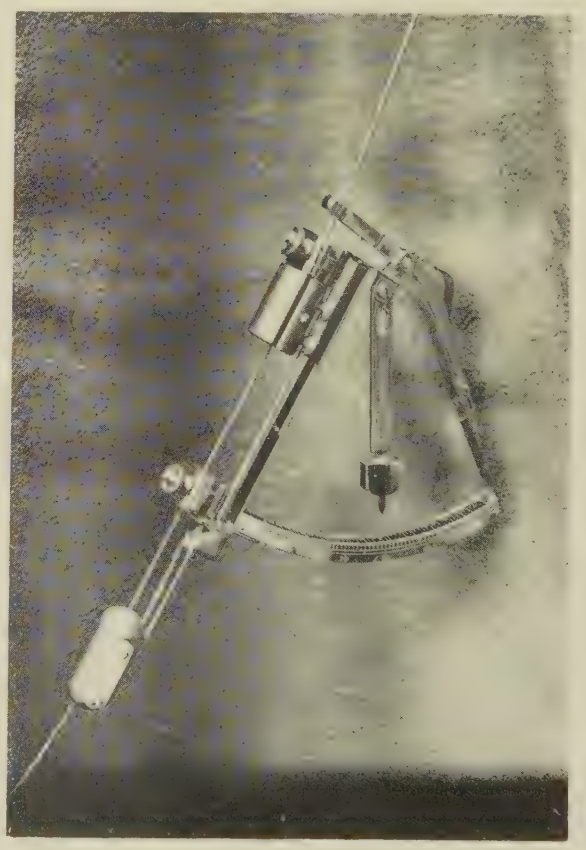

Fig. 9. Underwater clinometer.

Besides, we have been able to know from the investigation that the wire is kept straight between the lowest water bottle and the lead.

(**h**) As supposed, when the underwater clinometer is too heavy the wire curves locally and a large error is engendered in the depth calculation. In fact the first type of the instrument had the weight of 1.8 kg, and the wire angle measured with this differed from that calculated from the results of the thermometric sounding. We used it along with the second type of instrument (improved one) and could know the measurement with that was incorrect. We could know, too, that we made the breadth and the length of the frame of the underwater clinometer larger, the indication of the instrument is incorrectly as well, because of the drag force acting on these parts. In the improved one this defect has been amended.

7. Instrument (Underwater Clinometer)

As the instrument is used in the sea water, it must be easily cleaned and rustlessness is necessary. We made the most part of the instrument of brass and plated it with chromium. In the cover of the pendulum, we made slits for the cleaning of plumb.

In order to keep the instrument in the vertical plane, the weight was attached in a corner of the frame but the author gave his attention to make the instrument lighter.

The detail is shown in Fig. 9.

Acknowledgement

This research is partly financed by the funds of the Japanese National Commission for Unesco, Tokyo, Japan, to whom the author expresses his sincerest gratitude. He also wishes to thank Prof. K. Hidaka for his many helpful advices and suggestions, and to Mr. M. Iwamiya, President of the "Tsurumi Seiki Kosakusho" Co. for his help in making and improving the underwater clinometer. And the author also acknowledges the assistance and cooperation of the research workers on board the research vessel "Ryofu-Maru" in carrying out the experiment.

References

Carruthers, J. N. (1954): On the instrumental measurement of line shape under water—with technical descriptions by A. J. Wood and Appendix by A. J. Lee . Deutsche Hydrographische Zeitschrift, Band 7, Heft 1/2, 1954.

Hirano, T. (1952): An attempt to correct errors of the sounding by wire inclination. Journal of the Oceanographical Society of Japan, Vol. 8, No. 2.

Pollak, M. J. (1950): Notes on determining depths of sampling in serial oceanographic observations. J. M. R., Vol. 9, No. 1.

Records of Oceanographic Works
in Japan Vol. 4, No. 2,
March 1958

A Study on Upwelling

By
Kozo Yoshida
(Geophysical Institute, University of Tokyo)

1. Introduction

Upwelling is induced by horizontal divergence of horizontal component of flow which in most cases is generated by surface winds. Hence the vertical motion may respond to the wind action without time lag larger than a few days. In contrast, horizontal currents themselves are nearly geostrophic and vary with mass distributions which include some integral effects of winds. Vertical motion will cause the changes in mass distributions and consequently those in geostrophic currents, but these geostrophic currents are nearly non-divergent so that they may not alter the wind-generated vertical motion appreciably. In the lower layers, motions may be considered essentially not wind-driven but are induced by the changes in pressure field as a consequence of the horizontal divergence in the surface layer, and they occur so as to compensate the surface divergence in the upper layer.

These considerations may lead to the idea that the vertical motion can be determined from either of the information of wind or density distributions, or from the combination of these two informations. Obviously, the methods to estimate the vertical motion, which are based on dynamics involved, should depend largely upon the scale of processes concerned. Two typical examples of the determination of upwelling of different scales have so far been presented by the present author, which seem to show satisfactory agreement between theory and observations.

In the present article, only a summary of the present study will be given and more detailed discussion will be published in another paper.

2. Responses of Two-Layer Ocean to Variable Winds

The basic ideas of the discussions contained in this paper may simply be derived from a theory of dynamical responses of two-layer ocean to variable winds.* The dynamical model here assumed is essentially the same as that treated by Veronis

* The numerical values which result from the dynamics depend upon those assumed for various parameters, which are taken in the present study as

$$f=10^{-4}\,\mathrm{sec}^{-1},\quad \beta=2\times10^{-13}\,\mathrm{cm}^{-1}\,\mathrm{sec}^{-1},\quad H_1=10^{4}\,\mathrm{cm},\quad H_2=2\times10^{5}\,\mathrm{cm},\quad \frac{\Delta\rho}{\rho_2}=2\times10^{-3}$$

where f is the Coriolis parameter, $\beta=df/dy$, y being the horizontal coordinate directing northward, H_1 is the equilibrium thickness of the upper layer, is the one of the lower layer, and $\Delta\rho=\rho_2-\rho_1$, ρ_1 and ρ_2 being the densities of the upper and lower layers respectively.

and STOMMEL (1956), CHARNEY (1955) and the present author (YOSHIDA, 1956). By confining our present interest to the variations of the periods longer than a few days, we can gain much simplification of the whole discussion. Then the vorticity equations in the upper and lower layers yield the two equations, of which one gives the deviation of the interface between the two layers in response to the forcing function, the wind stress vorticity applied at the sea surface. The other equations gives the relation between the deviations at the sea surface and at the interface.

Various simplifications of the equations which may correspondingly lead to various method of determination of vertical motion can be made by assuming a criterion that the terms can be neglected if their magnitudes are less than, say, 10 % of the main terms in balance. This determines the ranges of L and T for which the approximations are valid, where L is the wave length and T is the period of the variations under consideration.

Particularly let us call our attention to the two ranges* which correspond to certain large-scale processes (Range 1) as described in the Section 3 and to small-scale processes (Range 2) as in the Section 4. The analysis indicates that the approximation for Range 1 will be valid, if (1) the period is longer than nearly one month, and if (2) the wave length is longer than the value as listed in Table 1. for different periods. The variations of periods shorter than one month or those of wavelength less than 1000 km should then be out of validity of this approximation.

Table 1.

T (in sec.)	2.6×10^6	0.8×10^7	3.2×10^7	6.4×10^7	1.6×10^8	2.2×10^8
	1 month	3 months	1 year	2 years	5 years	7 years
L (in km) (longer than)	8000	2500	1300	2600	6400	9100

Validity for Range 2 approximation will be secured, under the same criterion, if the period is between 7 days and 25 days, and if the wavelength falls within the ranges as shown in Table 2. The wavelength is limited between 24 km and 330 km.

Table 2.

T (in sec.)	6.5×10^5	1.3×10^6	2.0×10^6
	1 week	2 weeks	3 weeks
L (in km)	26–300	52–150	80–100

Another importance in this basic theory might be that relationship between changes in mean sea level and those in the vertical motion is obtained. This might

* The approximations for Range 1 tell that horizontal divergence is balanced by wind stress curl in the upper layer and by planetary vorticity in the lower layer. Range 2 corresponds to the balance between horizontal divergence and time change in relative vorticity.

give us a rough idea on a possibility of the determination of vertical motion from tide gage recording at coast or island stations.

3. An Example of Large-scale Upwelling

Discussion in this section is concerned with the scale as large as classified in Range 1. Table 1 shows that annual variations in vertical motion forced by those in wind stress curl of which wavelength is nearly 1000 km will belong to this range. The annual variations in the vertical motion off the California, when structure of scale smaller than 100 km and one month is smoothed out, are the examples. Indeed, a study by the present author and MAO (1954, unpublished) indicated that the vorticity balance seems to be valid well in the California waters. It was found from the observed data there, that density of water at depths of 100 to 150 meters increases from month to month in the cases when geostrophic northward (poleward) flow is present in lower layers and that it decreases when subsurface flow directs southward (or equatorward). At the same time, it was pointed out that seasonal shift of the regions of ascending motion off the coasts appears to coincide well with the shift of the regions of positive wind stress curl over the area. These facts which indicated satisfactory agreement between theory and observations would support the validity of our dynamical model and suggests strongly a possibility to determine the large-scale features of vertical motion in certain oceanic area. Under the assumption of the similar relationship between the steady meridional components of deep geostrophic flow and horizontal mass divergence, STROMMEL (1956) has determined the depth of no meridional motion for a particular oceanic area.

It might be worthwhile at this opportunity to comment on some remarkable features of isotherms or isopycnals which are frequently encountered especially in coastal regions where upwelling takes place. In examining the NORPAC temperature profiles, M. UDA* has paid a particular attention to a "vertical divergence" of isotherms at depths between 200 m and 500 m, revealed on a few east-west sections close to the Pacific coasts of North America. DEFANT (1936) presented the similar type of isothermal pictures along the western coasts of North Africa and of South Africa. Such a feature might give an impression that onshore flow in certain subsurface layer, as it strikes the coast, gives rise to upwelling in the layer above and sinking in the layer below. However, an alternative interpretation which seems more acceptable might be that the fall of isotherms toward the coast in the layers over several hundred meters above 1000 meter level should indicate the presence of northward current at and somewhat above these depths as usually known by the name of California Countercurrent. Then the present theory requires that upward motion is present also in the lower layer, contrary to the sinking features of isotherms, to compensate the upwelling in the surface layer.

* Personal communication.

4. An Example of Coastal Upwelling

It was empirically indicated that significant upwelling is likely to have taken place off the California coasts when the northerly winds blow along the coasts with duration as long as a week to several weeks. This upwelling is a kind of boundary phenomenon which differs materially from the upward motion described above and is not considered purely wind-driven. In actuality, conspicuous upwelling which has ever been described off California is likely to be a process confined within small distance such as 100 km from coasts. The coastal barrier and the stratification of water are essential to cause such a concentration of upwelling in narrow zone. This local but very important process of coastal upwelling belongs to the Range 2 stated in Section 2. A simple theory which appears to account for the process indicates that the speed of upwelling at the coasts is proportional to the wind stress and the width of upwelling zone depends upon latitude and stratification of the water. (Yoshida, 1955).

A question may arise whether or not strong offshore winds might also cause a significant upwelling along the coast. This problem must be of practical importance and is discussed in the first place. The approximate upwelling velocity at the coast is, when one considers the wind stress component normal to the coast in addition, given by

$$w_H=\frac{1}{\sqrt{gH_1\Delta\rho}}\left(\tau_y+\frac{1}{f}\frac{\partial\tau_x}{\partial t}\right)^{*}$$

In the result, upwelling velocity due to the increase in offshore winds is smaller by one order of magnitude in ordinary conditions than that due to the wind parallel to the coast, although it could still be quite significant, giving about 1 meter per day for $|\partial\tau_x/\partial t|$ of order of 10^{-5} cm^2 sec^{-3}. In the second place, annual variations in coastal upwelling are examined. Such variations are modified by the effect of planetary vorticity and do not belong to Range 2. In practice, however, the upwelling velocity at the coast is the same as the one for shorter periods if the amplitude of wind stress variations is the same. Only slight difference is that the width increases by 15 % and that vertical motion shows a lag of phase by one month.

There is a possibility that lateral mixing process may play a significant role in this case to reduce the amplitude and phase lag of the change appreciably. The observed annual changes in mean sea level along the Pacific of North America (Pattullo etal, 1955) might be explained well by applying this theory if we assume an additional role of lateral mixing by taking lateral eddy viscosity to be 10^5 to 10^6 cm^2 sec^{-1}. Should this be the case in reality, the tide gage recording would

---

* w_H is the vertical velocity, positively downward; τ_y is the component of wind stress parallel to the coast, positively northward, and τ_x is that normal to coast, positively onshore.

give very useful means to measure the vertical motion in subsurface layers for the areas. In the third place, definite means should be given to estimate the value of $\sqrt{gH_1\Delta\rho}$, although it is measurable and nothing of uncertain quantities like eddy viscosity and although errors due to this would be only a small matter of a factor of two or three. A difficulty may be encountered especially in coastal waters where the upper mixed layer is extremely thin or is absent. The best way perhaps will be that a depth where vertical density gradient is largest may be taken as H_1. An alternative method might be to measure the distance L, if possible, based on observed data of density change. Another way might be to measure the characteristics of long internal waves as $\sqrt{gH_1\Delta\rho}$ is the speed of propagation of such waves in the area concerned.

5. An Estimate of the Maximum Range of Vertical Displacement

Upwelling is of great importance to the productivity of waters because it brings nutrient salts into the euphotic zone. It might be desired to define upwelling in its proper sense by large upward transport of water from some deep layers into the surface layer. An occurrence of such a significant overturning of layers would require the upward displacement of water as large as the order of 100 meters at least. The duration of upwelling is only days in some cases and is months or could be many years in some other cases. It might be considered that the magnitude $|h|$ on the model given in the Section 2 gives a rough measure of the maximum amount of vertical shift of the thermocline so that this would give very rough idea of the possibilities of occurrence of upwelling on different scales of the variations.

Assumptions are made in computing $|h|$ from the theory that (1) the variations are represented by waves of a form $\exp\left[i\left(\frac{2\pi}{T}t-\frac{2\pi}{L_x}x\right)\right]\sin\frac{2\pi}{L_y}y$ and that (2) the magnitude of wind stress curl is given by $\sqrt{\left(\frac{2\pi}{L_x}\right)^2+\left(\frac{2\pi}{L_y}\right)^2}\,|\tau(T, L_x, L_y)|$ where $|\tau(T, L_x, L_y)|$ denotes the magnitude of wind stress vector for various periods and wave-lengths and is put here equal to 1 dyne cm^{-2} for all periods and wave-lengths.

Table 3.

$|h|$ in meters

(1) L_y=6000 km

T \ L_x	12000 km	6000 km	600 km	60 km
∞	500	250	250	250
10 years	45	42	170	220
1 year	5.4	5.0	42	100
1 month	0.4	0.4	4.2	13
1 week	0.1	0.1	1.0	3.3

(2) L_y=600 km

T \ L_x	12000 km	6000 km	600 km	60 km
∞	5000	2500	250	250
10 years	450	420	170	220
1 year	50	50	42	100
1 month	4.2	4.2	4.2	13
1 week	1.0	1.0	1.0	3.3

(3) L_y=60 km

T \ L_x	12000 km	6000 km	600 km	60 km
∞	5×10^4	2.5×10^4	2500	250
10 years	1600	1600	1000	200
1 year	170	170	160	70
1 month	14	14	14	8
1 week	3.3	3.3	3.3	2

In actuality, there is possibility that lateral mixing effect may emerge perhaps for longer periods. However, the present result shown in Table 3 gives the values of $|h|$ based on the model which is free from the unknown effect of lateral mixing.

For the coastal upwelling as described in section 4, $|h|$ is appreciable even for the period as short as a few weeks. (see Table 4)

Table 4

$|h|$ in meters

Period	1 week	1 month	2 months	3 months
$\|h\|$ at coast (in meters)	10	40	84	126

If we disregard the lateral mixing effect, $|h|$ for the annual variations amount to be 500 meters. Summarizing the above calculations, it follows that a significant amount of vertical displacement of water will not occur for variations of periods shorter than a year except for the coastal regions. Upwelling of practical importance would have a greatest change to occur in the coastal waters. There are some other mechanism of generating and maintaining upwelling under different conditions in different areas of the oceans. However, as far as our model is concerned, intense upwelling of duration as short as weeks to months would not occur in the open ocean.

References

CHARNEY, J. C. (1955): The generation of oceanic currents by wind. J. Mar. Res. **14** (4): 477-498.

DEFANT, A. (1936): Das Kaltwasserauftriebsgebiet wor der Küste Südwestafrikas. Landerkundliche Forschung, Festshrift Norcert Krebs zur Vollendung 60, Lebensjahres dargebracht, 52–66.

PATTULLO, J., W. H. MUNK, R. R. REVELLE and E. STRONG: The seasonal oscillation in sea. J. Mar. Res. **14** (1) : 88–155.

STOMMEL, H. (1956): On the determination of the depth of no meriodional motion Deep Sea Res. **3** : 273–278.

VERONIS, G., and H. STOMMEL (1956): The action of variable wind stresses on a stratified ocean. J. Mar. Res. **15** (1) : 43–75.

YOSHIDA, K. (1955): Coastal upwelling off the California Coast. Records of Oceanographic Works in Japan. **2** (2) : 8–20.

YOSHIDA, K. (1956): A note on the pressure changes of the two-layer ocean. J. Oceanogr. Soc. Japan. **12** (4) : 111–116.

Records of Oceanographic Works
in Japan Vol. 4, No. 2,
March 1958

Productivity of Plankton-feeders in the Off-shore Area of Japan*

By
Yoshio Hiyama and Fujio Yasuda
(Fisheries Department, Faculty of Agriculture, University of Tokyo)

1. Introduction

Roughly speaking, the area where the Japanese fishing activities are operating could be devided into three areas, according to the distance from the coast, namely: (1) Coastal area, (2) Off-shore area, and (3) Oceanic area. Though it is hard to define by the accurate measure of distance from the coast, the off-shore area, here the authors are going to deal with, is an area beyond the coastal area and about 5 to 50 miles off from the coast. This area is generally operated by the medium size boats, about 20 to 50 tons, furnished with about 50 to 100 H. P. engine. The length of fish cruise is often one day or night, and it is rarely a few days.

This area had been explored since thirty or forty years ago by the development of fishing boats of the modern type. Satisfactory historical statistics for the production and for the number of boats is available for the authors' reference.

The total production from these areas occupies about half of the total Japanese landing, fished by about 4,000 boats in recent years. Though a part of the catch is bottom livings, like plaice, turbot, crabs, shrimps and others, a much bigger part of the catch is either surface or middle-layer livings, such as sardine, anchovy, herring, mackerel, horse mackerel, skipper, squids and other plankton-feeders and carnivorous fishes such as yellow-tail, cod, skip-jack, tuna, salmon and others.

In the products from the off-shore area, which arises to one and a half million metric tons per year in some period, plankton-feeders occupy about 90% and are about 10 times of the carnivorous fish, in amount.

The historical review on the statistics of the amount of landing of these plankton-feeders from the off-shore area shows that the total landing of these species altogether is nearly the same in both the pre-war time and the post-war time, as shown in Figs. 1 and 2, though that for each species changed remarkably and the abundance for them also changed[3]. This is a peculiar circumstance in the world, and the authors here have tried to analyse how and why it is so.

2. Constant production of plankton

The area here that the authors are going to consider is so vast that a minor

* The present work was carried out under a financial support of the Japanese National Commission for Unesco.

local change in the condition related with the production of plankton could be neglected when considering the area as a whole. And, though there would be some annual change on the climatological or oceanographical condition in the area as a whole, if we could speak roughly, it would be possible to say that the total production of plankton of all species remain somewhat even throughout the entire period we are now considering.

3. Two groups of plankton-feeders

The landing statistics available for the analysis is merely for the species of economical value. However, we know through the evidence of the stomach contents of carnivorous fish such as tunas, salmon and others that there are so many species of plankton-feeders in the same area not utilised by man directly as the object of fishing.

Between the two groups of plankton-feeders, economical and non-economical species, there must be some competition for survival between the two groups, though also inter-special and intra-special competition is also certainly exist among them.

The total population of the two groups would be influenced by the population size of their predators, if the plankton production is constant. However, the population of the economical group has extra burden besides it, that is man's effort of fishing. Therefore, when man's demand for marine products for the food is large, the population of the economical group would be reduced, while the non-economical group would thrive.

4. The value of fish

Fundamentally, the economical value of a certain fish species would be decided by traditional choice and demand with regarded to the amount of supply. And, if the amount of fishing effort is constant, the supply would be decided by the density of the fish in the area, which means that it will depend on the size of the population when the area is the same, a case that we are now considering.

Generally speaking, the plankton-feeders here considered are abundant and cheap species, and have nearly equal value in Japan. This means that people here would select cheaper fish among these several species for their table use by substituting one another.

5. Man's fishing effort

Therefore, when the population of a certain species of this group decreases to a certain extent, accordingly the density decreases, and the supply of it becomes small, and then the price gets high. As a sequence, people buy other cheaper species. This calls upon man's effort to turn to aim at other relatively abundant species. Really such an "economical compensation[2])" would be easily achieved by

converting some equipment and gear of the same type of fishing boat, as it had actually happend when sardine density reduced, and many of the fishing boats turned for skipper and squid.

This statistics on the number of fishing boats in Japan has no division for each kind of fish, however, the total number of boats of sizes from 20 to 50 tons, as shown in Fig. 2, indicates the total amount of fishing effort for the several species of plankton-feeders altogether approximately.

6. Change of gear

(1) Sardine and anchovy is mainly fished by purse-seine, (2) herring by gill-net and set net, (3) horse mackerel by purse-seine and hand-line, (4) skipper by lift net, (5) mackerel by purse-seine and rod-and-line, (6) squid by hand-line, and all these are caught by almost the same type of boat. A few remarkable change or improvement in fishing gear took place during this period, especially after the recent war. The first is the development and the wide-spread use of the supersonic fish finders for sardine purse-seine, mackerel and horse mackerel fisheries. And the next is that of powerful fish attracting electric lamp for nocturnal operation of purse-seine for sardine, mackerel and horse mackerel, lift net for skipper, and hand-line for squid.

7. Interpretation of Figs. 1 and 2

Fig. 1, shows the fluctuation of the amount of annual catch of six major species of plankton-feeders from the off-shore area from 1926 to 1954 for each species, (anchovy is included in sardine).

This tells that the sardine was a major species in the pre-war period, but by the reduction of the density of sardine in this area, other five minor species had come up in the post-war period. Among these species the most remarkable increase (about 40 times of the pre-war catch) can be seen for squid, and the next (about 20 times) for skipper. On the other hand, sardine landing was reduced to the level less than half of the pre-war time peak.

Fig. 2, was prepared so as to show the annual landing of these species adding the one by the one, so the line at the top shows the total of all the six species, with the graph of the number of registered fishing boats (20 to 50 tons in size) supposedly engaged in these fishing.

This tells (1) that the total landing of the six species is about equal for both the pre-war and post-war periods, though the war-time reduction is remarkable, and (2) that the amount of fishing effort for this catch is more than twice of the pre-war level in the post-war time, which can be seen by the increase of the number of fishing boats and the improvement of fishing gear, though the latter is hard to enumerate in figure.

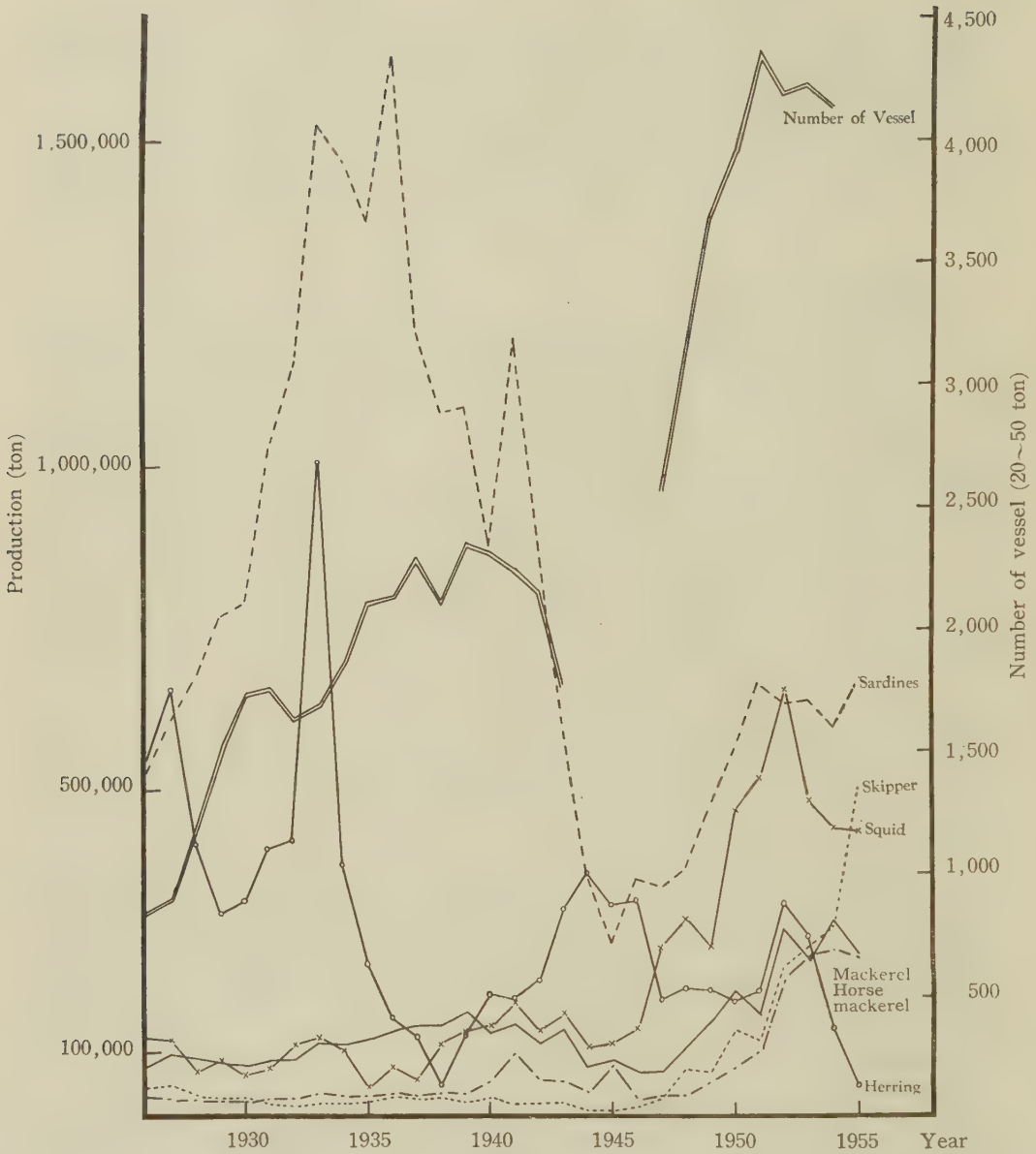

Fig. 1.

8. Interpretation of the tendency

By the fact that the total catch of the six plankton-feeders is nearly equal for both the pre-war and the post-war time, it is hard to say that the total amount or population of these as a whole is equal for the two periods. This phenomena tells (1) that the "economical compensation" above mentioned had taken place, and (2)

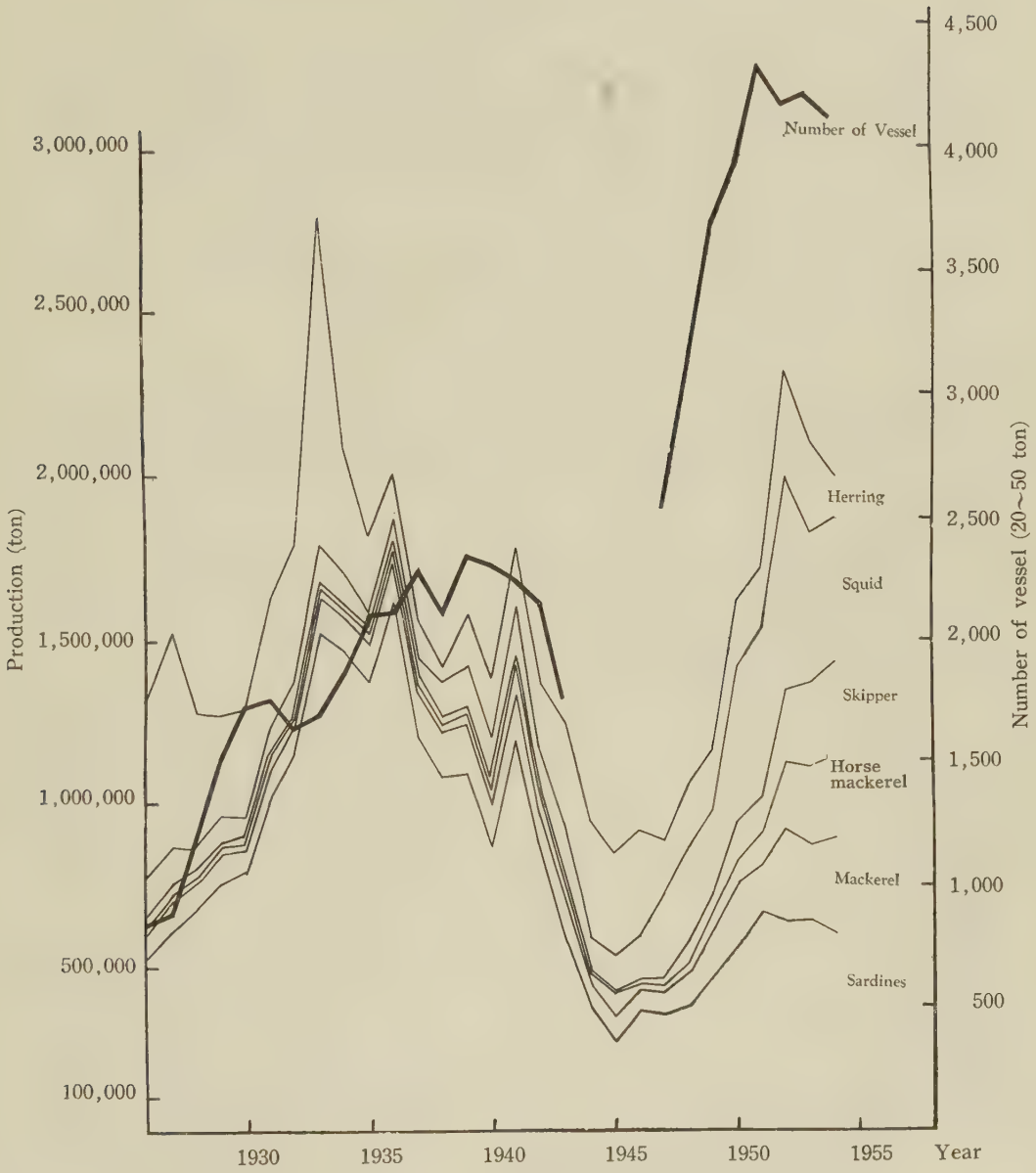

Fig. 2.

that the total demand by people for fish as a whole is nearly the same in both periods and though the increase of animal husbandry product is remarkable in recent years, it still has little influence for the supply of animal protein to this nation.

As catch per unit effort of fishing can indicate the density of the fish in the

area, it also can indicate the size of the population inhabiting a definite area, a case that we are now considering.

Considering the total population of the six major plankton-feeders altogether just as one species of fish, it decreased to a level of less than half of the pre-war time in the post-war time, because the number of the boats for this catch became about twice in the post-war time.

If, by the constant yield of plankton in this area, the total population or amount of the plankton-feeders could be constant during this period, then it can be expressed as C, and the following relation would exist.

$$A+B=C \qquad \text{and} \qquad A'+B'=C$$

where, A is the total population of economical group in the pre-war time and A' is that in the post-war time. B is that of non-economical group in the pre-war time, and B' is that in the post-war time. No information is available for the size of C, B and B', expect A' is about a half of A. Then B' would be larger than B in any degree.

Through the knowledge of the stomach contents of carnivorous fishes, such as tunas and salmon, B is supposed to be fairly larger than A at any time. And, B is composed by fairly more numerous species than A, though the density of each species is lower than any of A.

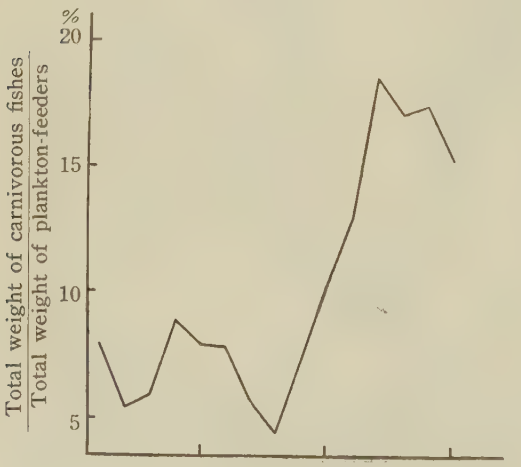

Fig. 3.

Because, if the density of any species becomes high enough to be easily caught, it would be fished commercially, if its quality is not bad for the table use of this fish eating nation.

The ratio of total catch of carnivorous species altogether to that of plankton-feeders was about 5–10% for pre-war time peak, and about 15–20% for post-war, as shown in Fig. 3. (local variation ref. to 4))

If the total number of fishing boats (20–50 tons) could be used for the fishing effort of the carnivorous fish also, the average catch, as well as the relative size of population, for carnivorous fish has no remarkable difference between pre-war and post-war periods.

This would tell that the total population or amount of plankton-feeders (C) to feed this population of carnivorous fish might have no significant change during this period, and the equilibrium between the two is still maintained now, though the population of economical group had reduced to almost a half now.

Literature

1) Statistics here used are from "Norinsho Tokei-hyo" for respective year by Japanese Government.
2) Y. HIYAMA, 1956. "Gyogyo to Suisan" (Fishing Industry and Fisheries).
3) F. YASUDA and Y. HIYAMA, 1957. Mechanism of Utilization of Plankton by Some Fishes (Record of Oceanographic Works in Japan 3 (1).)
4) T. HANAOKA, 1955. Problem on the Productivity in Water Area. (Aquiculture Science Series No. 10. Tokyo).

Records of Oceanographic Works
in Japan Vol. 4, No. 2,
March 1958

Morphometric Comparison of the Albacore from the Northwest, the Equatorial and the Southwest Pacific

By
Kenji Kurogane and Yoshio Hiyama
(Fisheries Department, Faculty of Agriculture, University of Tokyo)

1. Introduction

The albacore is distributed abundantly in the Northwest and the Southwest Pacific all the year round. Occasionally, the fish is also caught in plenty by the Japanese long line tuna boats in the Equatorial Pacific. The problem of whether or not these albacore are composed of a number of independent units, is not exactly analysed up to date from the standpoint of morphometry, excepting for the study by Godsil (1948)[1]. In order to approach this problem we have examined the morphometrical analysis for the albacore from these different areas of the Pacific. We have reported earlier about the relative growth and the morphometric characteristics of the albacore taken by the pole-and-line and the long line fishery from the Northwest Pacific[2]. In the present study the biometric data of specimens from the Equatorial and the Southwest Pacific are compared with the data of specimens from the Northwest Pacific.

We gratefully acknowledge and sincerely extend our gratitude to the chief and staff of the Nankai Regional Fisheries Research Laboratory, who have given us all the facilities for the collection of the samples.

2. Materials and Methods

In addition to the Northwest Pacific samples that were reported in our previous paper, we collected one sample from the Southwest Pacific in 1955, and four samples from the Equatorial Pacific, ranging from 150°E to 160°W in 1956 and 1957.

All specimens of samples from the Southwest and the Equatorial Pacific were caught by long line fishery boats and landed at the Tokyo Central Fish Market. These samples are tabulated in Table 1, showing the fishing grounds, fishing date, number of specimens, range and average of body length. As regards the samples from the Northwest Pacific, only those caught by the long line fishery were used in this present study.

Measurements and the comparison of data are similar to those employed in our reports on the yellowfin tuna and the albacore[2),3)]. Eighteen body characters were

Table 1

Origin, date taken, number of fish, range and average of body length for each sample.

Origin	Date taken	No. of fish	Range of body length (mm.)	Average of body length (mm.)
0°S- 7°S, 153°E -162°E	Mar.-May, 1956	30	821-1079	942
2°N- 2°S, 164°E -167°E	Apr., 1957	46	859-1050	955
0°S- 5°S, 170°E -177°W	Apr., 1957	30	878-1031	931
1°N- 3°S, 170°W-161°W	Apr.-May, 1956	35	879-1049	971
13°S-28°S, 153°E -158°E	July-Sept., 1955	42	798-1062	928

measured with slide calipers and a pair of dividers according to the techniques of Marr and Schaefer (1949)[4]. The statistical procedure used in comparing the regression as presented by Kendall (1948)[6] was followed.

Table 2

Comparison of body proportion of albacore by covariance analysis for the samples taken from the Equatorial Pacific. Data show variance ratio and its significance. F_r is the variance ratio to test the significance of the regression difference, F_b to test the regression coefficient difference and F_a to test the adjusted mean difference.

Body character	F_r	F_b	F_a
Head length	1.15	1.03	1.26
Snout to 1st dorsal	1.69	1.83	1.52
Snout to 2nd dorsal	2.64*	3.12*	(2.07)
Snout to anal	1.85	3.45*	(<1)
Snout to ventral	1.97	<1	3.75*
Snout to pectoral	2.25*	<1	3.51*
1st dorsal base	1.44	1.80	1.07
2nd dorsal to caudal	2.27*	1.38	4.11*
Anal to caudal	2.46*	<1	4.56*
1st dorsal spine length	1.04	1.53	<1
2nd dorsal length	1.89	<1	3.44*
Anal length	1.57	<1	2.82*
Pectoral length	<1	<1	<1
Body depth	3.31**	<1	6.45**
Spread caudal	2.61*	1.36	3.82*
Maxillary length	3.27**	2.79*	(3.61*)
Diameter of iris	4.28**	<1	8.07***

N.B. In the case where the regression coefficient difference is significant, the test of the adjusted mean difference becomes inappropriate, i.e. those figures within brackets under F_a.

* : Significant at 5% level

** : Significant at 1% level

*** : Significant at 0.1% level

3. Results

i) Morphometric characteristics of the albacore from the Equatorial Pacific

Prior to the comparison between regions, we attempted to analyse the problem of whether or not the four samples taken from the equatorial areas show any great difference in morphometrical characters. Samples were compared in 17 body characters by covariance analysis. The variance ratio to test the significance of the difference in the sample regression lines with each body character is shown in Table 2. The asterisks in the table show the significant level.

The difference of regression lines was highly significant in body depth, maxillary length and diameter of iris, and significant at 5% level in snout to second dorsal, snout to pectoral, second dorsal to caudal, anal to caudal and spread caudal. These differences were mainly caused by the differences of the adjusted means. A test of significance can decide merely whether or not there is a difference between samples, and if a difference is found we become interested in the quantity and direction of that difference. As such, we estimated the adjusted mean with its 99% confidence interval of each body character, basing on the regression coefficient estimated from the four samples, excepting in the three body characters, snout to second dorsal, snout to anal and maxillary length, which showed the significant difference in the regression coefficient. These values are tabulated in Table 3.

Table 3

Adjusted mean of each body part with its 99% confidence limits, mean standard length in millimeters and estimated regression coefficient.

Body character \ Sample	150°E in 1956	160°E in 1957	170°E in 1957	160°W in 1956	Mean standard length (mm.)	Estimated regression coefficient
Head length	279.8±1.92	278.6±1.54	279.5±1.94	278.0±1.81	951.1	0.2608
Snout to 1st dorsal	312.1±2.76	310.6±2.21	311.3±2.79	309.7±2.59	951.1	0.2880
Snout to ventral	316.2±2.52	315.0±2.02	314.6±2.54	312.0±2.37	951.1	0.3032
Snout to pectoral	286.2±2.21	282.9±1.77	281.5±2.23	283.5±2.08	951.1	0.2662
1st dorsal base	248.2±2.81	248.4±2.25	250.0±2.84	247.3±2.64	951.1	0.2638
2nd dorsal to caudal	429.3±3.45	423.8±2.77	424.3±3.49	424.3±3.24	951.1	0.4519
Anal to caudal	375.5±3.78	373.2±3.03	376.9±3.82	369.7±3.55	951.1	0.4036
1st dorsal spine length	115.4±2.81	113.7±2.12	114.0±2.44	113.9±2.50	947.8	0.1280
2nd dorsal length	119.6±2.31	120.2±1.81	122.2±2.25	118.4±2.13	950.1	0.1387
Anal length	116.1±2.22	114.7±1.72	116.9±2.22	113.8±2.02	951.1	0.1474
Pectoral length	418.6±7.61	417.2±6.16	417.2±7.69	415.4±7.15	2.9775	629.90
Body depth	247.1±3.54	245.6±2.78	245.6±3.56	240.3±3.26	951.4	0.2704
Spread caudal	329.0±5.88	320.7±4.72	328.7±6.10	323.7±5.52	950.7	0.4631
Diameter of iris	43.33±0.75	44.20±0.61	44.30±0.76	45.20±0.68	279.2	0.1162

For diameter of iris, the measurement was the greatest in the eastern sample and the least in the western one, and their difference was about 2 mm. However, a cline in the other direction was indicated for body depth (the western sample having the greater measurement), and the maximum difference between samples was about 7 mm..

In maxillary length, these four samples indicated significant difference in their regression coefficients, but there was no geographical tendency both in the slope and the level of the regression line.

The significant difference of 5% level were often recognized in repeated samples taken from the same area, as shown in the albacore from the Northwest Pacific. These heterogeneity have been obtained by Godsil (1948) and Schaefer (1952, 1955)[6),7)], too. Lund (1957)[8)] pointed in his report on the striped bass, *Roccus saxatilis*, that the 5% level is not considered biologically significant. Godsil said in his report, "In every series of duplicate samples there are significant differences (below the 1 percent level) in one or more of the characters investigated.—Under these circumstances it seems advisable (until these divergent sample regression lines can be correlated with and explained by the caudative factors) to regard the stock of yellowfin tuna as composed of a single (though statistically heterogeneous) population, the parameters of which are best estimated from the total sample."

We have pointed in our earlier reports that body depth and maxillary length show the great variability in repeated samples from the same region. The same kind of result was obtained from comparing the duplicated samples of specimens from the Equatorial Pacific.

However, great differences were not recognized in many body characters and we may consider that the four samples from the Equatorial Pacific belong to a simple population. This problem will be decided more exactly in the following section.

ii) Morphometric comparison of the albacore from the three waters of the Western Pacific

In order to compare statistically the albacore from the three different areas, the two samples from the Northwest Pacific and the four samples from the Equatorial Pacific were treated as a single unit sample from each area respectively. The results tabulated in Tables 4 and 5 are based on the analysis, identical in method with that previously described.

In head length, insertion ventral and pectoral fins, second dorsal to caudal, first dorsal spine length, pectoral length, spread caudal, maxillary length and diameter of iris, we observed the difference at 0.1% significant level. In four other body characters the difference was significant at 5% level and in the four remaining characters no significant difference was noted. Accordingly we may consider that

Table 4

Comparison of body proportion of albacore by covariance analysis, for the samples from the Northwest, the Equatorial and the Southwest Pacific. Data show variance ratio and its significance level.

Body character	F_r	F_b	F_a
Head length	36.27***	<1	71.83***
Snout to 1st dorsal	3.11*	<1	6.02**
Snout to 2nd dorsal	<1	<1	<1
Snout to anal	1.04	<1	1.78
Snout to ventral	6.46***	<1	12.79***
Snout to pectoral	19.26***	<1	38.04***
1st dorsal base	3.09*	<1	6.06**
2nd dorsal to caudal	5.32***	1.29	9.33***
Anal to caudal	<1	<1	1.43
1st dorsal spine length	22.01***	<1	43.74***
2nd dorsal length	2.35	<1	3.91*
Anal length	2.80*	<1	4.89**
Pectoral length	15.51***	13.18***	(16.42***)
Body depth	3.27*	3.37*	(3.11*)
Spread caudal	87.34***	5.53**	(162.94***)
Maxillary length	10.47***	1.63	19.23***
Diameter of iris	41.20***	7.68***	(71.05***)

Table 5

Adjusted mean of each body part with its 99% confidence limits, mean standard length in millimeters and estimated regression coefficient.

Body character \ Sample	Northwest	Equatorial	Southwest	Mean standard length (mm.)	Estimated regression coefficient
Head length	270.9±1.08	277.2±0.92	277.1±1.70	944.5	0.2530
Snout to 1st dorsal	306.6±1.49	308.9±1.26	309.5±2.33	944.5	0.2895
Snout to 2nd dorsal	548.8±1.61	549.0±1.36	549.2±2.52	944.5	0.5426
Snout to anal	601.9±1.80	600.3±1.53	601.9±2.82	944.5	0.5935
Snout to ventral	308.7±1.60	312.4±1.36	312.9±2.51	944.5	0.3028
Snout to pectoral	277.0±1.25	282.4±1.06	281.2±1.96	944.5	0.2538
1st dorsal base	249.4±1.57	246.7±1.33	246.7±2.46	944.5	0.2630
2nd dorsal to caudal	425.8±1.99	422.1±1.69	420.4±3.12	944.5	0.4649
Anal to caudal	371.4±2.13	371.0±1.81	373.5±3.34	944.5	0.3987
1st dorsal spine length	107.6±1.32	113.5±1.13	113.4±1.93	942.6	0.1204
2nd dorsal length	117.5±1.31	119.3±1.12	118.0±2.09	944.3	0.1314
Anal length	112.5±1.27	114.3±1.09	114.9±1.99	944.4	0.1339
Maxillary length	98.3±0.56	100.0±0.47	100.3±0.86	274.9	0.3555

the three samples do not agree with such a hypothesis that they might have been drawn by simple random sampling from a homogeneous population, but from the above facts they difinitely belong to separate populations.

When we consider the difference of regression lines, two questions are posed for any group of samples, namely: whether the variance between samples is caused by the regression coefficient difference or by the adjusted mean difference. As shown in Table 4, the difference between samples mainly depended on the difference in the adjusted means. We estimated the adjusted mean with its 99% confidence interval for each character (Table 5), excepting for four characters the regression coefficient of which cannot be considered as drawn from a common population. For characters that indicated heterogeneity in the regression coefficient, we estimated the regression coefficient b with its 95% confidence interval and y intercept a of each sample. These estimates of parameters are shown in Table 6.

Table 6

Estimates of the parameters of the albacore from the Northwest, the Equatorial and the Southwest Pacific.

Body character \ Sample	Northwest		Equatorial		Southwest	
Parameter	b	a	b	a	b	a
Body depth	0.2404±0.0108	14.2	0.2603±0.0245	−2.7	0.2776±0.0282	−18.1
Spread caudal	0.3763±0.0219	−59.9	0.4525±0.0400	−105.3	0.4062±0.0495	−64.6
Diameter of iris	0.1034±0.0092	12.88	0.1217±0.0062	10.34	0.1524±0.0063	1.09
Pectoral length	820.42±59.79	−2034.0	620.27±107.79	−1429.8	499.08±118.35	−1085.9

a) Comparison of the equatorial sample with the southwest sample

Two samples showed great difference in pectoral length and diameter of iris. But the other 15 body characters showed close similarity. This is also deduced from Table 5 and 6.

For diameter of iris, the variance was very large within samples from the equatorial area, above mentioned. As the samples did not show the difference in regression coefficient, we estimated the adjusted means. The diameter of iris of the Southwest Pacific albacore was a little larger than that of the western sample from the equatorial regions but was smaller than the remaining three. If we consider the equatorial samples as samples from a common population, we cannot say that the albacore taken from the two different areas do not belong to the common population as far as this character is concerned.

As to pectoral length, the difference was great. We must further examine this character basing on the repeated samples from these areas.

Generally, we may say that albacore taken from the Equatorial Pacific frequently

have very similar morphometrical characteristics with the Southwest Pacific sample.

b) Comparison of the northwest sample with the equatorial and the southwest samples

The comparison of three samples from the different areas showed great difference in many characters. But when we compared the equatorial with the southwest sample, we could not find such difference excepting for two characters. Accordingly, we may deduce that such differences depend on the heterogeneity of the Northwest Pacific sample and other samples. When we compared the northwest sample with the equatorial sample, the result was almost identical with the one shown in Table 4. This was also seen in the comparison of the northwest with the southwest sample. The specimens of albacore taken from the equatorial area had the following morphometrical characteristics; larger head and maxillary, more posteriorly positioned fin insertions, higher first dorsal spine and spread caudal, shorter body trunk and caudal regions. These characteristics were also recognized while comparing the southwest sample with that of the northwest.

The specimens of the northwest albacore had a shorter head, about 6 mm. for a body length of 95 cm. (near the grand mean) than the albacore from the equatorial and the southwest areas (Fig. 1A). The great difference in this character was not seen in the comparison of the samples from the same area. Ventral and pectoral fin insertions are good indicators to separate the albacore from the different areas, too. Comparing these samples, we could find 4 mm. of difference in the ventral fin insertion (Fig. 1B) and 5 mm. in the pectoral fin insertion (Fig. 1C).

In the fist dorsal spine length, the northwest albacore was shorter by about 6 mm. than the albacore of other areas (Fig. 1D), and in the spread caudal was less by about 20 mm.. Maxillary length of the Equatorial and the Southwest Pacific albacore was 2 mm. larger than the Northwest Pacific one, but this character showed the great variability that has been mentioned earlier in this paper. Maximum difference of the northwest samples by pole-and-line and long line fishery was about 1.5 mm. and in the equatorial samples, their positional difference was not so great. Accordingly, we can consider that 2 mm. difference was greater than the difference which would occur in the samples from the same area.

First dorsal base and second dorsal to caudal of the Northwest Pacific albacore were longer than that of the Equatorial and the Southwest Pacific samples. Their differences were about 3 mm. for first dorsal base and about 5 mm. for second dorsal to caudal.

For diameter of iris the regression coefficient showed heterogeneity, so we cannot compare the adjusted means directly. The Northwest Pacific sample had the smallest regression coefficient than the other two regions. Using each sample regression coefficient we estimated the diameter of iris of each sample for a head

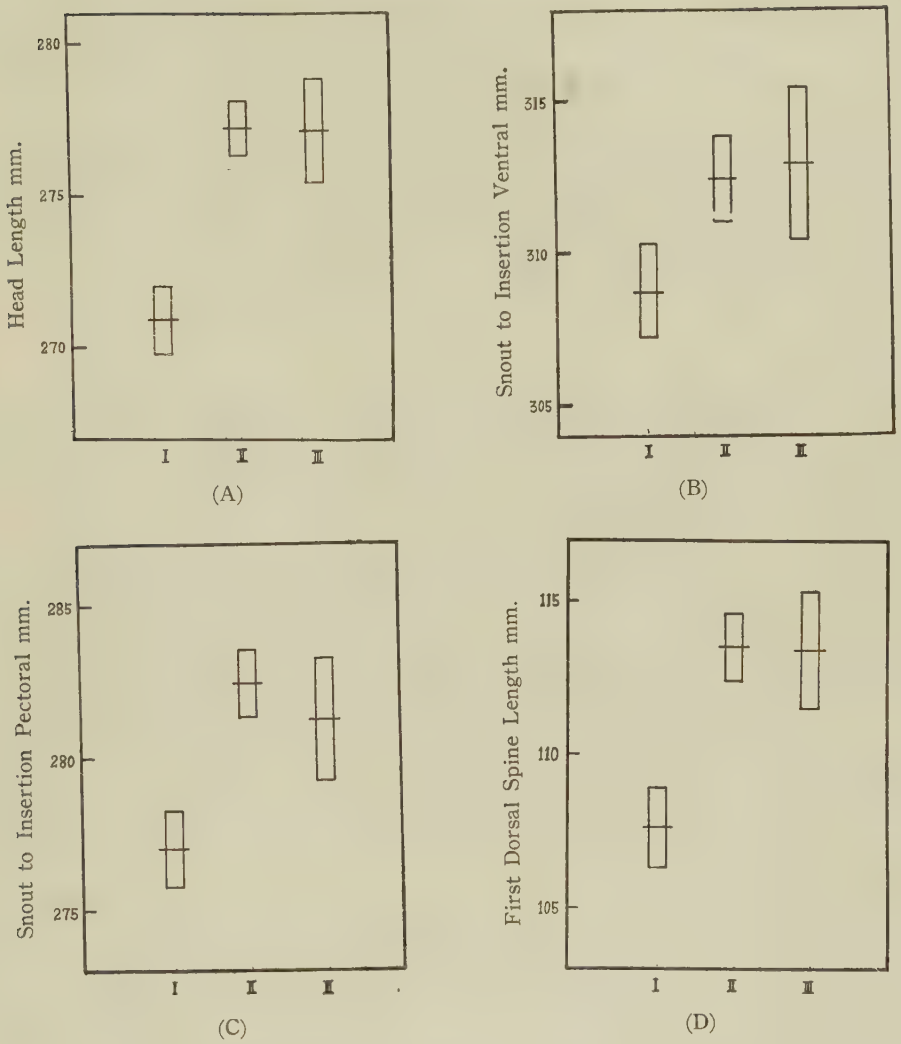

Fig. 1. Adjusted mean of body part and its 99% confidence interval.

(A): Head length at 944.5 mm. body length
(B): Snout to ventral fin insertion at 944.5 mm. body length
(C): Snout to pectoral fin insertion at 944.5 mm. body length
(D): First dorsal spine length at 942.6 mm. body length
I: Albacore from the Northwest Pacific
II: Albacore from the Equatorial Pacific
III: Albacore from the Southwest Pacific

length of 275 mm. (near the grand mean). The southwest sample was about 43.0 mm., the equatorial about 43.8 mm., and the northwest about 41.3 mm.. Consequently, the specimens of the Northwest Pacific albacore differed from the Southwest and the Equatorial Pacific one in the slope and in the level of regression line.

In pectoral length, three samples differed from each other. Generally, the speci-

mens of the equatorial sample had a longer pectoral fin and the northwest albacore had a relatively fast growing fin. The southwest albacore had a shorter and relatively slow growing fin.

Basing on these results we may consider that the Northwest Pacific albacore form a distinct unit from the Equatorial and the Southwest Pacific albacore. The albacore which appear in the equatorial area seasonally, are either the component of the Southwest albacore population or a sub-population having the intensive intermingling with each other.

4. Discussion

GODSIL (1948) suggested in his population study of the tunas, that the morphometry is a useful method to analyse the relationship of the albacore. We applied his procedure to our specimens from the several localities of the Western Pacific in order to know their relationship.

On the yellowfin tuna, racial studies have been undertaken by many workers in the form of investigations of morphometric characters. They all got the results that the yellowfin tunas of the Pacific could be considered to be separated into many independent or semi-independent populations. On the contrary, our results let us consider the existence of only two albacore populations in the Western Pacific from the standpoint of morphometry. Recently tagging programs for tunas have been actively promoted and they have revealed, basing on the data of the recovered albacore, that the albacore migrate in the area between the east and the west of the Northwest Pacific.

It was estimated by UEYANAGI (1957)[9] that the waters of the North Equatorial Current is the main spawning ground of the albacore that are distributed in the Northwest Pacific. The spawning ground of the Southwest Pacific albacore is not well known, but ISHII and INOUE (1956)[10] have suggested that the Coral Sea may be the spawning ground. According to the reports collected from tuna fishery boats, relatively small fish are richly distributed in the further southward area of our southwest region as well as in the Northwest Pacific. These seem to show positive evidence that the albacore population distributed in the southern hemisphere is independent from that in the northern hemisphere.

The four samples of albacore from the Equatorial Pacific (the South Equatorial Current) are similar morphometrically with that of the Southwest Pacific. We may deduce that the albacore of these two areas belong to a common population and the latter migrate northwards in the winter season, basing on both the results of morphometrical analysis and their fishing conditions and migrations connecting with the oceanographical structure of the adjacent waters around 10°S of the Western Pacific[11].

References

1) GODSIL, H. C. (1948): A preliminary population study of the yellowfin tuna and the albacore. Calif. Div. Fish and Game, Fish Bull. 70.
2) KUROGANE, K. and Y. HIYAMA (1957): Morphometric characteristics of the albacore, Germo germo, from the Northwest Pacific. Records. Oceano. Works. Japan, 4 (1).
3) KUROGANE, K. and Y. HIYAMA (1957): Morphometric comparison of the yellowfin tuna taken from the Equatorial Pacific. Bull. Jap. Soc. Sci. Fish., 23 (7 & 8).
4) MARR, J. C. and M. B. SCHAEFER (1949): Definitions of body dimensions used in describing tunas. U. S. Fish and Wildlife Service, Fish. Bull. 47.
5) KENDALL, M. G. (1948): The advanced theory of statistics. Charles Griffin and Co., London.
6) SCHAEFER, M. B. (1952): Comparison of yellowfin tuna of Hawaiian waters and of the American west coast. U. S. Fish and Wildlife Service, Fish. Bull. 72.
7) SCHAEFER, M. B. (1955): Morphometric comparison of yellowfin tuna from Southeast Polynesia, Central America, and Hawaii. Inter-American Tropical Tuna Comm., Bull. 1 (4).
8) LUND, W. A. (1957): Morphometric study of the striped bass, Roccus saxatilis. U. S. Fish and Wildlife Service, Special Scientific Report, Fish. 216.
9) UEYANAGI, S. (1957): Spawning of the albacore in the Western Pacific. Report. Nankai Regional Fish. Research Lab., No. 6.
10) ISHII, K. and M. INOUE (1956): Some notes on the ovary of albacore, Germo germo, taken from the Coral Sea. Bull. Jap. Soc. Sci. Fish., 22 (2).
11) YAMANAKA, H. (1956): Vertical structure of the ocean in relevant to fishing conditions for albacore adjacent to 10°S in the Western South Pacific. Bull. Jap. Soc. Sci. Fish., 21 (12).

PRINTED BY
KOKUSAI BUNKEN INSATSUSHA
CHIYODA-KU, TOKYO